Technische Universität München
TUM School of Engineering and Design

Multi-fidelity Optimization Methods with Applications to Automotive Crashworthiness and Deep Drawing

Arne Kaps

Vollständiger Abdruck der von der TUM School of Engineering and Design der Technischen Universität München zur Erlangung eines

Doktors der Ingenieurwissenschaften (Dr.-Ing.)

genehmigten Dissertation.

Vorsitz: Prof. Dr.-Ing. Michael Manhart

Prüfende der Dissertation:

1. Prof. Dr.-Ing. habil. Fabian Duddeck
2. Prof. Dr.-Ing. habil. Carola Doerr
3. Assoc. Prof. Dr. Jean-Marc Bourinet

Die Dissertation wurde am 15.04.2024 bei der Technischen Universität München eingereicht und durch die TUM School of Engineering and Design am 01.10.2024 angenommen.

Abstract

As the increase in simulation model resolution has at times outpaced the rapid increase in available computational power, the required effort to perform multi-query analyses, such as optimizations, can become prohibitive. MF (multi-fidelity) methods have been introduced as a remedy where the accurate but expensive, *high-fidelity*, simulation model is complemented with a cheaper-to-evaluate but also less accurate, *low-fidelity*, model in a way that benefits overall performance.

In the context of the present thesis and the appended publications, surrogate-based MF optimization techniques are applied to two challenging structural applications and different modifications are suggested. The two applications automotive crashworthiness and deep drawing are chosen because they involve similar challenges in the simulation models and therefore allow for some degree of generalizability in the findings. A recently proposed MF extension of the popular efficient global optimization method based on a *hierarchical kriging* surrogate model and the *variable-fidelity expected improvement* infill criterion is used as a basis to establish the potential of MF techniques. Beyond that, the novel contributions of this work include the investigation of various aspects of both, the algorithm and application problems and the suggestion of different modifications to further improve optimization performance. On the application side, the choice of low-fidelity model is investigated in the context of two examples from the automotive crashworthiness field, and the importance of careful definition of the objective function is illustrated on a deep drawing problem. It is shown that a novel modification to the initial *design of experiments* can benefit the optimization performance. Finally, it is investigated how input parameter uncertainties, which may be commonly encountered in real-world applications, can be included into the MF optimization. Therefore, a novel MF extension for a common infill criterion is suggested. Furthermore, it is shown that even optimization performance can benefit when integrating methods to consider input parameter uncertainties into the algorithm.

In summary, the chosen MF optimization technique is established in automotive crashworthiness and deep drawing here and various novel modifications to improve optimization performance are proposed. Based on the promising findings, various ideas for future work are developed.

Zusammenfassung

Da die Detailliertheit von Simulationsmodellen bisweilen schneller zunimmt als die verfügbare Rechenleistung, kann der erforderliche Rechenaufwand für die Durchführung von sogenannten multi-query Analysen, wie beispielsweise Optimierungen, prohibitiv werden. Als Abhilfe wurden MF (multi-fidelity) Methoden eingeführt, bei denen das genaue, aber teure, *high-fidelity* Simulationsmodell durch ein günstiger auszuwertendes, aber auch weniger genaues, *low-fidelity* Modell ergänzt wird, um die Gesamtleistung zu verbessern.

Im Rahmen der vorliegenden Arbeit und der beigefügten Veröffentlichungen werden Surrogat-basierte MF-Optimierungstechniken auf zwei anspruchsvolle Strukturprobleme angewendet und verschiedene Modifikationen vorgeschlagen. Die beiden Anwendungen automobile Crashsicherheit und Tiefziehen wurden ausgewählt, um ein gewisses Maß an Verallgemeinerbarkeit der Ergebnisse ermöglichen. Eine kürzlich vorgeschlagene MF-Erweiterung der beliebten *efficient global optimization* Methodik, die auf einem *hierarchical kriging* Surrogatmodell und dem *variable-fidelity expected improvement* basiert, wird als Grundlage verwendet, um das Potenzial der MF-Techniken zu ermitteln. Darüber hinaus gehören zu den neuen Beiträgen dieser Arbeit die Untersuchung verschiedener Aspekte sowohl des Algorithmus als auch der Anwendungsprobleme und der Vorschlag weiterer Modifikationen zur Verbesserung der Optimierungsleistung. Auf der Anwendungsseite wird die Wahl des Low-Fidelity-Modells im Zusammenhang mit zwei Beispielen aus dem Bereich der automobilen Crashsicherheit untersucht, und die Bedeutung einer sorgfältigen Definition der Zielfunktion wird anhand eines Tiefziehproblems veranschaulicht. Es wird gezeigt, dass eine neuartige Modifikation der anfänglichen Versuchsplanung die Optimierungsleistung verbessern kann. Schließlich wird untersucht, wie Unsicherheiten der Eingangsparameter, die in realen Anwendungen häufig vorkommen, in die MF-Optimierung einbezogen werden können. Daher wird eine neuartige MF-Erweiterung für ein gängiges Infill-Kriterium vorgeschlagen. Darüber hinaus wird gezeigt, dass sogar die Optimierungsleistung profitieren kann, wenn Methoden zur Berücksichtigung von Unsicherheiten der Eingangsparameter in den Algorithmus integriert werden.

Zusammenfassend wird hier die gewählte MF-Optimierungstechnik in Anwendungen der automobilen Crashsicherheit und im Tiefziehen etabliert und es werden verschiedene neuartige Modifikationen zur Verbesserung der Optimierungsleistung vorgeschlagen. Auf der Grundlage der vielversprechenden Ergebnisse werden verschiedene Ideen für zukünftige Arbeiten entwickelt.

Acknowledgements

This dissertation and the appended publications are the result of about three and a half years of research work conducted at the Associate Professorship of Computational Solid Mechanics at TU Munich. I am deeply grateful to all those whose continued support and encouragement have been instrumental not only in the completion of this doctoral thesis but also in making my time at the chair quite enjoyable.

First and foremost, I wish to thank Prof. Fabian Duddeck for the opportunity to work at the chair and pursue this research. His supervision, which included regular, highly interesting discussions, guidance and support but also allowing me to pursue my own ideas, is what ultimately made this thesis possible.

Special thanks go out to Dirk Lukaszewicz for agreeing to be my mentor, for the regular, highly interesting exchanges and his guidance during these exciting years!

I am grateful to Prof. Quek Ser Tong who co-supervised me at National University of Singapore and to Evan Cheok for very interesting research discussions and for making my stay overall very enjoyable.

I am also very thankful to all the (former) colleagues at the chair, Tobias Lehrer, Catharina Czech, Lisa Pretsch, Paolo Ascia, Elena Raponi, Philippa Weißinger, Giada Colella, Koushyar Komeilizadeh, Norbert Ludwig, Mathias Lesjak, Reza Barzanooni, Sonja Schlenz and Nivesh Dommaraju, for interesting scientific discussions, constructive collaborations and a very enriching environment in general.

Finally, I have to thank my friends and family for their encouragement, support, and interest in my work throughout this time.

Thank you Kyla for being there and for your unending love and support!

Appended publications

Publication I

Kaps A., Czech C., Duddeck F.: A hierarchical kriging approach for multi-fidelity optimization of automotive crashworthiness problems. Structural and Multidisciplinary Optimization **65**(4), 2022. DOI: https://doi.org/10.1007/s00158-022-03211-2

Publication II

Kaps A., Lehrer T., Lepenies I., Wagner M., Duddeck F.: Multi-fidelity optimization of metal sheets concerning manufacturability in deep-drawing processes. Structural and Multidisciplinary Optimization **66**(8), 2023. DOI: https://doi.org/10.1007/s00158-023-03631-8

Publication III

Kaps A., Lehrer T., Lepenies I., Wagner M., Quek S.T., Duddeck F.: A novel two-stage multi-fidelity optimization for manufacturability of deep-drawn metal sheets. 2024. (submitted for publication at Structural and Multidisciplinary Optimization)

Other contributions

Journal publications

- Komeilizadeh K., Kaps A., Duddeck F.: Isovolumetric adaptations to space-filling design of experiments. Optimization and Engineering **24**, 1267–1288 (2023). DOI: https://doi.org/10.1007/s11081-022-09731-6
- Lehrer T., Kaps A., Lepenies I., Duddeck F., Wagner M.: 2S-ML: A simulation-based classification and regression approach for drawability assessment in deep drawing. International Journal of Material Forming **16**(5), 2023. DOI: https://doi.org/10.1007/s12289-023-01770-3
- Lehrer T.[1], Kaps A.[1], Lepenies I., Raponi E., Wagner M., Duddeck F.: Complementing drawability assessment of deep-drawn components with surrogate-based global sensitivity analysis. ASCE-ASME Journal of Risk and Uncertainty in Engineering Systems Part B: Mechanical Engineering, 2024. DOI: https://doi.org/10.1115/1.4065143

[1]These authors contributed equally and should be regarded as co-first authors.

Conferences

- Kaps A., Komeilizadeh K., Duddeck F.: An Iso-volumetric Weighting Approach to Increase Efficiency of Stratified Samplings. *In:* 14th World Congress of Structural and Multidisciplinary Optimization, Boulder, CO, USA, 2021
- Kaps A., Lehrer T., Komeilizadeh K., Duddeck F.: Adaptation of multi-fidelity optimization schemes to nonlinear structural dynamics applications. *In:* 8th European Congress on Computational Methods in Applied Sciences and Engineering, Oslo, Norway, 2022
- Czech, C., Kaps A., Duddeck F.: Robust multi-fidelity optimization approach exploiting data-driven, non-linear model order reduction. *In:* Proceedings of the 8th International Symposium on Reliability Engineering and Risk Management, Hannover, Germany, 357-363, 2022. DOI: https://doi.org/10.3850/978-981-18-5184-1_MS-12-041-cd
- Lehrer T., Kaps A., Daiminger T., Lepenies I., Duddeck F., Wagner M.: Analysis of Global Sensitivities for One-Step and Multi-step Deep-Drawing Simulations. *In:* 16th German LS-DYNA Forum, Bamberg, Germany, 2022

Contents

List of Figures

List of Tables

List of Abbreviations

AEI	augmented expected improvement
BHF	blankholder force
BO	Bayesian optimization
CDF	cumulative distribution function
DE	differential evolution
DoE	design of experiments
EFF	expected feasibility function
EGO	efficient global optimization
EGRA	efficient global reliability analysis
EI	expected improvement
EU	European Union
FEA	finite element analysis
FLC	forming limit curve
FLD	forming limit diagram
FMVSS	Federal Motor Vehicle Safety Standard
GP	Gaussian process
HF	high-fidelity
HK	hierarchical kriging
IV	isovolumetric
LCB	lower confidence bound
LF	low-fidelity
LHS	Latin hypercube sampling
MC	Monte Carlo
MF	multi-fidelity
MF-DoE	multi-fidelity design of experiments
MLE	maximum likelihood estimation
MOR	model order reduction
MSE	mean squared error
NCAP	New Car Assessment Programme
OIVLH	optimal isovolumetric Latin hypercube
OLHS	optimal Latin hypercube sampling
PDF	probability density function
PE	potential energy
PI	probability of improvement
QMC	quasi-Monte Carlo
RBF	radial basis function
ROM	reduced order model
SF	single-fidelity
SVD	singular value decomposition
UN-ECE	United Nations Economic Commission for Europe
USA	United States of America

VFEI	variable-fidelity expected improvement
WLC	wrinkling limit curve

Chapter 1

Introduction

Optimization algorithms have been successfully applied to different structural applications not only in research work but also in industrial applications for many decades now. The rapid increase in available computational resources was at times even outpaced by the increase in simulation model resolution. This makes running hundreds or even thousands of simulations per optimization run computationally prohibitive in many practical applications. This is particularly true in cases where no additional information on the objective function is available. This means that it has to be considered a black box, and, for example, gradient-based techniques cannot be used.

There have historically been two closely related ideas on how to tackle this challenge without reducing the quality of simulation models. First, black-box optimization algorithms were tailored to reduce the number of required objective function evaluations. These techniques, such as EGO (efficient global optimization) (Močkus, 1975; Jones et al., 1998), commonly use surrogate models to guide the algorithms towards promising regions in the design space. Second, the idea of MF optimization techniques was developed whereby the accurate but expensive simulation model is combined with a faster to evaluate, yet less accurate LF (low-fidelity) model, for example, a simplified simulation model. Then, both models are combined in the optimization process in a way that is beneficial to overall optimization performance. In recent years, as both ideas gained increasing popularity, they have also been combined to generate highly efficient MF optimization techniques (Huang et al., 2006; Zhang et al., 2018a).

As MF methods have been widely adopted in the literature (Mainini et al., 2022; Park et al., 2017; Fernández-Godino, 2023) and used in various different applications, they also introduce additional challenges not encountered in ‘classical’, SF (single-fidelity), methods. One example is the appearance of additional hyperparameters in the optimization technique, which have to be defined in a sensible way to ensure reliable performance of the optimization. Another example is the need to define an LF model which typically requires human interaction and can be a time-consuming task depending on the problem at hand. Finally, it must be ensured that when assessing optimization algorithms against each other, particularly MF with SF techniques, hyperparameters are defined in a way that allows a fair comparison. These points, together with the fact that many aspects of the MF optimization technique which is the focus

in the present work, were only suggested very recently (e.g., Zhang et al. (2018a)); and they are the motivating factors for the research done in the context of the present thesis.

One of the fields of structural applications considered in the present thesis is automotive crashworthiness. As the field in general has been active in academia and industry since at least the 1970s, some of the first uses of optimization algorithms for this application also date back almost 30 years at the time of writing, e.g. (Etman et al., 1996). Since then, optimization algorithms have been extensively applied to structural crashworthiness problems (Fang et al., 2016) and also some work on MF optimization in this field has been published (e.g., Sun et al. (2010a); Acar et al. (2020)). Optimization problems in this field are typically characterized by a high degree of nonlinearity in the underlying dynamic simulation models which are based on explicit FEA (finite element analysis). Common sources of nonlinearity are highly nonlinear deformations, strain-rate dependencies, (self-)contact and others. Therefore, the objective functions are also commonly nonlinear and multimodal, usually having to be considered as black-boxes, which currently renders gradient-based optimization algorithms unsuitable.

The other application that is investigated in the present work is the deep-drawing process, which represents one of the most widespread sheet metal forming processes in industry. More specifically, it is investigated here how the drawability of a component can be improved through optimization, as this is one of the major challenges in the early design stages of new components. As with crashworthiness, optimization algorithms have been widely used in this field of application (see, for example, the review works by Wifi et al. (2007); Andrade-Campos et al. (2022)). Few works have been published that apply MF optimization in deep drawing problems; they are discussed in Section 3.2. Similar to structural crashworthiness problems, drawability optimization problems also have an underlying nonlinear simulation model based on explicit FEA that usually causes the objective function in the optimization problem to be multimodal. The main sources of nonlinearity in this case are large plastic deformations in the metal sheet and contacts.

1.1 Research Questions

The use of MF optimization techniques in challenging structural applications, such as automotive crashworthiness or deep drawing raises various interesting research questions. The focus on these two applications was chosen because, while they are different in the individual challenges and quantities involved, they both include highly nonlinear simulation models. Therefore, common findings in both applications allow at least some degree of generalizability of the conclusions. The research questions which initiated this research work and which are also behind the appended publications (Kaps et al., 2022, 2023, 2024), are listed below. Thereby, a distinction is made between the questions related to the optimization algorithm and the questions related to the application problem at hand.

First and foremost, it has to be established that modern MF optimization methods based on the idea of EGO such as the one based on HK (hierarchical kriging) and VFEI (variable-fidelity expected improvement) mainly applied in the present work can bring any benefit to the chosen applications at all (*Question 1*). When comparing optimization algorithms, the focus typically lies either on the quality of the optimum found or on the time / computational resources needed to find it. The focus in the present work lies more on the latter, as it is argued that in practical applications it matters more to find a decent optimum fast. Another essential aspect of using stochastic algorithms such as EGO is the consistency of the results when repeating optimization runs. This also strongly depends on the optimization problem under investigation. In a second step, the observed benefits have to be compared with previous publications using different optimization techniques to ensure the reliability of the assessments and quantify potentials (*Question 2*). The third question is how different steps of existing optimization algorithms, such as the initial design of experiments, can be modified to improve the overall optimization performance (*Question 3*). The different aspects of the optimization algorithm are reviewed in Chapter 2 and individual modifications of the appended publications are highlighted. It is investigated whether the overall algorithm architecture can be adjusted in a beneficial way (*Question 4*). Closely related, it is interesting to explore the question of how to effectively integrate input parameter uncertainties into the optimization scheme (*Question 5*). The latter would allow for more realistic problem definitions in real-world applications, where typically not all parameters can be controlled, but some information on their variation may be available.

Two further questions arise from the applications, but are also closely related to the remaining questions. First, can the low-fidelity model be chosen in a way that is beneficial for the overall performance of the algorithm in these two applications (*Question 6*)? Second, how much impact does the choice of objective function have in the context of a drawability optimization of a deep-drawn component (*Question 7*)?

A total of seven research questions have been formulated, which are investigated in the three appended publications (Kaps et al., 2022, 2023, 2024). An overview of how the research questions are distributed to the publications is given in Table 1.1.

Table 1.1 Attribution of research questions to appended publications. Formulations of the questions see text above.

Research questions	Publication I (Kaps et al., 2022)	Publication II (Kaps et al., 2023)	Publication III (Kaps et al., 2024)
Question 1	x	x	x
Question 2	x	x	x
Question 3	x	-	x
Question 4	-	-	x
Question 5	-	-	x
Question 6	x	-	-
Question 7	-	x	-

1.2 Thesis outline

The key contributions of this research work include the successful answering of research questions 1 and 2 formulated above. On the side of optimization methodology, a novel modification to DoE (design of experiments) techniques is proposed (Komeilizadeh et al., 2022) and successfully applied to the two fields of application in appended publications I and III (Kaps et al., 2022, 2024). Furthermore, a novel two-stage MF technique that allows for the consideration of input parameter uncertainties and improves the optimization performance is proposed in appended publication III (Kaps et al., 2024). Studies on the choice of LF model and the choice of objective function are performed in appended publications I and II (Kaps et al., 2022, 2023) using application examples from the fields of crashworthiness and deep drawing, respectively.

Based on these contributions, the remainder of this thesis is structured as follows. The state of the art for the MF optimization methods including the proposed improvements and the greater research context is presented in Chapter 2. The two application use cases automotive crashworthiness and deep drawing are reviewed in Chapter 3 incorporating the mechanical challenges and previous research by others on MF optimization in these applications. The appended publications are then summarized in Chapter 4 (the full length papers can be found in Appendix A). A discussion on the results and contributions of the appended publications along with a critical reflection on the formulated research questions in Chapter 5 is followed by concluding remarks and an outlook in Chapter 6.

Chapter 2

Methodology

In the appended publications (Kaps et al., 2022, 2023, 2024), a multi-fidelity EGO technique is investigated and extended in the context of automotive crashworthiness and sheet metal forming applications. The novel contributions here include a modified initial DoE, a novel MF infill criterion, and the study of different LF models. Therefore, a detailed overview of the utilized optimization methods is given in this chapter. DoE as the essential first step in this surrogate-based technique is introduced in Section 2.1. The concept of EGO is summarized in Section 2.2 and its extensions to an MF context are presented in Section 2.3.

2.1 Design of experiments

The problem of optimally distributing a finite number of design samples in a (hyperrectangular) design space is addressed by DoE. It represents an essential first step in many modern computer-based techniques, such as surrogate modeling, sensitivity analysis, or population-based optimization. As such, it has been extensively investigated and covered in the literature (Forrester et al., 2008; Montgomery, 2020; Niederreiter, 1992; Pronzato and Müller, 2011; Saltelli et al., 2007; Santner et al., 2003). In the context of the present work, a novel modification of popular DoE methods adapted for surrogate-based optimization techniques is proposed (Komeilizadeh et al., 2022) and investigated in structural applications (see also Sections 4.1, 4.3 and Chapter 5). Therefore, an overview of important concepts in modern DoE is given in the following.

Originally, deterministic methods for physical experiments or studies were developed many decades ago (Fisher, 1936). These methods, such as full-factorial or Box-Behnken design (Box and Behnken, 1960), usually place design samples in a regular pattern with many samples at or close to the design space boundaries. The variation over the full range of each design variable is then estimated after running the experiments. This branch of DoE is called classical DoE and remains relevant until today in many areas of research (Montgomery, 2020). One major disadvantage of this type of method is that the number of required samples may grow exponentially with the number of design variables, and, for example, with Box-Behnken designs, the number of samples may not be specified arbitrarily.

The focus in modern DoE, which may sometimes be called the *design of computer experiments*, is more on uniformly distributing samples across the entire design space. To that end, several space-filling criteria have been introduced to assess the quality of a sample data set. They can be broadly categorized into distance-based and uniformity-based criteria (Garud et al., 2017). For the latter, so-called *discrepancy* measures are defined that quantify the difference between a given design and a uniform design. Various definitions have been proposed and discussed in the literature (Hickernell, 1998; Fang and Ma, 2001; Fang et al., 2002). However, these criteria are rarely used when generating an DoE in an application use case due to their high computational costs. Efforts have been made to make them more feasible (Jin et al., 2005). Distance-based criteria are also defined in numerous different ways (Garud et al., 2017; Komeilizadeh et al., 2022). Two of the most popular criteria, which are very common due to their low computational cost, are *PE (potential energy)* (Audze and Eglais, 1977) and *Maximin* (Johnson et al., 1990). The former, which is also used in OLHS (optimal Latin hypercube sampling) throughout the present work, is defined as

$$\Phi_{PE} = \sum_{i=1}^{N-1} \sum_{j=i+1}^{N} d(\boldsymbol{x}^{(i)}, \boldsymbol{x}^{(j)})^{-2}. \tag{2.1}$$

Here, N is the number of samples $\boldsymbol{x}^{(i)}$ in the sample set and $d(\boldsymbol{x}^{(i)}, \boldsymbol{x}^{(j)})$ represents the Euclidean distance between two sample points.

Two of the most widely used classes of DoE techniques, namely (Quasi) MC (Monte Carlo) sampling and LHS (Latin hypercube sampling), are summarized below. MC sampling itself is arguably the most simple DoE technique in which samples are drawn (pseudo-)randomly from the design space. However, since samples are almost never uniformly distributed when using this approach, more efficient methods named QMC (quasi-Monte Carlo) were developed (Niederreiter, 1992). The idea is to place samples based on low-discrepancy sequences of prime numbers, where low-discrepancy refers to the uniform space-filling property. Popular examples of the sequences include Hammersley (Hammersley and Handscomb, 1964), Halton (Halton, 1964) and Sobol (Sobol', 1967). Following their introduction, numerous improvements to these sequences and their initialization have been suggested over the years to remedy some of the common problems, such as clustering of samples or poor lower-dimensional projections (Braaten and Weller, 1979; Bratley and Fox, 1988; Joe and Kuo, 2008; Morokoff and Caflisch, 1994).

LHS is a space-filling DoE technique that extends upon the concept of Latin squares. A Latin hypercube design for N samples in d dimensions is constructed by first dividing each dimension into N bins of equal probability, for example, uniformly. Of the total N^d cells created, N are randomly selected such that each bin in each dimension only contains a single sample (McKay et al., 1979). Typically, samples are placed in the center of a cell. However, other

approaches such as random placement have been suggested (Rajabi et al., 2015). As initial designs may suffer from problems such as sample correlations, OLHS was introduced as a remedy. The basic idea is to optimize an initial LHS with respect to a space-filling criterion such as PE or Maximin. An early approach utilizing a simulated annealing (Bohachevsky et al., 1986) optimization algorithm was proposed by Morris and Mitchell (1995). Due to its good balance between simplicity and performance, this is also the approach employed in all publications included in the present work. However, several modifications and improvements have been suggested over the years (Husslage et al., 2011; Jin et al., 2005; Vořechovský and Novák, 2009; Ye, 1998; Ye et al., 2000). A more detailed overview of the developments around OLHS is given by Viana (2015).

During the work for the present thesis, a novel modification to these DoE methods was suggested and named IV (isovolumetric) sampling by our group (Komeilizadeh et al., 2022). Developed for surrogate modeling and surrogate-based optimization, it is based on two ideas. First, it is well known that as the number of dimensions increases, so does the share of volume close to the boundaries in a hypercube. Second, surrogate models generally perform significantly better at interpolating between existing samples than at extrapolating. Based on these two observations, the idea of IV sampling, specifically IV LHS is to redefine the bin boundaries and sizes in a way that samples are pushed closer to design space boundaries depending on the number of design space dimensions. Instead of bin boundaries $p_i = \frac{i}{N}$ and sizes $a_j = \frac{1}{N}$ for classic LHS and uniformly distributed variables, they are defined as

$$p_i = \begin{cases} 0.5\left(1 - \left(\frac{N_v+1-i}{N_v}\right)^{1/d}\right), & i \in [1, N_v] \\ 0.5\left(1 + \left(\frac{i-(N_v+1)}{N_v}\right)^{1/d}\right), & i \in (N_v, N+1] \end{cases}, \tag{2.2}$$

$$a_j = p_{j+1} - p_j,\ j \in [1, N]. \tag{2.3}$$

Here, $N_v = \frac{N}{2}$ is introduced for clarity of notation. To illustrate the resulting pattern, an exemplary OIVLH (optimal isovolumetric Latin hypercube) design of eight samples in two dimensions is shown together with an OLHS and a QMC sampling based on the Sobol sequence in Figure 2.1. The concept can be straightforwardly extended to arbitrary DoE techniques and applied there as an a posteriori transformation. More details on that, as well as a more in-depth discussion of the approach, can be found in the original publication (Komeilizadeh et al., 2022). The performance of IV sampling is investigated in multi-fidelity optimization problems related to automotive crashworthiness and sheet metal forming in the appended publications I (Kaps et al., 2022) and III (Kaps et al., 2024), respectively.

When investigating MF optimization methods, it seems reasonable to also explore the use of MF-DoE (multi-fidelity design of experiments) techniques. The basic idea is to create a DoE for all fidelity levels involved while considering the existence of other fidelity levels instead of

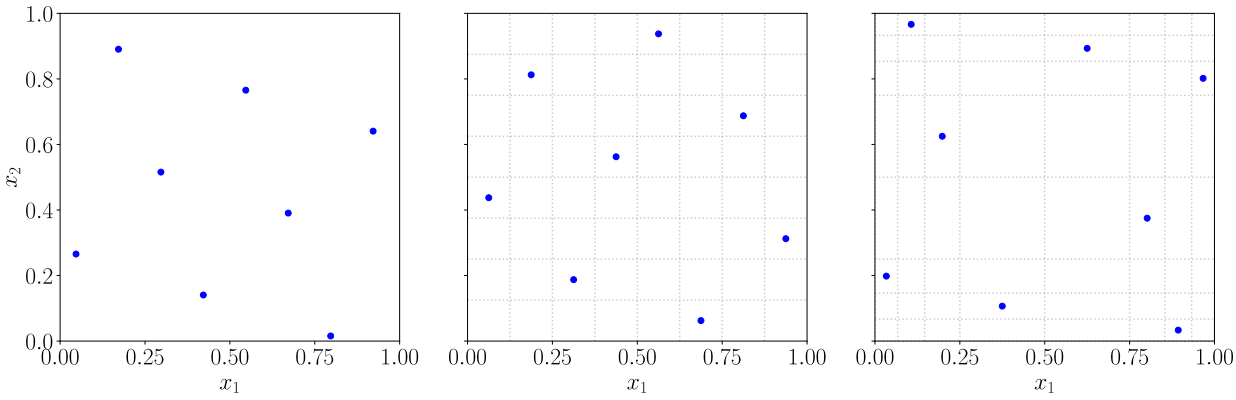

Figure 2.1 Exemplary design of experiments for eight samples in two dimensions. For both Latin hypercube methods, the bin boundaries are depicted as grey dotted lines. Left: Sobol' sampling; mid: optimal Latin hypercube sampling; right: optimal isovolumetric Latin hypercube sampling.

creating them separately for each individual fidelity level. Although it is not required for the methods used here, many MF techniques require that the HF (high-fidelity) sample set be a subset of the LF sample set. Various approaches have been suggested, for example, a nearest neighbor (Le Gratiet, 2013) or an exchange approach, Forrester et al. (2007). More information on the different available methods can also be found in one of the review articles covering the topic (Zhou et al., 2023; Fernández-Godino, 2023; Park et al., 2017). Within the present work, the use of MF-DoE techniques was only studied preliminarily within the scope of a Master's thesis (Wang (2022); see Appendix B for a summary). An in-depth assessment of the potential of MF-DoE in MF optimization remains open for future work.

2.2 Efficient global optimization

Surrogate-based optimization methods are commonly used when some form of expensive simulation is required to evaluate the objective function in a given optimization problem. In the most straightforward approach, the optimization is run completely on an initially fitted surrogate model, and the global optimum predicted by the surrogate model is then assumed to be the desired optimum of the objective function. However, this approach strongly depends on the quality of the surrogate model and may be very inefficient. Therefore, techniques have been developed that iteratively add design samples to the surrogate model, thus increasing model quality in promising areas of the design space. Throughout the present work, an optimization method called EGO that was originally proposed by Jones et al. (1998) and Schonlau et al. (1998) and its extensions to multi-fidelity are applied. It was originally inspired by and is sometimes used synonymously with BO (Bayesian optimization) (Močkus, 1975, 2012).

In the following, the general workflow of EGO is presented in Subsection 2.2.1. Subsequently, the underlying GP (Gaussian process) surrogate model and some available infill criteria for adaptive sampling are discussed in more detail in Subsections 2.2.2 and 2.2.3, respectively.

2.2.1 Introduction

When using adaptive surrogate-based optimization strategies, it is typically assumed that no additional information such as gradients is available for the objective function. That is, the objective function is treated as a black box. Other optimization techniques that take gradient information into account are available if this assumption is not valid (Kochenderfer and Wheeler, 2019; Rao, 2019). Recently, efforts have also been made to improve surrogate models with gradient information and thus make adaptive surrogate-based optimization methods more viable in these cases (Chen et al., 2020; Laurent et al., 2017).

The general workflow of EGO as an adaptive surrogate-based optimization algorithm is depicted in Figure 2.2. Initially, a sample data set $(\boldsymbol{S}, \boldsymbol{y}_S)$ consisting of input variable data $\boldsymbol{S} \in \mathbb{R}^{m \times d}$ and the corresponding objective function values $\boldsymbol{y}_S \in \mathbb{R}^m$ for m samples in a d-dimensional design space is constructed using DoE and then used to fit the initial GP model. The following steps are then repeated until a termination condition of the algorithm is reached. First, an infill criterion is optimized on the surrogate model to find the best design space location for a new adaptive sample. Second, the termination conditions of the algorithm are checked. Common conditions include a maximum number of adaptive iterations and a threshold value for the infill criterion, either absolute or relative to the magnitude of the objective function. The former criterion represents possible computation budget restrictions on the optimization, while the latter can be interpreted as convergence of the algorithm. Third, if the algorithm has not finished, the actual objective function value for the new adaptive sample is calculated and the sample is added to the sample data set. Finally, the surrogate model is refitted with the updated sample data set before a new infill criterion optimization begins.

Although adaptive surrogate-based optimization algorithms can be used with any surrogate model, EGO is defined with a GP surrogate model, which is sometimes also called kriging. This type of surrogate or variants of it are also utilized throughout the present work. The main reason for this is that GP surrogate models not only output a predicted response value, but also a predicted model variance, which can be interpreted as the prediction uncertainty. Two main search characteristics commonly required in black-box optimization techniques are exploration and exploitation. Exploration describes the search refinement in design space regions where little information on the objective is currently available. Exploitation refers to the improvement of model accuracy close to the best known samples. Using the prediction and variance output of GP models, infill criteria can be constructed that balance the exploration and exploitation behaviors of the algorithm. More details on infill criteria are discussed in Subsection 2.2.3.

In its most basic form, the optimization problem that is solved here can be formulated as

$$\min_{\boldsymbol{x}} \quad f(\boldsymbol{x}), \tag{2.4a}$$

$$\text{where } \underline{x}_i \leq x_i \leq \bar{x}_i, \;\; i \in [1,2,...,d]. \tag{2.4b}$$

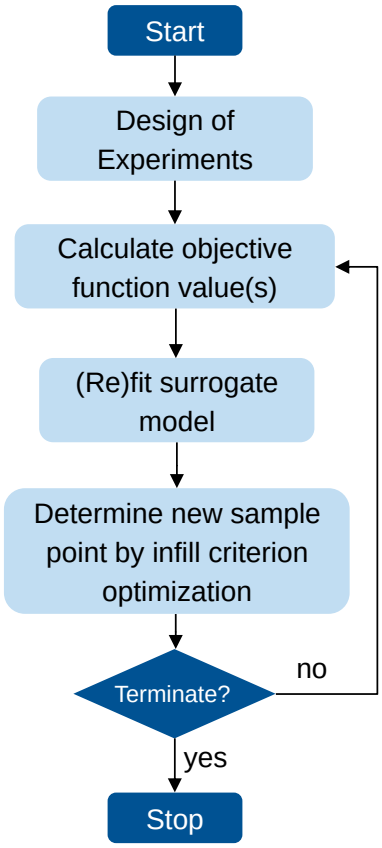

Figure 2.2 Schematic representation of the workflow in an adaptive surrogate-based optimization workflow.

Here, $\boldsymbol{x}$ is the vector of d design variables with entries x_i. $\underline{x}_i$ and $\bar{x}_i$ represent the lower and upper design space bounds of the i-th design variable, respectively. The objective function is denoted by $f(\boldsymbol{x})$. For analytical test problems, this may be a closed-form equation, while in structural optimization problems it involves multiple substeps. A typical workflow is described here, but details may vary, especially in a multi-fidelity context (see Section 2.3). First, the design variable values $\boldsymbol{x}$ have to be translated into an individual simulation model. Then, the simulation is performed, here typically an FEA. Subsequently, the results, e.g., the strain field of the component, are used to determine the objective function value.

In real-world applications of the optimization methods discussed in the following sections, additional aspects such as constraints, algorithm parallelization, multiple conflicting objectives, or input noise may become relevant (e.g., Keane and Nair (2005); Arsenyev (2017); Duddeck (2008); Koziel and Leifsson (2013); Antinori (2016)). These are not further considered throughout the present work because they can be integrated into an optimization in a modular way (Moustapha and Sudret, 2019) and due to the focus on algorithm aspects of the MF context here (see also Chapter 5).

2.2.2 Gaussian process surrogate

The concept of GP surrogate models was originally proposed in the geostatistics community by Krige (1951) and Matheron (1963), which is where the synonym *kriging* originates. It was later popularized for computer experiments in engineering design by Sacks et al. (1989) and has been widely used since.

Gaussian stochastic processes can be defined as a "collection of random variables, any finite number of which have a joint Gaussian distribution" (Rasmussen and Williams, 2005, p. 13). As such, they are conceptually a generalization of Gaussian random distributions to functions. A GP $Z(\boldsymbol{x})$ is fully defined by its mean $\mu(\boldsymbol{x})$ and covariance $C(\boldsymbol{x},\boldsymbol{x}')$ and is denoted as

$$Z(\boldsymbol{x}) \sim \mathcal{GP}\left(\mu(\boldsymbol{x}), C(\boldsymbol{x},\boldsymbol{x}')\right). \tag{2.5}$$

In the following, it is assumed that $\mu(\boldsymbol{x})$ is zero as is commonly done when working with GP surrogate models. The covariance is then denoted as

$$C(\boldsymbol{x},\boldsymbol{x}') = \sigma_z^2 R(\boldsymbol{x},\boldsymbol{x}'), \tag{2.6}$$

where σ_z^2 is the process variance and $R(\boldsymbol{x},\boldsymbol{x}')$ is a *correlation function* also called *kernel*. Throughout the present work, two of the most popular kernels, specifically the squared exponential kernel, also named the Gaussian RBF (radial basis function) kernel, and the Matérn kernel (Matérn, 1986) are used. They are defined as

$$R_{RBF}(\boldsymbol{x},\boldsymbol{x}') = \exp\left(-\frac{d^2}{\theta^2}\right), \tag{2.7}$$

$$R_{Matern}(\boldsymbol{x},\boldsymbol{x}') = \frac{2^{1-\nu}}{\Gamma(\nu)}\left(\frac{\sqrt{2\nu}d}{\theta}\right)^{\nu} K_\nu\left(\frac{\sqrt{2\nu}d}{\theta}\right), \tag{2.8}$$

where θ is the kernel hyperparameter, also called the *length scale*, $d = d(\boldsymbol{x},\boldsymbol{x}')$ is the Euclidean distance between the two design space locations, Γ is the gamma function and K_ν is the modified Bessel function of the second kind. ν is a separate parameter for the class of Matérn kernels that can be used to explicitly control the smoothness of the function. For $\nu \to \infty$, the two kernel functions above become identical. In the above equations, the hyperparameter θ is defined globally as a scalar. In this case, the correlation function is called *isotropic*. If greater flexibility with respect to different design variables is required, the correlation functions can also be defined to have individual hyperparameters for each design variable. They are then called *anisotropic*. More detailed derivations of kernel functions as well as an overview of numerous other functions that have been proposed can be found in the literature (Rasmussen and Williams, 2005; Duvenaud, 2014; Genton, 2002).

For the GP surrogate model, the actual unknown function $y = f(x)$ is represented by a GP as

$$Y(\boldsymbol{x}) = \mu(x) + Z(x), \tag{2.9}$$

Here, $\mu(x)$ is called the trend term and is assumed to be an unknown constant β_0. $Z(x)$ is a stationary GP, i.e., it is invariant with respect to translation. This property is fulfilled when the underlying GP has a constant mean, here it is zero, and a correlation function that depends only on the distance between samples as shown above. Given a correlation function as discussed above and a training data set $(\boldsymbol{S}, \boldsymbol{y}_S)$ as introduced in Subsection 2.2.1, this approach can be used to predict function values at unknown locations $\boldsymbol{x}^*$. The derivation shown here follows the one presented by Keane and Nair (2005). Numerous different approaches have been shown to essentially lead to the same predictor over the years (Sacks et al., 1989; Rasmussen and Williams, 2005; Forrester et al., 2008; Duvenaud, 2014). Based on the assumptions of a GP, the unknown output value y^* predicted here has a joint Gaussian distribution with the existing m samples $\boldsymbol{y}_S$. It can be written as

$$\begin{bmatrix} \boldsymbol{y}_S \\ y^* \end{bmatrix} \sim \mathcal{N}\left(\left[\beta_0 \mathbf{1}\right], \sigma_z^2 \begin{bmatrix} \boldsymbol{R} & \boldsymbol{r}(\boldsymbol{x}^*) \\ \boldsymbol{r}(\boldsymbol{x}^*)^T & R(\boldsymbol{x}^*, \boldsymbol{x}^*) \end{bmatrix} \right), \tag{2.10}$$

where $\mathbf{1} \in \mathbb{R}^{m+1}$ is a column vector filled with ones and $R(\bullet, \bullet)$ is a correlation function such as those defined in Equations (2.7) and (2.8). $\boldsymbol{r}(\bullet) = \left[R(\boldsymbol{x}^*, \boldsymbol{x}^{(1)}), R(\boldsymbol{x}^*, \boldsymbol{x}^{(2)}), ..., R(\boldsymbol{x}^*, \boldsymbol{x}^{(m)})\right] \in \mathbb{R}^m$ is a column vector representing the correlations between the existing sample points $\boldsymbol{x}^{(i)}$ and the new location $\boldsymbol{x}^*$. The matrix $\boldsymbol{R} \in \mathbb{R}^{m \times m}$ includes the correlation values between the existing sample points. Based on this distribution, the conditional distribution of y^* given $\boldsymbol{y}_S$ is given by

$$y^* | \boldsymbol{y}_S \sim \mathcal{N}\left(\beta_0 + \boldsymbol{r}^T(\boldsymbol{x}^*)\boldsymbol{R}^{-1}(\boldsymbol{y}_S - \beta_0 \mathbf{1}), \sigma_z^2\left(R(\boldsymbol{x}^*, \boldsymbol{x}^*) - \boldsymbol{r}(\boldsymbol{x}^*)^T \boldsymbol{R}^{-1} \boldsymbol{r}(\boldsymbol{x}^*)\right)\right). \tag{2.11}$$

The mean and variance of this distribution are exactly the surrogate model predictor $\hat{y}(\boldsymbol{x})$ and its MSE (mean squared error) for arbitrary design space locations that are then defined as

$$\hat{y}(\boldsymbol{x}) = \beta_0 + \boldsymbol{r}^T(\boldsymbol{x})\boldsymbol{R}^{-1}(\boldsymbol{y}_S - \beta_0 \mathbf{1}), \tag{2.12}$$

$$\sigma^2(\boldsymbol{x}) = MSE(\boldsymbol{x}) = \sigma_z^2\left(R(\boldsymbol{x}, \boldsymbol{x}) - \boldsymbol{r}(\boldsymbol{x})^T \boldsymbol{R}^{-1} \boldsymbol{r}(\boldsymbol{x})\right). \tag{2.13}$$

To be able to actually predict function values at new locations, the unknown parameters of the model, that is, the trend term β_0, the process variance σ_z^2, and the kernel length scale(s) θ, have to be determined. Typically, an approach of MLE (maximum likelihood estimation) is used to determine the set of parameters that most likely produced the sample data set. With

this approach, β_0 and σ_z^2 can be analytically determined as

$$\hat{\beta}_0 = \frac{\mathbf{1}^T \boldsymbol{R}^{-1} \boldsymbol{y}_S}{\mathbf{1}^T \boldsymbol{R}^{-1} \mathbf{1}}, \tag{2.14}$$

$$\sigma_z^2 = \frac{1}{m} (\boldsymbol{y}_S - \hat{\beta}_0 \mathbf{1})^T \boldsymbol{R}^{-1} (\boldsymbol{y}_S - \hat{\beta}_0 \mathbf{1}). \tag{2.15}$$

The MLE of the kernel length scale cannot be expressed analytically. Therefore, it must be determined by performing an internal optimization when fitting a GP surrogate model. Various strategies for this hyperparameter tuning have been discussed (Toal et al., 2008; Rasmussen and Williams, 2005; Butler et al., 2014). One of the most popular optimization algorithms due to the availability of gradient information from the MLE is the L-BFGS-B algorithm (Byrd et al., 1995) that is used in popular software implementations of GP surrogates such as *scikit-learn* in Python (Pedregosa et al., 2011).

It has to be noted here that the objective function and its underlying simulation model are treated as deterministic in the context of the derivation given above. Given the same set of input parameters, the results are assumed to be identical. Thus, the GP surrogate model introduced here is exactly interpolating existing design samples. While this is consistent with the generally deterministic nature of computer models, it may be problematic when considering, for example, real-world experiments. There are GP surrogate models available that allow for the regression of design samples instead of interpolation (Keane and Nair, 2005; Arsenyev, 2017; Forrester et al., 2008). Additionally, several authors (Sacks et al., 1989; Forrester et al., 2008; Gramacy and Lee, 2010; Ranjan et al., 2011) have suggested adding a small amount of Gaussian noise to the diagonal of the covariance matrix to improve the quality of the surrogate model and to avoid numerical problems due to ill-conditioning of the covariance matrix. This term, which is often called *nugget*, is also used throughout the present work.

2.2.3 Infill criteria

Following the fitting of an initial GP surrogate model, an infill criterion is used to iteratively determine new sampling locations to improve the surrogate model quality and find the function minimum. In the context of BO, infill criteria are also called acquisition functions. More in-depth reviews of available infill criteria are also available in literature (e.g., Jones (2001); Arsenyev (2017); Liu et al. (2017); Fuhg et al. (2020)).

Two of the most straightforward infill criteria are minimizing the surrogate predictor or maximizing the surrogate error. The former can be defined as $\boldsymbol{x}_{new} = \underset{x}{\operatorname{argmin}}(\hat{y}(\boldsymbol{x}))$ using the predictor from Equation (2.12). This criterion uses only exploitation and thus requires a globally accurate initial surrogate model to find the true optimum. Usually, the large initial DoE needed is not affordable for structural optimization problems, making this criterion somewhat impractical. The latter criterion is defined accordingly as $\boldsymbol{x}_{new} = \underset{x}{\operatorname{argmax}}(\sigma(\boldsymbol{x}))$. As it focuses solely on ex-

ploration and neglects exploitation, it is usually very inefficient. Additionally, the number of infill points required for an accurate global surrogate model grows exponentially with the number of design variables due to what is known as the curse of dimensionality. A criterion that can be considered a basic combination of the former two was proposed by Cox and John (1992) and named LCB (lower confidence bound). It is defined as $\boldsymbol{x}_{new} = \underset{x}{\operatorname{argmin}}(\hat{y}(\boldsymbol{x}) - b\sigma(\boldsymbol{x}))$ with a user-defined constant b. While this approach may remedy some of the major challenges with the previous criteria, it can also run into problems depending on the objective function as observed by Jones (2001).

To combine the concepts of exploration and exploitation in infill criteria in a more elaborate way, a measure called improvement is introduced using the currently best calculated objective function value y_{min} and can be written as

$$I(\boldsymbol{x}) = \max(y_{min} - Y(\boldsymbol{x}), 0). \tag{2.16}$$

The new sample points are then found by maximizing one of the following infill criteria. The PI (probability of improvement) criterion (originally proposed by Kushner (1964) for a one-dimensional problem) is defined as follows

$$P[I(\boldsymbol{x})] = \begin{cases} \Phi\left(\frac{y_{min} - \hat{y}(\boldsymbol{x})}{\sigma(\boldsymbol{x})}\right), & \text{if } \sigma(\boldsymbol{x}) > 0, \\ 0, & \text{if } \sigma(\boldsymbol{x}) = 0, \end{cases} \tag{2.17}$$

where $\Phi(\bullet)$ is the CDF (cumulative distribution function) of the standard normal distribution. As the name suggests, PI estimates the probability that a new sample brings an improvement over the best known sample.

Another very popular infill criterion that was formulated by Jones et al. (1998) for the EGO approach with early ideas dating back to Močkus (1975) is EI (expected improvement). It is defined as

$$EI(\boldsymbol{x}) = \begin{cases} (y_{min} - \hat{y}(\boldsymbol{x}))\Phi\left(\frac{y_{min} - \hat{y}(\boldsymbol{x})}{\sigma(\boldsymbol{x})}\right) + \sigma(\boldsymbol{x})\phi\left(\frac{y_{min} - \hat{y}(\boldsymbol{x})}{\sigma(\boldsymbol{x})}\right), & \text{if } \sigma(\boldsymbol{x}) > 0, \\ 0, & \text{if } \sigma(\boldsymbol{x}) = 0, \end{cases} \tag{2.18}$$

where $\Phi(\bullet)$ and $\phi(\bullet)$ are the CDF and PDF (probability density function) of the standard normal distribution. The first term in the sum reflects the exploitation of existing good values, as it is dominated by $(y_{min} - \hat{y}(\boldsymbol{x}))$ whereas the second term represents exploration of unknown regions in the design space because it is proportional to $\sigma(\boldsymbol{x})$. Contrary to PI, EI can quantify the amount of improvement expected from a new sample location and not just the probability of any improvement.

Over the years, several variations and extensions of the EI criterion have been proposed. Two of the first popular variants are *generalized EI* (Schonlau, 1997; Schonlau et al., 1998) and *weighted EI* (Sóbester et al., 2005) both of which aim to better tune the balance of exploration and exploitation during the optimization process. Other variants include handling design constraints (Parr et al., 2010; Sasena et al., 2002) and the ability to utilize simulation parallelism by adding multiple samples at once (Schonlau, 1997; Ponweiser et al., 2008; Ginsbourger et al., 2010). A more recent in-depth review of the developments around EI and its variants is given by Zhan and Xing (2020).

A second class of infill criteria, which is not technically used for optimization but is strongly inspired by the EGO method, is used for reliability analysis. Here, instead of minimizing the objective function, the aim is to improve the prediction quality along a limit state of the function (i.e. a given threshold value) to improve the predicted probability of failure. This methodology has been called active learning kriging or EGRA (efficient global reliability analysis) (Bichon et al., 2008). As this class of infill criteria is used in appended publication III (Kaps et al., 2024) to extend an optimization algorithm, two popular criteria are briefly introduced below. In reliability analysis, these criteria are commonly defined with respect to a failure constraint because the computation of the probability of failure is done with that constraint. Here, they are denoted with respect to the predictor of the objective function as introduced above in Equations (2.12) and (2.13) for consistency of notation.

First, the EFF (expected feasibility function) (Bichon et al., 2008) which is inspired by EI, can be defined as

$$\begin{aligned} EFF(\boldsymbol{x}) =& (\hat{y}(\boldsymbol{x}) - a)\left[2\Phi(\bar{u}) - \Phi\left(u^-\right) - \Phi\left(u^+\right)\right] \\ &- \sigma(\boldsymbol{x})\left[2\phi(\bar{u}) - \phi\left(u^-\right) - \phi\left(u^+\right)\right] \\ &+ \varepsilon\left[\Phi\left(u^+\right) - \Phi\left(u^-\right)\right], \\ \text{where} \qquad \bar{u} =& \frac{a - \hat{y}(\boldsymbol{x})}{\sigma(\boldsymbol{x})}, \\ u^+ =& \frac{(a+\varepsilon) - \hat{y}(\boldsymbol{x})}{\sigma(\boldsymbol{x})}, \\ u^- =& \frac{(a-\varepsilon) - \hat{y}(\boldsymbol{x})}{\sigma(\boldsymbol{x})}. \end{aligned} \tag{2.19}$$

Here, a represents the limit state value of the function at hand, commonly 0, and $\varepsilon = 2\sigma(\boldsymbol{x})$ is used to define a close region around a. Like EI, this function is maximized to determine a new sampling location. Due to the high similarity with EI, EFF is also capable of exploration and exploitation while improving the prediction quality of the limit state of a function.

The second criterion, which is called the U learning function, was initially proposed by Echard et al. (2011) and can be written as

$$U(\boldsymbol{x}) = \frac{|\hat{y}(\boldsymbol{x})|}{\sigma(\boldsymbol{x})}. \tag{2.20}$$

This function is minimized. To handle the case of $\sigma(\boldsymbol{x}) = 0$ for which the above definition is no longer valid, a large problem-dependent constant is defined to prevent that location from ever being chosen as a new adaptive sample. This is done because $\sigma(\boldsymbol{x}) = 0$ is mainly encountered when existing sample locations are evaluated. Contrary to EFF, the U learning function focuses more on sample locations close to the predicted limit state rather than exploring the design space (Echard et al., 2011).

Due to the highly multimodal nature of infill criteria in general and EI in particular, infill criterion optimization is in itself a challenging problem. Different techniques have been studied to optimize infill criteria (see, for example, Schonlau et al. (1998)). Throughout the present work, a DE (differential evolution) algorithm (Storn and Price, 1997) is used to optimize infill criteria. Although it is certainly not the most efficient algorithm in terms of the number of required function evaluations, it shows good performance and is readily available in popular software libraries such as *scikit-learn* in Python (Pedregosa et al., 2011). Also, the time spent in infill criterion optimization in the structural application problems studied here is in the order of magnitude of a fraction of one percent of the total optimization time.

2.3 Multi-fidelity optimization

The rapid increase in computational cost and complexity of simulation models may render even optimization algorithms specifically designed for expensive black box functions, such as EGO infeasible. As a potential remedy, multi-fidelity methods were introduced many years ago. Their main idea is to complement the accurate but expensive simulation model, which is then called the HF model, with a cheaper but also less accurate, so-called LF, model. Both of these models are then used, for example, in an adaptive surrogate-based optimization algorithm, to gain a benefit either in result quality or in computational cost over a classical SF technique. Most MF optimization algorithms and surrogate models, including all the approaches introduced in the following, allow the use of an arbitrary number of fidelity levels by design. In the present work and in most published research works, problems are limited to the *bi-fidelity* case with two levels of fidelity for the purpose of practicability. Recently, there have also been a few works in which three or more levels of fidelity were utilized (Fischer, 2021; Baheri, 2023). It should be noted here that the classical EGO method introduced in Section 2.2 above can be classified as an MF method with the GP surrogate as the LF model and the simulation model as the HF model (see, for example, Peherstorfer et al. (2018)). In the context of the present work, the term *multi-fidelity* is used with respect to the input models of the optimization algorithm. Therefore, the classical EGO method is referred to here as an SF method. This has the additional benefit of making the distinction between EGO and its multi-fidelity variants explored in the present work significantly easier.

The general workflow of a multi-fidelity adaptive surrogate-based optimization is the same as that shown in Figure 2.2 for the SF case. The primary difference is that each individual step gains some complexity due to the existence of LF and HF models. For example, this requires either the generation of two separate DoEs or the use of an MF-DoE technique. As discussed in Section 2.1, the former is done in the appended publications (Kaps et al., 2022, 2023, 2024) while some early investigations of the latter were performed within the scope of a Master's thesis (Wang (2022); see Appendix B for a summary) based on previously published methods. A review of available MF surrogate models that are an essential component of this type of optimization algorithm is given in Subsection 2.3.1 below. This also includes a discussion on the choice of LF model depending on the application problem (compare appended publication I (Kaps et al., 2022)). Finally, an overview of different multi-fidelity infill criteria is given in Subsection 2.3.2.

2.3.1 Multi-fidelity surrogate models

MF surrogate models can be broadly categorized into hierarchical and non-hierarchical approaches (Zhou et al., 2023). The latter generally refers to all cases where some of the models involved on the input side cannot be hierarchically ordered, such as when a single HF model is combined with multiple LF models. This category is not considered further in the present work. For hierarchical MF surrogate models, it is generally assumed that the LF and HF models can be clearly identified and that the LF model is cheaper to evaluate and less accurate than the HF model. The general idea of hierarchical surrogate models is then to use a high number of LF evaluations to capture the general trend in the response function, and then to use a lower number of HF evaluations to correct the LF predictions. Below, the term *hierarchical* is skipped when discussing MF surrogates but it is implied unless explicitly stated otherwise.

Another aspect of the classification of MF surrogate models is with respect to how the models of the different fidelities are combined to generate the MF model. Different taxonomies for categorizing approaches that may be similar and somewhat overlapping have been suggested. Peherstorfer et al. (2018) suggest three categories named *adaptation*, *fusion* and *filtering*, which are used for uncertainty propagation, surrogate modeling, and optimization methods. Two separate groups named *multi-fidelity surrogate modeling* and *multi-fidelity hierarchical modeling* are proposed by Fernández-Godino (2023) whereby the first is comparable to the *fusion* category and the second integrates *adaptation* and *filtering* from Peherstorfer et al. (2018). Another division that has been suggested for MF surrogate models (Zhou et al., 2023) makes a distinction between *scaling-function-based methods*, *space-mapping-based methods* and *cokriging methods*. Because the focus in the present work lies on surrogate modeling, the latter classification is used as an orientation below when discussing different types of MF surrogate models. It should be mentioned that regardless of how the methods are categorized, hybrid methods and combinations of methods from different categories are possible.

In the following, a brief discussion of different options for the definition of the LF model is followed by a more in-depth overview of the different available MF surrogate models. Subsequently, cokriging and HK are introduced in more detail.

Throughout the appended publications (Kaps et al., 2022, 2023, 2024), HK is used as the MF surrogate model. Reasons for this choice are discussed at the end of this section after introducing HK and cokriging. The latter is introduced in detail here to illustrate the differences between the two models and because it was studied in the scope of a Master's thesis (Krivacic (2023); see Appendix B for a summary) during the present research work.

Choice of low-fidelity model

The definition of the LF model is an essential part of MF surrogate modeling, although it is generally independent of the choice of surrogate model. LF models can be assigned to one of three categories, *simplified models*, *projection-based methods*, and *data-fit models* (Peherstorfer et al., 2018). The last two have been subsumed into the term *surrogate models* by Fernández-Godino (2023). Both works also list various publications that use LF models from the different categories.

The first category, *simplified models*, refers to the simplification of the simulation model which in structural applications is typically an FEA. Typical simplifications that can be integrated include a coarser mesh, a larger time step size, or the linearization of nonlinear phenomena. This type of LF is applied in the appended publications II and III (Kaps et al., 2023, 2024) and used as a reference in appended publication I (Kaps et al., 2022). It is also the type of LF model most commonly used in literature.

The second category, *projection-based methods*, refers to the use of MOR (model order reduction) techniques to project an HF simulation model into a lower-dimensional subspace that is significantly less expensive to evaluate but still captures the essential phenomena of the model. Depending on the knowledge required about the problem structure, the MOR methods are classified as *intrusive* or *non-intrusive*, where the latter is essentially a data-driven approach and the former requires knowledge of the problem structure (e.g., the stiffness matrix). A review of the developments around non-intrusive methods is given by Yu et al. (2019). While methods were initially developed for linear(ized) problems (compare, for example, the review by Benner et al. (2015)), MOR methods have only recently been extended to nonlinear problems (Rutzmoser, 2018; Guo and Hesthaven, 2018; Swischuk et al., 2019) and in particular to automotive crashworthiness (Bach et al., 2019b,a; Kneifl et al., 2021; Czech et al., 2022). In the appended publication I (Kaps et al., 2022) a non-intrusive ROM (reduced order model) obtained by using an incremental SVD (singular value decomposition) (Baker et al., 2012) is studied as an LF model in two MF crash problems.

The last category, *data-fit models*, refers to surrogate models that are fitted directly from existing DoE data from the HF model. Some methods available for surrogate modeling in general include polynomial regression, k-nearest neighbor regression, GP surrogate models / kriging, and support vector regression. For more details on available surrogate modeling techniques, readers are referred to one of the textbooks on the topic (Forrester et al., 2008) or popular software libraries such as *scikit-learn* in Python (Pedregosa et al., 2011) that include numerous different techniques.

Types of multi-fidelity models

One of the first MF surrogate models was proposed in the early 1990s (Haftka, 1991). In it, the author proposes to model the HF predictor through a multiplicative correction factor applied to the LF surrogate model. The approach was then successfully applied, for example, to aerospace structures or composite design (McQuade et al., 1992; Chang et al., 1993; Mason et al., 1998; Balabanov et al., 1998). A variation using an additive correction factor was introduced a few years later (Balabanov et al., 1998; Lewis and Nash, 2000). Gano et al. (2005) proposed a hybrid scaling approach that combines additive and multiplicative scaling factors. Although some modifications have been proposed from the methods originally developed, these techniques have been widely and successfully applied in different fields of application (see, for example, Viana et al. (2014); Peherstorfer et al. (2018); Zhou et al. (2023) for an overview).

Space-mapping methods were originally proposed by Bandler et al. (1994). The idea here is to project the input parameter space of the HF model onto the parameter space of the LF model while keeping the output characteristics of the two models similar. This allows the LF and HF models to have a different number of input dimensions. Although this class of methods is less prevalent in structural design optimization, it has been widely used in electromagnetic optimization, and various review articles documenting its development and popularization are available (Bandler et al., 2004; Koziel et al., 2008; Rayas-Sanchez, 2016).

Cokriging-type surrogate models represent an MF extension to the kriging or GP surrogate model. Originating from the geostatistics community (Journel and Huijbregts, 1978) the cokriging technique was popularized for computer experiments by Kennedy and O'Hagan (2000). The general idea is to combine the available sample data from the LF and HF models by modeling their combined covariance matrix. Although its mathematical formulation is somewhat different, HK (Han and Görtz, 2012), which is used throughout the present work, is conceptually very similar to cokriging as it also represents an MF extension of kriging. Both cokriging and HK are discussed in more detail in separate sections below.

Cokriging

The presentation of cokriging in the present work loosely follows the one given by Forrester et al. (2007), which is very close to the model originally proposed by Kennedy and O'Hagan

(2000). As with many multi-fidelity models, it is assumed that there are two sample data sets $(\boldsymbol{S}_{LF}, \boldsymbol{y}_{S,LF})$ and $(\boldsymbol{S}_{HF}, \boldsymbol{y}_{S,HF})$ consisting of m_{LF} and m samples available for LF and HF models, respectively. For cokriging, it is commonly assumed that the HF sample data set is a subset of the LF set with respect to the sample input locations. The reason for this assumption is discussed below. The cokriging model is then built using the following Gaussian processes

$$Y(\boldsymbol{x}) = Z_{HF}(\boldsymbol{x}) = \rho Z_{LF}(\boldsymbol{x}) + Z_d(\boldsymbol{x}), \tag{2.21}$$

where $Z_{LF}(\boldsymbol{x})$ and $Z_{HF}(\boldsymbol{x})$ are Gaussian processes representing the LF and HF model, respectively. ρ denotes an unknown scaling factor, and $Z_d(\boldsymbol{x})$ is a Gaussian process representing the difference between the scaled LF model $\rho Z_{LF}(\boldsymbol{x})$ and the HF model $Z_{HF}(\boldsymbol{x})$. To obtain the difference model, the two sample sets are merged as follows

$$\boldsymbol{S} = \begin{pmatrix} \boldsymbol{S}_{LF} \\ \boldsymbol{S}_{HF} \end{pmatrix} = \left[\boldsymbol{x}_{LF}^{(1)}, \boldsymbol{x}_{LF}^{(2)}, ..., \boldsymbol{x}_{LF}^{(m_{LF})}, \boldsymbol{x}_{HF}^{(1)}, \boldsymbol{x}_{HF}^{(2)}, ..., \boldsymbol{x}_{MF}^{(m)} \right]^T \tag{2.22}$$

$$\boldsymbol{y}_S = \begin{pmatrix} \boldsymbol{y}_{S,LF} \\ \boldsymbol{y}_{S,HF} \end{pmatrix} = \left[y_{LF}^{(1)}, y_{LF}^{(2)}, ..., y_{LF}^{(m_{LF})}, y_{HF}^{(1)}, y_{HF}^{(2)}, ..., y_{HF}^{(m)} \right]^T. \tag{2.23}$$

Thus, the structure of the covariance matrix of the difference model $Z_d(\boldsymbol{x})$ is different from that in standard GP surrogate models (compare Equation (2.6)). It can be written as

$$\boldsymbol{C} = \begin{pmatrix} \sigma_{Z_{LF}}^2 \boldsymbol{R}_{LF}(\boldsymbol{S}_{LF}, \boldsymbol{S}_{LF}) & \rho \sigma_{Z_{LF}}^2 \boldsymbol{R}_{LF}(\boldsymbol{S}_{LF}, \boldsymbol{S}_{HF}) \\ \rho \sigma_{Z_{LF}}^2 \boldsymbol{R}_{LF}(\boldsymbol{S}_{HF}, \boldsymbol{S}_{LF}) & \rho^2 \sigma_{Z_{LF}}^2 \boldsymbol{R}_{LF}(\boldsymbol{S}_{HF}, \boldsymbol{S}_{HF}) + \sigma_d^2 \boldsymbol{R}_d(\boldsymbol{S}_{HF}, \boldsymbol{S}_{HF}) \end{pmatrix} \in \mathbb{R}^{(m_{LF}+m)\times(m_{LF}+m)}, \tag{2.24}$$

where $\sigma_{Z_{LF}}$ and σ_d are the process variances of the LF and difference GPs, respectively. $\boldsymbol{R}(\boldsymbol{X}, \boldsymbol{X}')$ represents the correlation function evaluated on the input sample data sets $\boldsymbol{X}$ and $\boldsymbol{X}'$. Subscripts are added to these terms to illustrate that the correlation function can be defined independently for the two GPs.

The model is fitted using MLE as for the SF case, whereby the LF model can be fitted as described in Subsection 2.2.2. For the difference model, the MLE of process mean and variance can be determined as

$$\hat{y}_d = \frac{\boldsymbol{1}^T \boldsymbol{R}_d(\boldsymbol{S}_{HF}, \boldsymbol{S}_{HF})^{-1} \boldsymbol{d}}{\boldsymbol{1}^T \boldsymbol{R}_d(\boldsymbol{S}_{HF}, \boldsymbol{S}_{HF})^{-1} \boldsymbol{1}}, \tag{2.25}$$

$$\sigma_z^2 = \frac{1}{m} (\boldsymbol{d} - \hat{y}_d \boldsymbol{1})^T \boldsymbol{R}_d(\boldsymbol{S}_{HF}, \boldsymbol{S}_{HF})^{-1} (\boldsymbol{d} - \hat{y}_d \boldsymbol{1}). \tag{2.26}$$

Here, $\boldsymbol{d} = \boldsymbol{y}_{HF} - \rho \boldsymbol{y}_{LF}(X_{HF})$ contains the LF function values at the HF sample locations and therefore illustrates why it is helpful for cokriging if the HF sample data set is a subset of the LF set. As for SF kriging, the correlation function hyperparameters cannot be determined analytically and must be found through internal optimization. Furthermore, the scaling parameter ρ is also found by maximizing an MLE.

Over the years, various modifications to cokriging have been suggested. Among others, a scaling factor ρ that can vary across the design space was proposed (Qian and Wu, 2008), Han et al. (2012) introduced a different approach to construct the covariance matrix and a recursive formulation of cokriging that is computationally more efficient than the original formulation was proposed by Le Gratiet (2013) and Le Gratiet and Garnier (2014).

Hierarchical kriging

HK is an MF extension to kriging that was originally proposed by Han and Görtz (2012). While the model is introduced here for two levels of fidelity, it can be readily extended to more levels as was shown by the authors in the original publication. As before, it is assumed that two sampling data sets $(\boldsymbol{S}_{LF}, \boldsymbol{y}_{S,LF})$ and $(\boldsymbol{S}_{HF}, \boldsymbol{y}_{S,HF})$ evaluated using the low- and high-fidelity models, respectively, are available. The first step is then to fit a normal kriging model (see Subsection 2.2.2) to the LF data set. The result is the LF predictor $\hat{y}_{LF}(\boldsymbol{x})$ as defined in Equation (2.12). To obtain the HK predictor, the following random process is considered

$$Y(\boldsymbol{x}) = \beta_0 \hat{y}_{LF}(\boldsymbol{x}) + Z(\boldsymbol{x}), \tag{2.27}$$

where the LF predictor scaled by an unknown factor β_0 represents the trend term and $Z(\boldsymbol{x})$ is a stationary random process with zero mean and a covariance matrix of the same structure as introduced for the normal GP surrogate model in Equation (2.6). The HK predictor can then be written as

$$\hat{y}(\boldsymbol{x}) = \beta_0 \hat{y}_{LF}(\boldsymbol{x}) + \boldsymbol{r}^T(\boldsymbol{x}) \boldsymbol{R}^{-1} (\boldsymbol{y}_{S,HF} - \beta_0 \boldsymbol{F}) \tag{2.28}$$

Here, $\boldsymbol{F} = \left[\hat{y}_{LF}(\boldsymbol{x}^{(1)}), \hat{y}_{LF}(\boldsymbol{x}^{(2)}), ..., \hat{y}_{LF}(\boldsymbol{x}^{(m)})\right]^T$ is the LF prediction on the HF sample locations $\boldsymbol{x}^{(i)} \in \boldsymbol{S}$, $\boldsymbol{r}(\boldsymbol{x})$ and $\boldsymbol{R}$ are the correlations between the new point and the existing points and the correlations between the existing points, respectively (compare Equation (2.10)). β_0 is identified as a scalar factor that indicates the correlation between the LF and HF models. It is determined together with the process variance σ_z through an MLE approach analogous to the one applied in classical SF kriging (compare Subsection 2.2.2) to be

$$\hat{\beta}_0 = (\boldsymbol{F}^T \boldsymbol{R}^{-1} \boldsymbol{F})^{-1} \boldsymbol{F}^T \boldsymbol{R}^{-1} \boldsymbol{y}_{S,HF}, \tag{2.29}$$

$$\hat{\sigma}_z = \frac{1}{m} (\boldsymbol{y}_{S,HF} - \hat{\beta}_0 \boldsymbol{F})^T \boldsymbol{R}^{-1} (\boldsymbol{y}_{S,HF} - \hat{\beta}_0 \boldsymbol{F}). \tag{2.30}$$

As with SF kriging models, the MLE for the correlation function hyperparameter(s) cannot be analytically expressed and an internal optimization must be performed when fitting the model.

The MSE of the HK prediction is then defined as

$$\sigma^2_{HK}(\boldsymbol{x}) = MSE_{HK}(\boldsymbol{x}) = \sigma_z^2 (1 - \boldsymbol{r}^T(\boldsymbol{x}) \boldsymbol{R}^{-1} \boldsymbol{r}(\boldsymbol{x}) + \left[\boldsymbol{r}^T(\boldsymbol{x}) \boldsymbol{R}^{-1} \boldsymbol{F} - \hat{y}_{LF}(\boldsymbol{x})\right]^2 \left(\boldsymbol{F}^T \boldsymbol{R}^{-1} \boldsymbol{F}\right)^{-1}). \tag{2.31}$$

The derivation of HK is not shown in full detail here, as it is very similar to the one presented for the classical kriging model (see Subsection 2.2.2) but it can be found in the original publication (Han and Görtz, 2012).

It should be noted that the only terms in Equations (2.28) and (2.31) that depend on the new design space location $\boldsymbol{x}$ are $\boldsymbol{r}(\boldsymbol{x})$ and $\hat{y}_{LF}(\boldsymbol{x})$. Therefore, all other terms and products can be precalculated at model fitting time to increase the efficiency of the HK predictor.

When comparing cokriging with HK there are two main reasons why HK is used in the appended publications (Kaps et al., 2022, 2023, 2024) of the present work. First, cokriging in its original formulation is more expensive to compute because of the larger covariance matrix and has additional assumptions, e.g., regarding the input sample data sets. These points have been somewhat alleviated by the modifications suggested by Le Gratiet (2013) and Le Gratiet and Garnier (2014). The second and arguably more important point is that HK can provide more reasonable estimates of the prediction uncertainty compared to cokriging (Han and Görtz, 2012; Zhou et al., 2023). This is beneficial for the multi-fidelity infill criteria used in optimization problems which are introduced below (see Subsection 2.3.2). More discussions on the optimization performance and the various influence parameters on MF surrogate models can be found in Chapter 5.

2.3.2 Multi-fidelity infill criteria

When considering MF surrogate-based optimization techniques, there are generally two options available with respect to the infill criterion. First, an SF infill criterion (see Subsection 2.2.3) can be applied after the initial MF surrogate model is fitted to iteratively add samples to the data set. That way, the newly added samples can only come from one fidelity level, typically HF, and it has to be decided before the start of optimization which fidelity level it is. As this restricts the MF context to the initial surrogate modeling only and not the optimization itself, it could be argued, depending on exact definitions, that this should not even be called MF optimization. Therefore, it is not further considered in the following. The second option involves the use of MF infill criteria, which determine not only the location of a new design sample but also the fidelity level. Typically, these criteria are extensions of popular SF criteria that can also distinguish different fidelity levels. In the following, an overview of some MF infill criteria is presented, including the ones used in the appended publications.

One of the first MF infill criteria is based on the original EI function and was named AEI (augmented expected improvement) in the original publication (Huang et al., 2006). It is defined as

$$EI_a(\boldsymbol{x}, L) = EI(\boldsymbol{x}, 1)\alpha_1(\boldsymbol{x}, L)\alpha_2(L), \tag{2.32}$$

where $L \in \{0, 1\}$ represents the fidelity level whereby 0 for LF and 1 for HF are used throughout the present work. $EI(\boldsymbol{x}, 1)$ therefore represents the EI criterion (see Equation (2.18)) calculated

at the highest fidelity level. The correction factor $\alpha_1(\boldsymbol{x}, L)$ models the reduction in improvement of the HF model when an LF sample is added. In the original publication, it is defined as the correlation between LF and HF surrogate models. Here, $\alpha_2(L)$ denotes the cost per evaluation relative to an HF evaluation, that is, $\alpha_2(1) = 1$. A third scaling factor that is introduced in the original publication to account for random errors in the model output is skipped here because the models are assumed to be deterministic in the present work. In its original form, AEI works best when combined with a cokriging surrogate model because the model already includes the correlation needed for the α_1 factor. A modified formulation for α_1 that also works for other surrogate models has been proposed (Reisenthel and Allen, 2014). The AEI criterion is slightly modified by Di Fiore et al. (2021) to include another correction factor that allows the inclusion of engineering knowledge about the design space into the adaptive sampling.

Another MF extension to EI that is somewhat different from AEI is called VFEI (Zhang et al., 2018a). It can be written in a similar form to EI (compare Equation (2.18)) as

$$EI_{vf}(\boldsymbol{x}, L) = \begin{cases} (y_{min} - \hat{y}(\boldsymbol{x}))\Phi\left(\frac{y_{min} - \hat{y}(\boldsymbol{x})}{\sigma_{vf}(\boldsymbol{x}, L)}\right) + \sigma_{vf}(\boldsymbol{x}, L)\phi\left(\frac{y_{min} - \hat{y}(\boldsymbol{x})}{\sigma_{vf}(\boldsymbol{x}, L)}\right), & \text{if } \sigma_{vf}(\boldsymbol{x}, L) > 0, \\ 0, & \text{if } \sigma(\boldsymbol{x}, L) = 0. \end{cases} \tag{2.33}$$

The primary difference to the EI lies in the prediction uncertainty $\sigma_{vf}(\boldsymbol{x}, L)$ that is defined depending on the fidelity level here. It is used to model the expected improvement in the HF function through a new LF sample point and is defined using the correction factor β_0 in the HK model as

$$\sigma_{vf}(\boldsymbol{x}, L) = \begin{cases} \beta_0^2 \cdot \sigma_{LF}(\boldsymbol{x}), & L = 0, \\ \sigma_{HK}(\boldsymbol{x}), & L = 1, \end{cases} \tag{2.34}$$

with $\sigma_{LF}(\boldsymbol{x})$ the prediction uncertainty of the LF kriging model and $\sigma_{HK}(\boldsymbol{x})$ the HK prediction uncertainty (see Equation (2.31)). This criterion is used in all the appended publications (Kaps et al., 2022, 2023, 2024) as it was designed for use with HK surrogate models and was found to work well. Additionally, it does not require external or empirical parameters to be specified prior to optimization.

Similarly to EI, MF extensions have also been suggested for other popular infill criteria. LCB has been extended in two different ways with both approaches named *variable-fidelity LCB* in the original publications (Jiang et al., 2019; Ribeiro et al., 2023). Extensions to PI are named *extended PI* (Ruan et al., 2020) and *variable-fidelity PI* (Ribeiro et al., 2023). For both criteria, the former MF extensions suggested by Jiang et al. (2019) and Ruan et al. (2020) are somewhat inspired by the AEI extension to EI, whereas the latter ones by Ribeiro et al. (2023) are inspired by the VFEI extension to EI.

In recent years, MF extensions have also been suggested to the infill criteria used for reliability analysis. An MF variant of EFF that appears to be conceptually inspired by the AEI criterion

was named *augmented EFF* (Yi et al., 2020). The original EFF is combined with a new information gain criterion to determine the fidelity level of new samples by Chaudhuri et al. (2021). A modified MF approach called *collective learning function* that is somewhat independent of the specific infill criterion is proposed by Zhang et al. (2022). The U learning function was first applied in an MF setting by Dhulipala et al. (2022) with cokriging surrogate models as a basis. In appended publication III (Kaps et al., 2024), a novel MF extension to the U learning function is proposed and combined with VFEI in a two-stage optimization approach to improve optimization performance in a deep-drawing application problem. The novel MF U learning function is defined as

$$U_{MF}(\boldsymbol{x}, L) = \frac{|\hat{y}(\boldsymbol{x})|}{\sigma_{vf}(\boldsymbol{x}, L)}, \tag{2.35}$$

with the prediction uncertainty as defined in Equation (2.34).

As discussed for the SF infill criteria in Subsection 2.2.3 above, DE is also used for MF infill criteria optimization throughout the present work.

Chapter 3

Applications

MF optimization techniques are developed for and studied in two fields of structural design in the appended publications, automotive crashworthiness and deep drawing. In the following sections, the most relevant aspects of the respective fields are outlined. Additionally, an overview of recent research by others on structural optimization methods in these applications is presented to contextualize the contributions of the appended publications, which are summarized in Chapter 4 and further discussed in Chapter 5. While the applications are very different with respect to the processes and objectives, the relevant mechanical phenomena are similar between the two. Both crashworthiness assessment and sheet metal forming are transient dynamics problems usually solved using explicit FEAand are driven by highly nonlinear deformations, contacts as well as plastic material behavior. These two applications are therefore chosen over other structural problems due to their highly challenging nature and to ensure reliability of findings.

Automotive crashworthiness, which is studied in appended publication I (Kaps et al., 2022) is covered in Section 3.1. In Section 3.2, an overview of sheet metal forming, or more specifically, deep drawing, which is the structural application in appended publications II and III (Kaps et al., 2023, 2024) is given.

3.1 Automotive crashworthiness

The study of crashworthiness dates back many decades. While the following overview is about road vehicles, the underlying mechanics in crash scenarios are obviously similar for other types of vehicles such as trains, ships or aircraft. For automotive crashworthiness, the development process of new components, and thus the setup of optimization problems, are typically driven by two sets of requirements. First, there are legal regulations such as the UN-ECE (United Nations Economic Commission for Europe) in the EU (European Union) or the FMVSS (Federal Motor Vehicle Safety Standard) in the USA (United States of America) which are mandatory for any new model. Second, consumer test programs such as Euro NCAP (New Car Assessment Programme) in the EU and NCAP in the USA may define additional tests going beyond the legal requirements. These test programs were established worldwide

starting in the late 1970s to improve road vehicle safety. Deriving from these regulations, a number of different categories of scenarios that have to be considered in the development process can be identified. Popular examples include frontal impact, side impact, or vulnerable road user protection. The number of different scenarios, the sometimes conflicting requirements especially when considering manufacturing costs, and the fact that all these regulations vary slightly between different countries makes the development of a globally sold car model a highly complex process.

Early overview works from the 1970s and 1980s focus mainly on analytical description of the involved mechanics, experimental results and early numerical simulations, e.g. Johnson and Mamalis (1978); Pifko and Winter (1981); Jones and Wierzbicki (1983); Davies and Morton (1984). Some of the key mechanics phenomena in an automotive crash setting are highly nonlinear deformations, plastic material behavior, (self-)contact and strain-rate dependent material characteristics due to the small timescales involved. With the rapid increase in available computational power, numerical simulations increased in popularity. One of the earliest studies of optimization algorithms in a crashworthiness application was published in 1996 (Etman et al., 1996). Here, the authors use a sequential linear programming technique to optimize a restraint system in a frontal impact. The development in the following years is best summarized by some of the earlier comparative and overview works on both the method side (Fang et al., 2005; Forsberg and Nilsson, 2006) and the industrial application side (e.g., Duddeck (2008)). A more recent review work (Fang et al., 2016) illustrates the variety of approaches in structural crashworthiness. This extends to both the initial question of how to define the optimization problem and how to quantify the crashworthiness of a component, as well as the optimization methodology.

Arguably the most-used components for crashworthiness studies are so-called crashboxes. These, in their most classical form, hollow rectangular metal tubes are part of the frontal load paths of a vehicle. In a frontal impact, a crashbox is crushed to absorb the kinetic energy of the vehicle and protect the passenger cell of the vehicle. In the past years, variants of crashboxes with different shapes, materials, or fillings, such as foam, have been extensively studied (compare Fang et al. (2016); Abdullah et al. (2020); Yao et al. (2023)). An exemplary crashbox as it is studied in appended publication I (Kaps et al., 2022) is depicted in Figure 3.1, where the component would be crushed from the top left.

When optimizing a component, such as a crashbox for its crashworthiness, there are numerous different metrics that have been used both in literature and in industrial applications of optimization. They may be included as objective functions or as constraints. One obvious example that can usually not stand without either other objective functions or constraints is the component mass (see also the first application example in appended publication I (Kaps et al., 2022)). The remaining measures can be divided into two categories, injury-based and

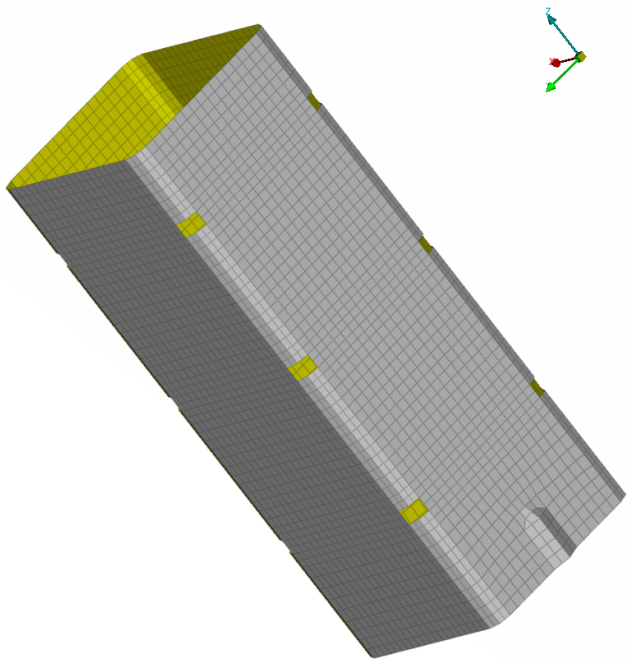

Figure 3.1 Exemplary crashbox geometry (adapted from Kaps et al. (2022)). The removed corner elements are used in the original publication to initiate folds during the crushing of the component.

energy-based criteria (Fang et al., 2016). For the former, three of the simplest criteria are the peak acceleration, the peak crash force, and the intrusion into the occupant compartment of the vehicle, as they are correlated with a high risk of injury for vehicle occupants. Other metrics, such as the head injury criterion, which is also assessed by regulatory and consumer tests, are derived from biomechanical observation with respect to injury mechanisms in the human body. Energy-based metrics are focused on the energy absorption characteristics of the component or system under investigation. One of the most straightforward criteria is to maximize the *energy absorption* of the investigated part(s). This measure can be a bit misleading though, as the total energy absorption at least on component level is typically equal to the kinetic energy in the system prior to impact. To ameliorate this potential shortcoming, *specific energy absorption* can be used, whereby the total energy absorption is divided by the component mass. Another popular metric considers the force displacement curve of, for example, a crashbox. It is also desirable with respect to vehicle occupants if this curve is as uniform as possible. Two reciprocal measures that have been defined here are the *load uniformity* which is defined as the mean crushing force divided by the maximum crushing force and its inverse the *crash load efficiency*. The former is used in the second application example in appended publication I (Kaps et al., 2022).

Relatively few works have been published on the use of MF optimization techniques in the context of crashworthiness. In one of the first works, a hybrid scaling factor approach (see Subsection 2.3.1) is combined with particle swarm optimization (Eberhart and Kennedy, 1995) to optimize the specific energy absorption of a honeycomb structure (Sun et al., 2010a). A

bumper system under frontal impact was studied by Acar et al. (2020) utilizing a very similar surrogate modeling technique (Zhang et al., 2018b) in combination with a genetic algorithm for optimization. An MF technique for the crashworthiness discipline within a multidisciplinary optimization was studied by Anselma et al. (2020). More recently, an extension to cokriging (Perdikaris et al., 2017) was combined with DE for global search and a trust region approach for local fine-tuning to optimize a crashbox bumper problem (Lualdi et al., 2023). As part of the present dissertation, two crash examples are studied in appended publication I (Kaps et al., 2022) in the context of an MF optimization scheme. The contributions of the publication are summarized in Section 4.1 and discussed in more detail in Chapter 5.

Another relevant aspect of MF techniques is the choice of LF model (compare Subsection 2.3.2). Some overviews of LF modeling techniques in crash scenarios have been given in literature (Lange et al., 2018; Noorsumar et al., 2021). In the works on MF optimization in crashworthiness, simplified simulation models are utilized as LF models in most publications (Sun et al., 2010a; Acar et al., 2020; Lualdi et al., 2023). This type of LF model is compared with a non-intrusive MOR approach in appended publication I (Kaps et al., 2022). An analytical formulation is used as an LF model by Anselma et al. (2020).

3.2 Deep drawing

Deep drawing is one of the most popular metal forming processes and has been used for many decades. As such, it has been widely covered in textbooks, e.g. Banabic (2010); Tschaetsch (2006); Siegert (2015), and review articles are published rather regularly such as by Tiwari et al. (2022); Takalkar and Chinnapandi (2018). In the following, an overview of the deep drawing process in general is given. Initially, the individual process steps are introduced to motivate the subsequent overview of different measures of drawability some of which are also studied in appended publication II (Kaps et al., 2023). Finally, the existing literature on optimization with deep drawing problems and, in particular, MF optimization is summarized.

A typical deep drawing setup consists of several components, for example, blank, die, punch, and blankholder. The components along with the most relevant process steps are shown in Figure 3.2. Initially, the blank is placed in between the die and the blankholder. The drawing process then begins with the blankholder holding the blank in the place with a predefined force, the so-called BHF (blankholder force), and the punch moving into contact with the blank. As the punch moves further downward, the blank is plastically deformed into its shape. The required material originates either from a thickness reduction in the blank, technically called *stretch forming*, or by material flowing in from the outside, which is called *deep drawing* and is thus where the name of the process originates. So-called *drawbeads* may be added to the blankholder and die to control the flow of material into the component more accurately. Once

the punch reaches its final position, it moves back out. This, in combination with the removal of the blank holder, leads to an elastic springback in the component.

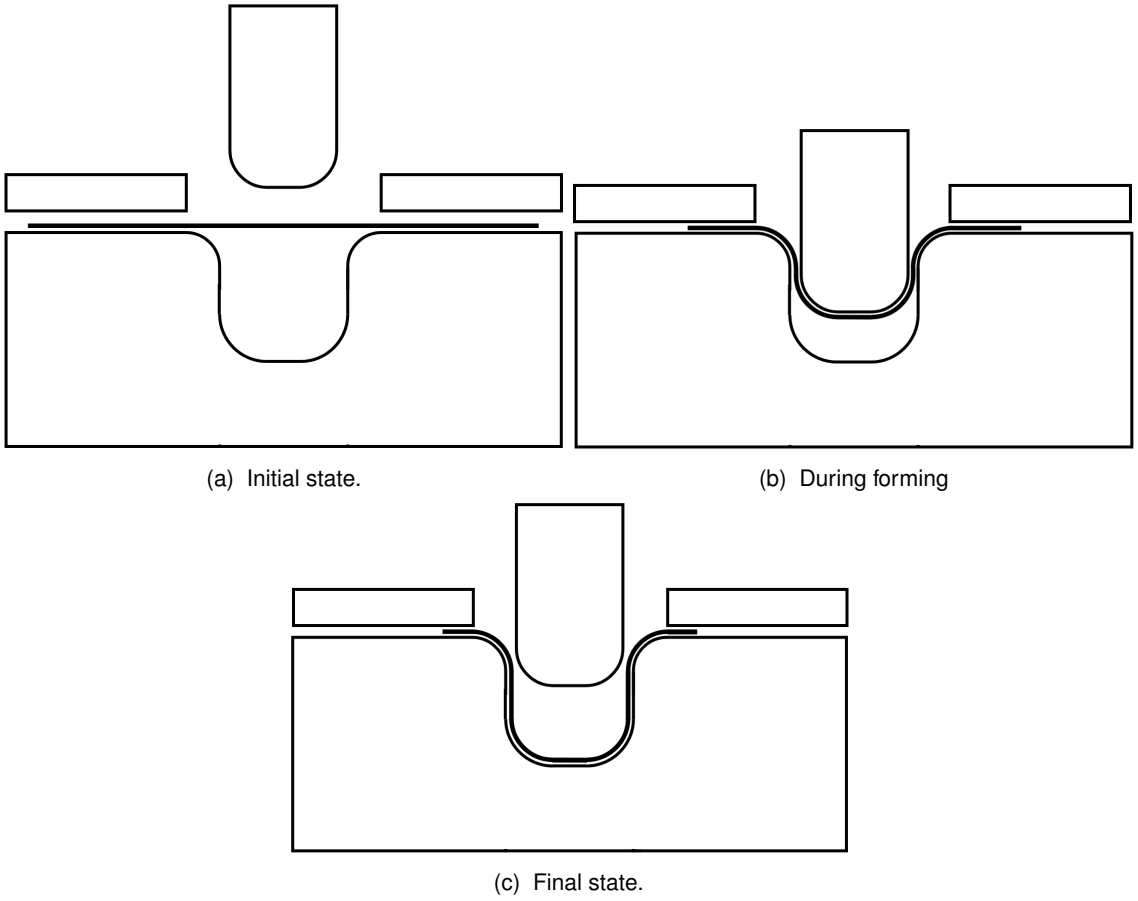

(a) Initial state. (b) During forming

(c) Final state.

Figure 3.2 Schematic of a deep drawing process. Initially (top left), the blank is placed on the die before it is fixed by the blankholder while the punch is brought in contact with the blank. The punch then deforms the blank into the desired shape (top right) and moves back up (bottom).

One of the major challenges in the product development cycle directly related to the deep drawing process is to ensure as early as possible in the development process that the component is drawable. The drawability of an exemplary deep-drawn component is used as an application problem in appended publications II and III (Kaps et al., 2023, 2024). As is commonly done for problems of formability, the elastic springback at the end of the process is not considered further in the following. Although it is highly relevant for manufacturing a geometrically accurate part, it is not relevant in the consideration of drawability.

Two of the major phenomena in limiting the drawability of a component are fracture and wrinkling. Both can be visualized in an FLD (forming limit diagram) which was originally introduced (then without the wrinkling component) in the 1960s (Goodwin, 1968; Keeler, 1968). An exemplary FLD is shown in Figure 3.3. Each dot represents an element in the simulation model. The red and pink lines are the FLC (forming limit curve) and WLC (wrinkling limit curve), respectively, which mark the limits of fracture and wrinkling as the name suggests. The black

line shows the limit of principal strain definitions, that is $\varepsilon_1 \geq \varepsilon_2$. Cracked and wrinkled elements are colored accordingly in the figure. Due to their widespread use, the determination of FLCs has also been standardized for example internationally in ISO 12004-2 (ISO, 2021). Many modifications and improvements have been suggested for FLD to address some of the limitations in the original concept, such as the assumption of linear strain paths for each element (for example, Stoughton and Zhu (2004); Volk and Suh (2013)). This assumption may be somewhat reasonable for components manufactured in a single step of drawing such as the cross-die investigated in appended publications II and III (Kaps et al., 2023, 2024). In industrial applications, where there are commonly multiple drawing steps with other processing steps in between, it does not hold. Other developments and influencing factors in FLDs have been reviewed fairly regularly in literature (Obermeyer and Majlessi, 1998; Stoughton and Zhu, 2004; Paul, 2013, 2021).

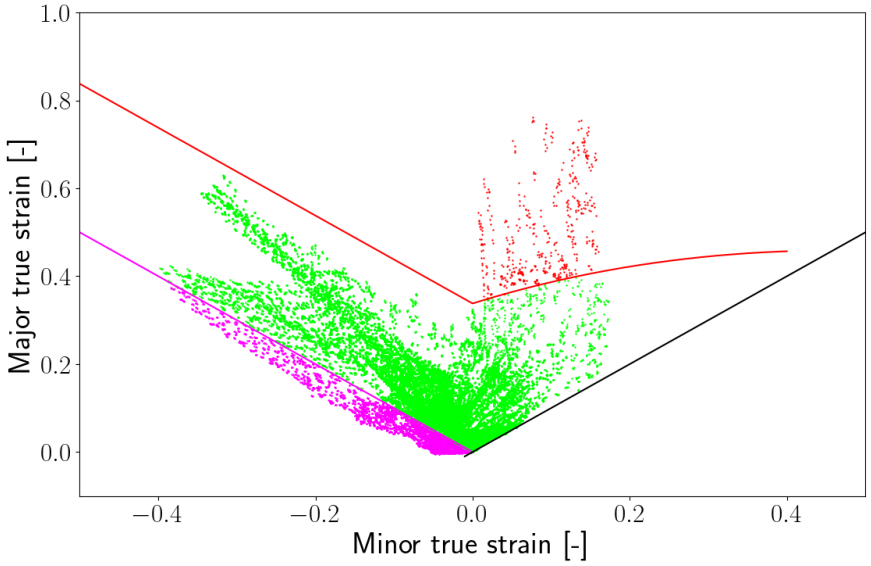

Figure 3.3 Exemplary forming limit diagram. Each dot represents an element in the simulation model. The black line represents the strain definition limit, that is $\varepsilon_1 \geq \varepsilon_2$. The red and purple lines represent the FLC and WLC, respectively. (Kaps et al., 2024)

There are many ways to simulate the deep drawing process as described above (compare, for example, Ablat and Qattawi (2016)). Two particular approaches are described further here, because they are used both in previous MF optimization literature and in appended publications II and III (Kaps et al., 2023, 2024). First, an incremental explicit simulation can be used, whereby the process and the involved components are modeled. Due to the involved nonlinearities in contact, deformations, and material models as well as the required mesh resolution, these simulations may be very expensive to run for real-world components. The second option is to use an inverse approach, where the final component geometry and deformation theory are used to derive stresses, strains, and thickness in the final component (Guo et al., 1990; Lee and Huh, 1997; Guo et al., 2000). Other components and effects, such as blankholder,

drawbeads, or friction, are not directly included in the simulation model here and are commonly modeled by equivalent restraining forces to increase the accuracy of the model.

Optimization techniques have been studied for deep drawing problems since the 1990s. Some overviews of different works have been published (for example, Wifi et al. (2007); Andrade-Campos et al. (2022)). When running an optimization, the definition of drawability measures as an objective function is an essential part of the process. In literature, different quantities have been used for optimizing the drawability of deep-drawn components. A very common definition involves the average of either the thinning over the drawing process or thickness variation in the final component (Ohata et al., 1998; Guo et al., 2000; Padmanabhan et al., 2007; Sattari et al., 2007; Manoochehri and Kolahan, 2014). These definitions are somewhat closely related to strain-based FLDs but do not make direct use of them. The FLD was first used by Naceur et al. (2004) in the definition of an objective function. Here, the authors define the objective as the sum of vertical distances of all failed elements to the FLC. The definition was extended to the wrinkling elements by Chengzhi et al. (2004). Later, it was applied in a very similar form (Sun et al., 2010b). The measure was extended to drawable elements by our group (Lehrer et al., 2023) to decrease mesh dependency and avoid potential numerical issues during optimization and surrogate modeling. A separate, partially FLD-based objective function was introduced by Jakumeit et al. (2005), where the number of cracked and wrinkled elements is combined with two other criteria in the process design of two academic deep drawing problems. Other objective functions such as the minimization of earing (Kishor and Kumar, 2002), the minimization of trimmed material (Hino et al., 2006), or a user-defined combination of failure mechanisms (Gantar et al., 2005) have been proposed. Three different measures of drawability based on average thinning and the two FLD-based functions are applied in an MF context and compared with each other in appended publication II (Kaps et al., 2023).

Similar to automotive crashworthiness, relatively few works using MF optimization in the context of deep drawing have been published. Space mapping techniques are one of the first MF surrogate modeling methods that were applied to deep drawing problems (Jansson et al., 2005; Hu et al., 2007). Another approach for a deep drawing blank design problem was proposed by Hino et al. (2006). The authors combine a finer and coarser mesh for HF and LF models, respectively, in a scaling factor approach and use a multipoint approximation method for optimization to illustrate a benefit over an SF optimization. Another scaling factor approach combining a moving least squares regression model with particle swarm optimization is used for the optimization of drawbead holding forces by Sun et al. (2010b). The authors later expanded the study to other surrogate models such as kriging and support vector regression using an artificial bee colony algorithm (Sun et al., 2012). An inverse one-step simulation model is used as an LF model and an explicit incremental simulation as an HF model in both publications. The same model combination for the two fidelity levels is utilized in appended

publications II and III (Kaps et al., 2023, 2024). The contributions of all appended publications are summarized in Chapter 4 and discussed together with the results in Chapter 5.

Chapter 4

Summary of appended publications

In the following, the appended publications are summarized and contributions to the research context outlined. The contributions of all individual authors are listed. The full length papers can be found in Appendix A. A more detailed discussion of the results and contributions of the papers is given in Chapter 5 below.

4.1 Publication I

As previously illustrated, MF optimization schemes have gained popularity in recent years and have also sometimes been applied to automotive crashworthiness problems. In the appended publication, an HK surrogate model is combined with the VFEI infill criterion as the basic MF technique. The novelty of this publication lies in the two modifications that are proposed to the optimization scheme. First, the IV sampling, or more specifically OIVLH, (compare Section 2.1 and Komeilizadeh et al. (2022)) is applied as the first step of an optimization for the first time. Second, instead of the very commonly used simplified simulation model, a projection-based non-intrusive MOR technique is proposed to simplify the LF model generation.

The proposed techniques are assessed on two application problems from automotive crashworthiness. One is a size optimization problem for a simplified side sill under lateral impact, and the other is a shape optimization problem for the triggers of a crashbox under frontal impact. The MF techniques are compared with a baseline SF EGO method. All optimizations are repeated ten times to ensure the reliability of the assessments.

For the lateral impact example, it is found that both tested methods SF, the baseline, and a version with OIVLH as the initial DoE method, reliably converge to the same optimum, which is therefore considered the global optimum. While the basic MF technique also finds this optimum in some repetitions, results are a little more inconsistent. Here, the proposed modifications individually and especially combined improve result quality to the point, that the technique with both modifications yields essentially the same results as the SF methods. The findings for the second application example are essentially the same except that results vary considerably more throughout, which is presumably caused by a more nonlinear objective function used

here. It is observed that all MF approaches save between 35% and about 55% in optimization time across both examples, whereby higher savings are observed for the novel modifications individually and especially combined.

Contributions of Authors

- Arne Kaps
  Conceptualization, Methodology, Software, Investigation, Writing - original draft, Writing - review and editing
- Catharina Czech
  Methodology, Writing - original draft, Writing - review and editing
- Fabian Duddeck
  Writing - review and editing, Supervision

4.2 Publication II

Previous publications on MF optimization in the context of drawability of deep-drawn parts so far have been using either space mapping or scaling factor type techniques for the surrogate model (see also Section 3.2). Therefore, the contributions of this appended publication are twofold. First, it represents one of the first times that an EGO-type MF optimization technique based on an HK surrogate model and the VFEI infill criterion is applied to a drawability optimization problem. Second, from the application side it appears to be one of the first publications, where different drawability measures are compared to each other on the same optimization problem.

Investigations in this publication are performed on a cross-die geometry that is also applied by Lehrer et al. (2023) in a metamodeling context. Three different drawability measures are selected for comparison, which include the share of bad elements in the FLD, the average violation of bad elements in the FLD and the average thickness reduction in the blank over the drawing process (compare also the overview given in Section 3.2). A total of six design variables including the initial sheet thickness, die radius, a form of drawing depth, the BHF as well as a friction coefficient and the Lankford coefficient are chosen.

The results of this study depend significantly on the objective function which illustrates the need for careful selection when using optimization techniques. The first function that uses the share of bad elements in FLD is found not to be well-suited for optimizing the drawability of the component. The best explanation is the limited influence of design variables on the objective function. The other two objective functions show the potential of the MF technique. For the distance-based FLD function, MF optimization requires significantly less computation time with comparable result quality. For the average thickness reduction function, the MF

technique even outperforms the reference SF approach while also needing more computation time.

Contributions of Authors

- Arne Kaps
  Conceptualization, Methodology, Software, Formal analysis and investigation, Writing - original draft, Writing - review and editing
- Tobias Lehrer
  Software, Writing - review and editing
- Ingolf Lepenies
  Software, Writing - review and editing
- Marcus Wagner
  Writing - review and editing, Supervision
- Fabian Duddeck
  Writing - review and editing, Supervision

4.3 Publication III

In appended publication III, a novel two-stage MF optimization approach is proposed and evaluated on the same cross-die deep drawing part that is also used in appended publication II. The novel approach is inspired by a previous publication (Pei et al., 2023) that introduces a similar approach for a reliability-based optimization example in an SF setting. The key idea is to perform a global enrichment phase between the initial DoE and the iterative infill criterion optimizations. The enrichment phase uses a different infill criterion from reliability analysis (see also the overview given in Subsection 2.2.3) to improve the surrogate model quality around a certain limit state. In the case of the drawability optimization used in this publication, the limit state is clearly defined as the drawability limit but other (arbitrary) definitions could be used. To facilitate the enrichment phase inside an MF optimization, a novel MF extension to the popular U learning function is proposed here. In addition, the OIVLH sampling strategy that was already successfully applied in appended publication I is investigated here as another modification to the optimization technique.

The application example in this publication is very similar to the one in appended publication II, except that fewer design variables are used and two noise variables, the material yield strength and the static friction coefficient, are defined to illustrate the simplicity of extending the proposed methodology to a context of optimization under uncertainty. As an objective function, the extension of the FLD-based average violation distance measure proposed by Lehrer et al. (2023) is utilized. Compared to the distance-based function studied in appended

publication II, this function can distinguish drawable components from each other but is the same for non-drawable components.

The optimization results show that the novel two-stage approach reduces the computation time by between 12% and 33% at minor impact on result quality compared to a classic single-stage method. The combination of the two-stage approach with the IV sampling is found to reduce the computation times by about 64% with also minor impact on result quality compared to the SF reference. Overall, the results again highlight the potential of MF techniques in structural optimization problems. Additionally, it is illustrated in this publication how the proposed two-stage approach can be used to consider input uncertainties in the optimization process.

Contributions of Authors

- Arne Kaps
  Conceptualization, Methodology, Software, Formal analysis and investigation, Writing - original draft, Writing - review and editing
- Tobias Lehrer
  Software, Writing - review and editing
- Ingolf Lepenies
  Software, Writing - review and editing
- Marcus Wagner
  Writing - review and editing, Supervision
- Ser Tong Quek
  Writing - review and editing, Supervision
- Fabian Duddeck
  Writing - review and editing, Supervision

Chapter 5

Discussion of contributions

In the following, the contributions of the appended publications (Kaps et al., 2022, 2023, 2024) that are summarized in Chapter 4 are discussed in more detail and the results are compared to previous works in the literature. Furthermore, it is assessed how the appended publications contribute to answering the research questions formulated in Chapter 1. Therefore, the publications are first discussed individually before a wider context is given. The limitations and remaining open questions of the present work and possible opportunities for future work are presented along with them.

5.1 Publication I

In appended publication I (Kaps et al., 2022), the novelty is twofold with an investigation of the modified DoE method named OIVLH and the integration of a non-intrusive ROM as LF into the MF optimization scheme. Additionally, it represents the first time that a surrogate model based on HK is combined with VFEI for MF optimization in this application. Both modifications are investigated using two application examples from the field of automotive crashworthiness. The first two research questions related to the benefit of the MF technique (compare Chapter 1) can be answered in this case. All four MF optimization techniques provide a computation time benefit that is approximately consistent between both application examples, while also maintaining the result quality at an acceptable level compared to the SF baseline. The observed computation time reductions for the baseline MF scheme match well with values previously reported in the literature for the same field of application (e.g., Acar et al. (2020)) as well as in the publication originally proposing the VFEI infill criterion (Zhang et al., 2018a). The findings are more differentiated with respect to the algorithm and LF model modifications investigated here (compare Questions 3 and 6 formulated in Chapter 1).

The OIVLH sampling alone has a limited impact in terms of optimization run time, which is reduced by a maximum of 14% for one method but remains similar for the others and even increases by about 10% in one case (the MF baseline for the lateral impact example) compared to OLHS. Interestingly, the use of OIVLH in MF techniques appears to improve the consistency of the results between repetitions of the same method. The likely reason is that OIVLH focuses

sampling on the design space boundaries where the optimum is found in both application examples. Therefore, it likely provides a higher initial surrogate model quality in the relevant regions of the design space, leading to slightly more consistent results compared to OLHS. In the present work, the same DoE method is used on both fidelity levels. One potential for future work is to use different methods for the fidelity levels, e.g., OIVLH for the HF model and OLHS for the LF model, or to use an MF-DoE technique in the first place. In particular, the latter approach has not been adapted in application examples in the literature even though various different MF-DoE methods have been proposed (compare Section 2.1).

The use of a non-intrusive ROM as LF model is found to have a similar effect in that it slightly reduces average optimization run times with little impact on the result. A slight improvement in the consistency of the results is observed compared to the use of a simplified simulation model as LF model. These findings are attributed to the higher model quality of the non-intrusive ROM (compare Tables 2 and 3 in Kaps et al. (2022)) and the higher simulation speed compared to the simplified simulation model. For the latter, the ROM achieves a speed-up factor of about 50 to 150 across the application examples as opposed to about four to six for the reference LF model compared to the HF model, respectively. The speed-up factor of the ROM appears to be low in the present study compared to what has been reported in the literature where values in the (ten)thousands are found (e.g., Le Guennec et al. (2018); Czech et al. (2022)). The best explanation is the comparatively small size of the application examples in the present study, where even the HF model is computed in less than ten minutes. A potentially interesting question for future research is regarding the quality of the ROM. In the version of the optimization algorithm proposed in the appended publication, the ROM is calculated on the initial DoE of the HF model and then used as LF model for the remainder of the iterative improvement phase of the optimization. At the same time, more HF evaluations are available as more adaptive samples are added. For future work, it appears very reasonable to try to update the ROM with each new HF data point that becomes available. That way, the quality of the LF model should increase as the optimization progresses and potentially bring further performance improvements compared to the technique shown in the appended publication.

5.2 Publication II

As previously summarized, the novelties in appended publication II (Kaps et al., 2023) are twofold. On the one hand, it is the first publication using an MF extension of EGO with a cokriging-type surrogate model, specifically HK, in the context of drawability optimization of deep-drawn components. On the other hand, it is one of the first works comparing different drawability measures in optimizations. The three objective functions are chosen here for their intuitiveness in the sense of comprehensibility by a human and their use in previous works on drawability optimization of deep-drawn components (compare Sections 3.2 and 4.2). The find-

ings in this publication vary significantly between the different objective functions and therefore illustrate the importance of careful consideration when setting up an optimization problem.

The first objective function, which is based on the share of cracked and wrinkled elements in the FLD is found to not be suitable for optimization. The results vary significantly between repetitions of the same technique and there is almost no real objective function improvement in the iterative phase of the optimization. These findings are attributed to the fact that the influence of design variables on the objective function values is potentially limited because the objective function cannot quantify the degree of violation for individual elements. Interestingly, a similar objective function that was previously used in the literature (Jakumeit et al., 2005) produced reasonable results for two different deep drawing examples. The best explanation is that the authors defined the objective function consisting of four components of which the first two are the shares of the cracked and wrinkled elements used as the first objective function in the appended publication. The remaining two consider springback and thinning. A variant of the thinning factor is chosen as the third objective function in the appended publication and found to work well. Details are discussed below.

The second objective function uses the average Euclidean distance of all 'bad' elements to their respective limit curve. Results for this function are very similar to the ones in appended publication I discussed above. The MF technique produces results that are slightly less consistent but of essentially the same quality as the HF reference but does so in about 46% less run time. These results fit into what was previously reported for MF techniques in literature although other authors have reported even greater time savings for the MF approach than what is found here, e.g. a factor of about four (Hu et al., 2007), about six (Jansson et al., 2005) or even about ten (Hino et al., 2006). As a caveat, it should be noted that in all the previous publications, it appears that the respective optimizations were only run once and not repeated. Therefore, it is assumed that there is some variation to these numbers.

Interestingly, the focus in other previous works on MF optimization for drawability of deep-drawn components is less on a reduction in optimization run time and more on an improvement of the obtained results (Sun et al., 2010b, 2012). For example, it is reported by Sun et al. (2012) that the optimization time remains roughly unchanged while the result quality improves. This is also the observation made for the third objective function in appended publication II, which is the average thinning in the blank over the drawing process. It is found here that the MF approach both improves result quality and finds the better optimum more consistently than the SF reference. At the same time, the MF technique actually takes on average about 31% longer here to terminate. Although this behavior does not seem excessively unusual in the context of other publications, it is the only example in the scope of the present work where the MF technique takes longer and improves results compared to the SF reference. While some reasonable assumptions for the reasons for this phenomenon are discussed in the appended

publication (Kaps et al., 2023), an in-depth analysis that could include an exploratory landscape analysis of the objective function goes beyond the scope of the publication and remains open for future work.

5.3 Publication III

The focus in appended publication III lies on proposing a novel two-stage MF optimization technique for a very similar optimization problem to the one applied in appended publication II. Additionally, the OIVLH sampling method that was shown to be promising in appended publication I is assessed here. The idea is to add an adaptive enrichment phase after the initial DoE to improve the surrogate model prior to the following global optimization. Specifically, the surrogate model is sampled around the drawability limit using a newly proposed infill criterion which is an MF extension to the U learning function which is popular in reliability analysis. It is found that the two-stage approach and particularly the IV sampling bring a benefit to the MF optimization technique and in the best case speeds optimizations up by a factor of almost three. This makes the observed benefits again fall in the same order of magnitude as in previous appended publications and literature as discussed above. This appended publication therefore contributes to the state of research and to answering the previously formulated research questions (see Chapter 1) in two ways. First, it illustrates the potential for improvement in optimization performance by changing the architecture of the algorithm similarly to what was suggested by Pei et al. (2023) in an SF optimization of a different application problem. The global enrichment phase increases the resolution of the surrogate model around the drawability limit. Therefore, the actual adaptive improvement phase of the algorithm using VFEI has a smaller region of the design space to search for the desired optimum and the algorithm converges faster. Second, the novel two-stage approach represents the first step towards fully integrating input parameter uncertainties into the MF optimization. MF reliability analyses which are the inspiration for the novel infill criterion proposed here, have been applied in literature in recent years (for example, by Chakroborty et al. (2023); Chaudhuri et al. (2021); Dhulipala et al. (2022); Yi et al. (2020)). However, the full integration into an optimization remains open, particularly in challenging structural applications. One example could be to use the drawability measure defined here as a failure constraint and define a different objective function for the optimization. Similarly, a more in-depth investigation into the MF extension to the U learning function which is inspired by the VFEI extension to EI remains open for future work.

5.4 Synthesis

Having discussed and contextualized the individual contributions of the appended publications, there are a few points of discussion that apply to two or all three appended publications. All these are discussed in the following.

The use of multiple levels of fidelity in the input simulation models introduces several additional hyperparameters compared to a 'classical' SF optimization. Especially in the initial DoE step and the surrogate modeling these can play a significant role. Two of the most relevant ones are the cost ratio between the HF and LF models as well as the quality of the LF simulation model, for example, in the form of the correlation between the LF and HF objective functions. The latter is usually not known a priori so it can generally not be considered in the optimization setup. However, MF surrogate models and infill criteria usually model the covariance between the fidelity levels, for example using the covariance matrix (compare Subsection 2.3.1). The cost ratio is directly included in some infill criteria such as AEI to balance the addition of LF and HF samples. The influence of both the cost ratio and the correlation between fidelity levels on optimization performance has also been studied in literature (Ruan et al., 2020). In that work, the authors find that the performance of different infill criteria varies and, for example, VFEI appears to perform better with weak correlations between the LF and HF models. The influence of these quantities adds to the need to report, for example, the cost ratio of the different models for better contextualization of results. This point of reporting for MF surrogate modeling is also discussed in more details in the review work by Fernández-Godino (2023).

Another part of this lies in the sensible definition of the initial DoE size and the distribution of samples to the LF and HF models. In the appended publications, the common rule of thumb $10d$ with d the number of design space dimensions which was established by Jones et al. (1998); Loeppky et al. (2009) is used to determine the DoE size for the SF reference optimization. For the MF methods, the approximately same computation budget as for the SF methods is distributed somewhat evenly between the LF and HF levels to determine the initial DoE size. When comparing MF methods, the same initial DoE size is used. Different ways of distributing samples between the fidelity levels were studied via a Master's thesis (Wang (2022); see Appendix B for a summary) in the context of MF-DoE methods. The findings are transferable to the cases studied in the appended publications. They illustrate the need to balance the LF and HF samples in the initial DoE, as too many LF or HF samples lead to a deterioration in both surrogate model quality and optimization performance. This is particularly the case, when a priori information on the quality of the LF model is not available.

The choice of LF model is another essential aspect of the MF optimization process. Two of the three LF model categories proposed by Peherstorfer et al. (2018) and summarized in Subsection 2.3.1 are utilized in the appended publications. Even though the non-intrusive ROM that is

integrated into the optimization in appended publication I, contains a surrogate model on the projected space, it is counted here as a projection-based LF model. The category of *data-fit models* is not investigated in the present work as the optimization itself is already surrogate-based. Therefore, using a surrogate model as the LF model appears somewhat redundant. Nevertheless, it should be mentioned that *data-fit models* are potentially the type of LF model with the lowest computation time required, maybe comparable with *projection-based models* depending on the specific methods used. There is however also a second reason, that only *simplified models* and *projection-based models* are investigated here and that is explainability. Both of these types of models allow for a full reconstruction of, for example, the displacement field in the component. The calculated objective function values can therefore be checked for numerical or other errors if that is deemed necessary. *Data-fit models* do not inherently provide this option. While *simplified models* are currently the most widespread approach used in literature for the applications considered here (compare Chapter 3) the author believes that *projection-based models* have great potential as already discussed with the results of appended publication I.

An added benefit of using the ROM as an LF model is that it removes the need to create a simplified simulation model, which in practical applications may not be needed elsewhere. Steps like remeshing, particularly of more complex geometries, are usually not only time-intensive but also require some form of human interaction. Using an intrusive ROM can lead to very good model predictions with very few training simulations, as the model follows the underlying physical laws. On the other hand, intrusive ROMs require access to the source code of the finite element solver and the speed-up factors they can achieve compared to non-intrusive models are often limited (Bach et al., 2019a; Czech et al., 2022). Mostly for these two reasons, a non-intrusive ROM was chosen in appended publication I. There are also a few limitations when using non-intrusive ROMs in optimization techniques. The ROM is commonly used to approximate the displacement field of the simulation model (e.g., Le Guennec et al. (2018); Gstalter et al. (2020); Czech et al. (2022)). This is because the displacement field is typically smooth and, therefore, can be well-approximated in a lower-dimensional subspace. Other fields calculated in the simulation model, such as the stress field do not necessarily have this property. Therefore, care must be taken if the objective function of the optimization problem requires stress values to be evaluated.

An argument can be made that the optimization problems defined in the appended publications are too far away from real-world examples to give any meaningful insights beyond the examples themselves. There are different aspects to this potential argument that are discussed here to make it clear, that the author believes it to not be substantiated.

First, regarding the chosen components and the HF simulation models, it is clear that the examples considered in the appended publications are academic examples and not necessar-

ily real-world components. As such, they represent simplified versions of potentially realistic application problems. These types of problems have also been used very commonly in the literature (compare, for example, Hino et al. (2006); Sattari et al. (2007); Manoochehri and Kolahan (2014)). They include the most relevant mechanical phenomena, such as nonlinear deformations and self-contact in the crashbox example of appended publication I (Kaps et al., 2022) while simplifying others, such as the addendum of blankholder and drawbeads in the cross-die example of appended publications II and III (Kaps et al., 2023, 2024). Therefore, while the exact location of the optimum and the exact individual simulation results would vary with higher model resolution, the fundamental landscape of the defined objective function likely would not change too significantly. Therefore, the observed comparisons between SF and MF optimization techniques are likely to be transferable with the limitations of the other influence factors for MF methods, which are discussed above.

The second aspect is the definition of the optimization problems itself. As already mentioned previously (compare Subsection 2.2.1), the optimization problems defined in the appended publications do not include constraints (except for the lateral impact example in appended publication I), algorithm parallelization, multiple objective functions, etc. It has been well-established that all or most of these aspects are relevant in actual industrial applications (e.g., Keane and Nair (2005); Duddeck (2008); Koziel and Leifsson (2013); Antinori (2016); Arsenyev (2017)). It is argued here, that it makes more sense to first establish the potential of MF-EGO techniques in an application as is done in the appended publications and then extend the scope of the problems considered, which is left open for future work here. A benefit of EGO as an algorithm is that it is inherently modular in that, for example, the infill criterion can be straightforwardly extended to include constraints or to allow for the parallel addition of multiple samples (compare Zhan and Xing (2020)). Another point here is that the number of design variables used here is rather low with between four and six design variables in the published examples. While this is realistic for some real-world problems, there are certainly others where a significantly higher number of design variables is required. However, the same reasoning from before still holds that it makes more sense to first establish the potential of the MF techniques by themselves and then increase the complexity of the considered problems. In this second step, the extensive research that has been put into extending EGO to higher-dimensional problems in SF settings (e.g., Raponi et al. (2020)) can then be used as a basis for further work.

Overall, the majority of the research questions formulated in Chapter 1 can be answered here. It is established, that MF EGO techniques can be beneficial in challenging structural applications, such as automotive crashworthiness and deep drawing simulations (*Question 1*). Additionally, the optimization time reduction observed is in the same order of magnitude as in previous publications on MF optimization in various applications (*Question 2*). A modified DoE technique called IV sampling is proposed and successfully applied in two of the appended

publications. Extensive research already done in literature has shown that the infill criteria also have a major impact on optimization performance. In appended publication III, it is shown that the addition of a second phase of adaptive improvement to the optimization inspired by reliability analysis techniques and the existence of a limit state in the investigated objective function(s) can also increase the quality of the result. (*Questions 3 and 4*). And while the effective integration of input parameter uncertainties into the optimization problem is only exemplarily established, the optimization scheme proposed in appended publication III marks the first steps in this direction (*Question 5*). It is found that the use of non-intrusive ROM as LF models inside the MF optimization can be beneficial compared to the commonly used simplified simulation models (*Question 6*). Finally, it is again established with appended publication II that the choice of objective function has a major impact on computational resources required and results going beyond the difference between SF and MF techniques (*Question 7*).

Chapter 6

Conclusions and outlook

Different aspects of MF optimization in two challenging structural applications are investigated in the context of this thesis, including the three appended publications and surrounding work. In the first appended publication, two application examples from the field of automotive crashworthiness, a lateral side-sill impact and a frontal crashbox impact, are evaluated. The remaining two publications are focused on the drawability optimization of a deep-drawn component. The MF optimization technique used as a baseline for comparisons in the present work is an MF extension of the popular EGO approach which is one of the most efficient optimization methods for expensive black-box functions. Instead of kriging as a surrogate model and EI as the infill criterion, HK and VFEI are utilized here, respectively.

In all investigations, the quality of the optimization algorithms is assessed in three ways. First, the result quality in the sense of location and objective function value of the final optimum is considered. Second, the computational resources required for finding the optimum are taken into account, as it is arguably also valuable to find the same optimum faster rather than finding a better optimum. Third, due to the stochastic nature of the optimization algorithm, the reliability of the assessments is ensured by repeating all optimization runs.

The appended publications include various novel contributions, which are summarized in the following.

The type of MF optimization scheme employed here has not been applied in either of the two applications investigated. Therefore, the observation that the baseline MF-EGO technique can already be beneficial in the two fields of application is a contribution in itself. Furthermore, the observed benefits in terms of optimization run time at comparable result quality for the baseline MF technique are in the same order of magnitude as previously reported values. This is true for both other MF optimization methods in the same applications and the same optimization technique applied in different fields of application.

In a second step, different novel modifications to the algorithm are suggested and implemented. A novel modification to DoE technique that aims at better resolving design space boundaries in surrogate models is first proposed in Komeilizadeh et al. (2022) and then successfully applied in an optimization context in appended publications I and III. It is found to be

beneficial on its own but particularly when combined with other modifications such as in the two-stage approach proposed in appended publication III. A non-intrusive ROM is integrated into the optimization scheme as the LF model in appended publication I and shown to be beneficial both in terms of result quality and optimization run times. The ROM is found to be both higher quality and faster to evaluate compared to a reference LF model that is the most commonly used simplified simulation model.

Appended publication II creates the basis for the latter work done in appended publication III by establishing the general usability of the MF-EGO optimization technique in drawability optimization problems. Additionally, it represents one of the first works where different drawability measures are directly compared to each other in the same application problem. The very differentiated findings for different drawability measures again highlight the need for careful consideration in the definition of an optimization problem.

In appended publication III, a novel two-stage MF optimization is proposed, whereby the initial surrogate model is adaptively enriched prior to the actual optimization stage. The enrichment phase is inspired by methods from reliability analysis where the investigated functions share the feature of having a limit state with the objective function in the deep drawing application problem assessed in the appended publication. It is found that the two-stage approach cannot only reduce the optimization run times further at limited impact on result quality. Furthermore, it enables the inclusion of input parameter uncertainties, for example through uncontrollable noise variables, and as exemplarily illustrated in the appended publication, the surrogate-based estimation of their influence on optimization results.

Based on the promising results throughout the present work, numerous ideas for interesting future work are identified, which are also detailed in the outlooks of the appended publications (Kaps et al., 2022, 2023, 2024) and in Chapter 5 of the present thesis. A generally interesting idea is to extend the somewhat small application examples used here to more realistic larger examples. Depending on the exact nature, this may necessitate the use of algorithm parallelization techniques as well as methods to remedy the influence of the curse of dimensionality encountered in higher-dimensional problems. Much work has already been done on both aspects in SF settings, but previous work is very limited for MF techniques and in the fields of application investigated here. Future work could also build upon the algorithm modifications suggested here and, for example, include the IV sampling into an MF-DoE technique, which also on its own might be a very interesting subject of investigation. In addition, the integration of the non-intrusive ROM as an LF model can be extended by updating the model during the optimization run or by exploring different MOR techniques to improve model quality. Finally, the inclusion of input parameter uncertainties into the MF optimization appears very promising. Little previous work has been done, and especially in real-world applications there are always

some uncertain parameters that have to be considered to ensure the reliability of the obtained results.

Bibliography

Abdullah N, Sani M, Salwani M, Husain N (2020) A review on crashworthiness studies of crash box structure. Thin-Walled Structures 153:106,795, DOI: 10.1016/j.tws.2020.106795

Ablat MA, Qattawi A (2016) Numerical simulation of sheet metal forming: a review. The International Journal of Advanced Manufacturing Technology 89(1-4):1235–1250, DOI: 10.1007/s00170-016-9103-5

Acar E, Yilmaz B, Güler MA, Altin M (2020) Multi-fidelity crashworthiness optimization of a bus bumper system under frontal impact. Journal of the Brazilian Society of Mechanical Sciences and Engineering 42(9):1–17, DOI: 10.1007/s40430-020-02572-3

Andrade-Campos A, Coppieters S, Strano M (2022) Optimization and inverse analysis in metal forming: scientific state-of-the-art and recent trends. International Journal of Material Forming 15(3), DOI: 10.1007/s12289-022-01690-8

Anselma PG, Niutta CB, Mainini L, Belingardi G (2020) Multidisciplinary design optimization for hybrid electric vehicles: component sizing and multi-fidelity frontal crashworthiness. Structural and Multidisciplinary Optimization 62(4):2149–2166, DOI: 10.1007/s00158-020-02603-6

Antinori G (2016) Uncertainty analysis and robust optimization for low pressure turbine rotors. PhD thesis, Technical University of Munich, Munich, Germany, URL: http://nbn-resolving.de/urn/resolver.pl?urn:nbn:de:bvb:91-diss-20160804-1279009-0-6

Arsenyev I (2017) Efficient surrogate-based robust design optimization method. PhD thesis, Technical University of Munich, Munich, Germany, URL: http://nbn-resolving.de/urn/resolver.pl?urn:nbn:de:bvb:91-diss-20171213-1360924-0-4

Audze P, Eglais V (1977) New approach to the design of experiments. Problems of Dynamic and Strength 35:104–107, [published in Russian]

Bach C, Ceglia D, Song L, Duddeck F (2019a) Randomized low-rank approximation methods for projection-based model order reduction of large nonlinear dynamical problems. International Journal for Numerical Methods in Engineering 118(4):209–241, DOI: 10.1002/nme.6009

Bach C, Duddeck F, Song L (2019b) Fixed-precision randomized low-rank approximation methods for nonlinear model order reduction of large systems. International Journal for Numerical Methods in Engineering 119(8):687–711, DOI: 10.1002/nme.6068

Baheri A (2023) Exploring the role of simulator fidelity in the safety validation of learning-enabled autonomous systems. AI Magazine 44(4):453–459, DOI: 10.1002/aaai.12141

Baker C, Gallivan K, Van Dooren P (2012) Low-rank incremental methods for computing dominant singular subspaces. Linear Algebra and its Applications 436(8):2866–2888, DOI: 10.1016/j.laa.2011.07.018

Balabanov V, Grossman B, Watson L, Mason W, Haftka R (1998) Multifidelity response surface model for HSCT wing bending material weight. In: 7th AIAA/USAF/NASA/ISSMO Symposium on Multidisciplinary Analysis and Optimization, American Institute of Aeronautics and Astronautics, St. Louis, MO, USA, DOI: 10.2514/6.1998-4804

Banabic D (2010) Sheet Metal Forming Processes. Springer Berlin Heidelberg, DOI: 10.1007/978-3-540-88113-1

Bandler J, Biernacki R, Chen SH, Grobelny P, Hemmers R (1994) Space mapping technique for electromagnetic optimization. IEEE Transactions on Microwave Theory and Techniques 42(12):2536–2544, DOI: 10.1109/22.339794

Bandler J, Cheng Q, Dakroury S, Mohamed A, Bakr M, Madsen K, Sondergaard J (2004) Space mapping: The state of the art. IEEE Transactions on Microwave Theory and Techniques 52(1):337–361, DOI: 10.1109/tmtt.2003.820904

Benner P, Gugercin S, Willcox K (2015) A survey of projection-based model reduction methods for parametric dynamical systems. SIAM Review 57(4):483–531, DOI: 10.1137/130932715

Bichon BJ, Eldred MS, Swiler LP, Mahadevan S, McFarland JM (2008) Efficient global reliability analysis for nonlinear implicit performance functions. AIAA Journal 46(10):2459–2468, DOI: 10.2514/1.34321

Bohachevsky IO, Johnson ME, Stein ML (1986) Generalized simulated annealing for function optimization. Technometrics 28(3):209–217, DOI: 10.1080/00401706.1986.10488128

Box GEP, Behnken DW (1960) Some new three level designs for the study of quantitative variables. Technometrics 2(4):455–475, DOI: 10.1080/00401706.1960.10489912

Braaten E, Weller G (1979) An improved low-discrepancy sequence for multidimensional quasi-Monte Carlo integration. Journal of Computational Physics 33(2):249–258, DOI: 10.1016/0021-9991(79)90019-6

Bratley P, Fox B (1988) Algorithm 659: Implementing Sobol's quasi-random sequence generator. ACM Trans Math Softw 14(1):88–100, DOI: 10.1145/42288.214372

Butler A, Haynes R, Humphries T, Ranjan P (2014) Efficient optimization of the likelihood function in Gaussian process modelling. Computational Statistics & Data Analysis 73:40–52, DOI: 10.1016/j.csda.2013.11.017

Byrd RH, Lu P, Nocedal J, Zhu C (1995) A limited memory algorithm for bound constrained optimization. SIAM Journal on Scientific Computing 16(5):1190–1208, DOI: 10.1137/0916069

Chakroborty P, Dhulipala SLN, Che Y, Jiang W, Spencer BW, Hales JD, Shields MD (2023) General multifidelity surrogate models: Framework and active-learning strategies for efficient rare event simulation. Journal of Engineering Mechanics 149(12), DOI: 10.1061/jenmdt.emeng-7111

Chang KJ, Haftka RT, Giles GL, Kao PJ (1993) Sensitivity-based scaling for approximating structural response. Journal of Aircraft 30(2):283–288, DOI: 10.2514/3.48278

Chaudhuri A, Marques AN, Willcox K (2021) mfEGRA: Multifidelity efficient global reliability analysis through active learning for failure boundary location. Structural and Multidisciplinary Optimization DOI: 10.1007/s00158-021-02892-5

Chen L, Qiu H, Gao L, Jiang C, Yang Z (2020) Optimization of expensive black-box problems via gradient-enhanced kriging. Computer Methods in Applied Mechanics and Engineering 362:112,861, DOI: 10.1016/j.cma.2020.112861

Chengzhi S, Guanlong C, Zhongqin L (2004) Determining the optimum variable blank-holder forces using adaptive response surface methodology (ARSM). The International Journal of Advanced Manufacturing Technology 26(1–2):23–29, DOI: 10.1007/s00170-003-1979-1

Cox D, John S (1992) A statistical method for global optimization. In: [Proceedings] 1992 IEEE International Conference on Systems, Man, and Cybernetics, IEEE, Chicago, IL, USA, DOI: 10.1109/icsmc.1992.271617

Czech C, Lesjak M, Bach C, Duddeck F (2022) Data-driven models for crashworthiness optimisation: intrusive and non-intrusive model order reduction techniques. Structural and Multidisciplinary Optimization 65(7), DOI: 10.1007/s00158-022-03282-1

Davies GAO, Morton J (eds) (1984) Structural Impact and crashworthiness, Elsevier, London, UK

Dhulipala SL, Shields MD, Spencer BW, Bolisetti C, Slaughter AE, Labouré VM, Chakroborty P (2022) Active learning with multifidelity modeling for efficient rare event simulation. Journal of Computational Physics 468:111,506, DOI: 10.1016/j.jcp.2022.111506

Di Fiore F, Maggiore P, Mainini L (2021) Multifidelity domain-aware learning for the design of re-entry vehicles. Structural and Multidisciplinary Optimization 64(5):3017–3035, DOI: 10.1007/s00158-021-03037-4

Duddeck F (2008) Multidisciplinary optimization of car bodies. Structural and Multidisciplinary Optimization 35(4):375–389, DOI: 10.1007/s00158-007-0130-6

Duvenaud D (2014) Automatic model construction with Gaussian processes. PhD thesis, University of Cambridge, Cambridge, UK, DOI: 10.17863/CAM.14087

Eberhart R, Kennedy J (1995) A new optimizer using particle swarm theory. In: MHS'95. Proceedings of the Sixth International Symposium on Micro Machine and Human Science, IEEE, MHS-95, DOI: 10.1109/mhs.1995.494215

Echard B, Gayton N, Lemaire M (2011) AK-MCS: An active learning reliability method combining kriging and Monte Carlo simulation. Structural Safety 33(2):145–154, DOI: 10.1016/j.strusafe.2011.01.002

Etman LFP, Adriaens JMTA, Slagmaat MTP, Schoofs AJG (1996) Crash worthiness design optimization using multipoint sequential linear programming. Structural Optimization 12(4):222–228, DOI: 10.1007/bf01197360

Fang H, Rais-Rohani M, Liu Z, Horstemeyer M (2005) A comparative study of metamodeling methods for multiobjective crashworthiness optimization. Computers & Structures 83(25-26):2121–2136, DOI: 10.1016/j.compstruc.2005.02.025

Fang J, Sun G, Qiu N, Kim NH, Li Q (2016) On design optimization for structural crashworthiness and its state of the art. Structural and Multidisciplinary Optimization 55(3):1091–1119, DOI: 10.1007/s00158-016-1579-y

Fang KT, Ma CX (2001) Wrap-around L2-discrepancy of random sampling, Latin hypercube and uniform designs. Journal of Complexity 17(4):608–624, DOI: 10.1006/jcom.2001.0589

Fang KT, Ma CX, Winker P (2002) Centered L2-discrepancy of random sampling and Latin hypercube design, and construction of uniform designs. Mathematics of Computation 71(237):275–296, DOI: 10.1090/S0025-5718-00-01281-3

Fernández-Godino MG (2023) Review of multi-fidelity models. ArXiv Preprint, DOI: 10.48550/ARXIV.1609.07196v4

Fischer CC (2021) Bayesian inspired multi-fidelity optimization with aerodynamic design. PhD thesis, Wright State University, Dayton, OH, USA, URL: http://rave.ohiolink.edu/etdc/view?acc_num=wright1621948051637597

Fisher RA (1936) Design of experiments. British Medical Journal 1(3923):554

Forrester A, Sobester A, Keane A (2008) Engineering Design via Surrogate Modelling. John Wiley & Sons Inc, DOI: 10.1002/9780470770801

Forrester AI, Sóbester A, Keane AJ (2007) Multi-fidelity optimization via surrogate modelling. Proceedings of the Royal Society A: Mathematical, Physical and Engineering Sciences 463(2088):3251–3269, DOI: 10.1098/rspa.2007.1900

Forsberg J, Nilsson L (2006) Evaluation of response surface methodologies used in crashworthiness optimization. International Journal of Impact Engineering 32(5):759–777, DOI: 10.1016/j.ijimpeng.2005.01.007

Fuhg JN, Fau A, Nackenhorst U (2020) State-of-the-art and comparative review of adaptive sampling methods for kriging. Archives of Computational Methods in Engineering 28(4):2689–2747, DOI: 10.1007/s11831-020-09474-6

Gano SE, Renaud JE, Sanders B (2005) Hybrid variable fidelity optimization by using a kriging-based scaling function. AIAA Journal 43(11):2422–2433, DOI: 10.2514/1.12466

Gantar G, Kuzman K, Filipič B (2005) Increasing the stability of the deep drawing process by simulation-based optimization. Journal of Materials Processing Technology 164-165:1343–1350, DOI: 10.1016/j.jmatprotec.2005.02.099

Garud SS, Karimi IA, Kraft M (2017) Design of computer experiments: A review. Computers & Chemical Engineering 106:71–95, DOI: 10.1016/j.compchemeng.2017.05.010

Genton MG (2002) Classes of kernels for machine learning: A statistics perspective. Journal of Machine Learning Research (JMLR) 2:299–312, DOI: 10.5555/944790.944815

Ginsbourger D, Le Riche R, Carraro L (2010) Kriging Is Well-Suited to Parallelize Optimization, Adaptation Learning and Optimization, vol 2, Springer Berlin Heidelberg, pp 131–162. DOI: 10.1007/978-3-642-10701-6_6

Goodwin GM (1968) Application of strain analysis to sheet metal forming problems in the press shop. In: SAE Technical Paper Series, SAE International, DOI: 10.4271/680093

Gramacy RB, Lee HKH (2010) Cases for the nugget in modeling computer experiments. Statistics and Computing 22(3):713–722, DOI: 10.1007/s11222-010-9224-x

Gstalter E, Assou S, Tourbier Y, De Vuyst F (2020) Toward new methods for optimization study in automotive industry including recent reduction techniques. Advanced Modeling and Simulation in Engineering Sciences 7:1–16, DOI: https://doi.org/10.1186/s40323-020-00151-8

Guo M, Hesthaven JS (2018) Reduced order modeling for nonlinear structural analysis using Gaussian process regression. Computer Methods in Applied Mechanics and Engineering 341:807–826, DOI: 10.1016/j.cma.2018.07.017

Guo Y, Batoz J, Naceur H, Bouabdallah S, Mercier F, Barlet O (2000) Recent developments on the analysis and optimum design of sheet metal forming parts using a simplified inverse approach. Computers & Structures 78(1-3):133–148, DOI: 10.1016/s0045-7949(00)00095-x

Guo YQ, Batoz JL, Detraux JM, Duroux P (1990) Finite element procedures for strain estimations of sheet metal forming parts. International Journal for Numerical Methods in Engineering 30(8):1385–1401, DOI: 10.1002/nme.1620300804

Haftka RT (1991) Combining global and local approximations. AIAA Journal 29(9):1523–1525, DOI: 10.2514/3.10768

Halton JH (1964) Algorithm 247: Radical-inverse quasi-random point sequence. Communications of the ACM 7(12):701–702, DOI: 10.1145/355588.365104

Hammersley JM, Handscomb DC (1964) Monte Carlo Methods. Springer Netherlands, DOI: 10.1007/978-94-009-5819-7

Han ZH, Görtz S (2012) Hierarchical kriging model for variable-fidelity surrogate modeling. AIAA Journal 50(9):1885–1896, DOI: 10.2514/1.J051354

Han ZH, Zimmermann R, Görtz S (2012) Alternative cokriging method for variable-fidelity surrogate modeling. AIAA Journal 50(5):1205–1210, DOI: 10.2514/1.j051243

Hickernell F (1998) A generalized discrepancy and quadrature error bound. Mathematics of Computation 67(221):299–322, DOI: 10.1090/S0025-5718-98-00894-1

Hino R, Yoshida F, Toropov VV (2006) Optimum blank design for sheet metal forming based on the interaction of high- and low-fidelity FE models. Archive of Applied Mechanics 75(10-12):679–691, DOI: 10.1007/s00419-006-0047-3

Hu W, Enying L, Li GY, Zhong ZH (2007) Optimization of sheet metal forming processes by the use of space mapping based metamodeling method. The International Journal of Advanced Manufacturing Technology 39(7–8):642–655, DOI: 10.1007/s00170-007-1253-z

Huang D, Allen TT, Notz WI, Miller RA (2006) Sequential kriging optimization using multiple-fidelity evaluations. Structural and Multidisciplinary Optimization 32(5):369–382, DOI: 10.1007/s00158-005-0587-0

Husslage BG, Rennen G, Van Dam ER, Den Hertog D (2011) Space-filling Latin hypercube designs for computer experiments. Optimization and Engineering 12(4):611–630, DOI: 10.1007/s11081-010-9129-8

International Organization for Standardization (2021) Metallic materials — determination of forming-limit curves for sheet and strip — part 2: Determination of forming-limit curves in the laboratory, (ISO Standard No. 12004-2:2021). URL: https://www.iso.org/standard/78138.html, (last accessed 05.04.2024)

Jakumeit J, Herdy M, Nitsche M (2005) Parameter optimization of the sheet metal forming process using an iterative parallel kriging algorithm. Structural and Multidisciplinary Optimization 29(6):498–507, DOI: 10.1007/s00158-004-0455-3

Jansson T, Andersson A, Nilsson L (2005) Optimization of draw-in for an automotive sheet metal part. Journal of Materials Processing Technology 159(3):426–434, DOI: 10.1016/j.jmatprotec.2004.06.011

Jiang P, Cheng J, Zhou Q, Shu L, Hu J (2019) Variable-fidelity lower confidence bounding approach for engineering optimization problems with expensive simulations. AIAA Journal 57(12):5416–5430, DOI: 10.2514/1.j058283

Jin R, Chen W, Sudjianto A (2005) An efficient algorithm for constructing optimal design of computer experiments. Journal of Statistical Planning and Inference 134(1):268–287, DOI: 10.1016/j.jspi.2004.02.014

Joe S, Kuo FY (2008) Constructing Sobol sequences with better two-dimensional projections. SIAM Journal on Scientific Computing 30(5):2635–2654, DOI: 10.1137/070709359

Johnson ME, Moore LM, Ylvisaker D (1990) Minimax and maximin distance designs. Journal of Statistical Planning and Inference 26(2):131–148, DOI: 10.1016/0378-3758(90)90122-B

Johnson W, Mamalis AG (1978) Crashworthiness of Vehicles. Mechanical Engineering Publications Limited, London, UK

Jones DR (2001) A taxonomy of global optimization methods based on response surfaces. Journal of Global Optimization 21(4):345–383, DOI: 10.1023/A:1012771025575

Jones DR, Schonlau M, Welch WJ (1998) Efficient global optimization of expensive black-box functions. Journal of Global Optimization 13(4):455–492, DOI: 10.1023/A:1008306431147

Jones N, Wierzbicki T (1983) Structural Crashworthiness. Butterworths London, London, UK

Journel AG, Huijbregts C (1978) Mining Geostatistics. Academic Press, New York, DOI: 10.1180/minmag.1979.043.328.34

Kaps A, Czech C, Duddeck F (2022) A hierarchical kriging approach for multi-fidelity optimization of automotive crashworthiness problems. Structural and Multidisciplinary Optimization 65(4), DOI: 10.1007/s00158-022-03211-2

Kaps A, Lehrer T, Lepenies I, Wagner M, Duddeck F (2023) Multi-fidelity optimization of metal sheets concerning manufacturability in deep-drawing processes. Structural and Multidisciplinary Optimization 66(8), DOI: 10.1007/s00158-023-03631-8

Kaps A, Lehrer T, Lepenies I, Wagner M, Quek ST, Duddeck F (2024) A novel two-stage multi-fidelity optimization for manufacturability of deep-drawn metal sheets, (submitted for publication at Structural and Multidisciplinary Optimization)

Keane A, Nair P (2005) Computational Approaches for Aerospace Design. John Wiley & Sons Inc, DOI: 10.1002/0470855487

Keeler SP (1968) Circular grid system — a valuable aid for evaluating sheet metal formability. In: SAE Technical Paper Series, SAE International, DOI: 10.4271/680092

Kennedy MC, O'Hagan A (2000) Predicting the output from a complex computer code when fast approximations are available. Biometrika 87(1):1–13, DOI: 10.1093/biomet/87.1.1

Kishor N, Kumar DR (2002) Optimization of initial blank shape to minimize earing in deep drawing using finite element method. Journal of Materials Processing Technology 130-131:20–30, DOI: 10.1016/s0924-0136(02)00790-2

Kneifl J, Grunert D, Fehr J (2021) A nonintrusive nonlinear model reduction method for structural dynamical problems based on machine learning. International Journal for Numerical Methods in Engineering DOI: 10.1002/nme.6712

Kochenderfer MJ, Wheeler TA (2019) Algorithms for Optimization. MIT Press Ltd, Cambridge, ISBN: 9780262039420

Komeilizadeh K, Kaps A, Duddeck F (2022) Isovolumetric adaptations to space-filling design of experiments. Optimization and Engineering 24(2):1267–1288, DOI: 10.1007/s11081-022-09731-6

Koziel S, Leifsson L (2013) Surrogate-Based Modeling and Optimization. Springer New York, DOI: 10.1007/978-1-4614-7551-4

Koziel S, Cheng Q, Bandler J (2008) Space mapping. IEEE Microwave Magazine 9(6):105–122, DOI: 10.1109/mmm.2008.929554

Krige DG (1951) A statistical approach to some basic mine valuation problems on the Witwatersrand. Journal of the Southern African Institute of Mining and Metallurgy 52(6):119–139, DOI: 10520/AJA0038223X_4792

Krivacic D (2023) Multi-fidelity optimization schemes in nonlinear structural applications. Master's thesis, Technical University of Munich, Munich, Germany

Kushner HJ (1964) A new method of locating the maximum point of an arbitrary multipeak curve in the presence of noise. Journal of Basic Engineering 86(1):97–106, DOI: 10.1115/1.3653121

Lange VA, Fender J, Song L, Duddeck F (2018) Early phase modeling of frontal impacts for crashworthiness: From lumped mass–spring models to deformation space models. Proceedings of the Institution of Mechanical Engineers, Part D: Journal of Automobile Engineering 233(12):3000–3015, DOI: 10.1177/0954407018814034

Laurent L, Le Riche R, Soulier B, Boucard PA (2017) An overview of gradient-enhanced metamodels with applications. Archives of Computational Methods in Engineering 26(1):61–106, DOI: 10.1007/s11831-017-9226-3

Le Gratiet L (2013) Multi-fidelity Gaussian process regression for computer experiments. PhD thesis, Université Paris-Diderot - Paris VII, Paris, France, URL: https://theses.hal.science/tel-00866770v2

Le Gratiet L, Garnier J (2014) Recursive co-kriging model for design of computer experiments with multiple levels of fidelity. International Journal for Uncertainty Quantification 4(5):365–386, DOI: 10.1615/int.j.uncertaintyquantification.2014006914

Le Guennec Y, Brunet JP, Daim FZ, Chau M, Tourbier Y (2018) A parametric and non-intrusive reduced order model of car crash simulation. Computer Methods in Applied Mechanics and Engineering 338:186–207, DOI: 10.1016/j.cma.2018.03.005

Lee C, Huh H (1997) Blank design and strain prediction of automobile stamping parts by an inverse finite element approach. Journal of Materials Processing Technology 63(1-3):645–650, DOI: 10.1016/s0924-0136(96)02700-8

Lehrer T, Kaps A, Lepenies I, Duddeck F, Wagner M (2023) 2S-ML: A simulation-based classification and regression approach for drawability assessment in deep drawing. International Journal of Material Forming 16(5), DOI: 10.1007/s12289-023-01770-3

Lewis R, Nash S (2000) A multigrid approach to the optimization of systems governed by differential equations. In: 8th Symposium on Multidisciplinary Analysis and Optimization, American Institute of Aeronautics and Astronautics, Long Beach, CA, USA, DOI: 10.2514/6.2000-4890

Liu H, Ong YS, Cai J (2017) A survey of adaptive sampling for global metamodeling in support of simulation-based complex engineering design. Structural and Multidisciplinary Optimization 57(1):393–416, DOI: 10.1007/s00158-017-1739-8

Loeppky JL, Sacks J, Welch WJ (2009) Choosing the sample size of a computer experiment: A practical guide. Technometrics 51(4):366–376, DOI: 10.1198/tech.2009.08040

Lualdi P, Sturm R, Siefkes T (2023) A multi-fidelity successive response surface method for crashworthiness optimization problems. Applied Sciences 13(20):11,452, DOI: 10.3390/app132011452

Mainini L, Serani A, Rumpfkeil MP, Minisci E, Quagliarella D, Pehlivan H, Yildiz S, Ficini S, Pellegrini R, Di Fiore F, Bryson D, Nikbay M, Diez M, Beran P (2022) Analytical benchmark problems for multifidelity optimization methods. ArXiv Preprint, DOI: 10.48550/ARXIV.2204.07867

Manoochehri M, Kolahan F (2014) Integration of artificial neural network and simulated annealing algorithm to optimize deep drawing process. The International Journal of Advanced Manufacturing Technology 73(1-4):241–249, DOI: 10.1007/s00170-014-5788-5

Mason BH, Haftka RT, Johnson ER, Farley GL (1998) Variable complexity design of composite fuselage frames by response surface techniques. Thin-Walled Structures 32(4):235–261, DOI: 10.1016/s0263-8231(98)00016-0

Matheron G (1963) Principles of geostatistics. Economic Geology 58(8):1246–1266, DOI: 10.2113/gsecongeo.58.8.1246

Matérn B (1986) Spatial Variation, vol 36, 2nd edn. Springer New York, DOI: 10.1007/978-1-4615-7892-5

McKay MD, Beckman RJ, Conover WJ (1979) Comparison of three methods for selecting values of input variables in the analysis of output from a computer code. Technometrics 21(2):239–245, DOI: 10.1080/00401706.1979.10489755

McQuade P, Eberhardt S, Livne E (1992) Optimization of a 2D scramjet-vehicle using CFD and simplified approximate flow analysis techniques. In: 28th Joint Propulsion Conference and Exhibit, American Institute of Aeronautics and Astronautics, Nashville, TN, USA, DOI: 10.2514/6.1992-3673

Močkus J (1975) On Bayesian methods for seeking the extremum. In: Optimization techniques IFIP technical conference, Springer, pp 400–404, DOI: 10.1007/3-540-07165-2_55

Močkus J (2012) Bayesian Approach to Global Optimization: Theory and Applications, vol 37. Springer Netherlands, DOI: 10.1007/978-94-009-0909-0

Montgomery DC (2020) Design and analysis of experiments, 10th edn. Wiley, Hoboken, NJ, ISBN: 978-1-119-49244-3

Morokoff WJ, Caflisch RE (1994) Quasi-random sequences and their discrepancies. SIAM Journal on Scientific Computing 15(6):1251–1279, DOI: 10.1137/0915077

Morris MD, Mitchell TJ (1995) Exploratory designs for computational experiments. Journal of Statistical Planning and Inference 43(3):381–402, DOI: 10.1016/0378-3758(94)00035-T

Moustapha M, Sudret B (2019) Surrogate-assisted reliability-based design optimization: a survey and a unified modular framework. Structural and Multidisciplinary Optimization 60(5):2157–2176, DOI: 10.1007/s00158-019-02290-y

Naceur H, Delaméziere A, Batoz J, Guo Y, Knopf-Lenoir C (2004) Some improvements on the optimum process design in deep drawing using the inverse approach. Journal of Materials Processing Technology 146(2):250–262, DOI: 10.1016/j.matprotec.2003.11.015

Niederreiter H (1992) Random number generation and quasi-Monte Carlo methods. SIAM, DOI: 10.1137/1.9781611970081

Noorsumar G, Rogovchenko S, Robbersmyr KG, Vysochinskiy D (2021) Mathematical models for assessment of vehicle crashworthiness: a review. International Journal of Crashworthiness 27(5):1545–1559, DOI: 10.1080/13588265.2021.1929760

Obermeyer E, Majlessi S (1998) A review of recent advances in the application of blank-holder force towards improving the forming limits of sheet metal parts. Journal of Materials Processing Technology 75(1-3):222–234, DOI: 10.1016/s0924-0136(97)00368-3

Ohata T, Nakamura Y, Katayama T, Nakamachi E, Omori N (1998) Improvement of optimum process design system by numerical simulation. Journal of Materials Processing Technology 80-81:635–641, DOI: 10.1016/s0924-0136(98)00170-8

Padmanabhan R, Oliveira M, Alves J, Menezes L (2007) Influence of process parameters on the deep drawing of stainless steel. Finite Elements in Analysis and Design 43(14):1062–1067, DOI: 10.1016/j.finel.2007.06.011

Park C, Haftka RT, Kim NH (2017) Remarks on multi-fidelity surrogates. Structural and Multidisciplinary Optimization 55(3):1029–1050, DOI: 10.1007/s00158-016-1550-y

Parr J, Holden CM, Forrester AI, Keane AJ (2010) Review of efficient surrogate infill sampling criteria with constraint handling. In: 2nd International Conference on Engineering Optimization, Lisbon, Portugal, URL: http://eprints.soton.ac.uk/id/eprint/336169

Paul SK (2013) Theoretical analysis of strain- and stress-based forming limit diagrams. The Journal of Strain Analysis for Engineering Design 48(3):177–188, DOI: 10.1177/0309324712468524

Paul SK (2021) Controlling factors of forming limit curve: A review. Advances in Industrial and Manufacturing Engineering 2:100,033, DOI: 10.1016/j.aime.2021.100033

Pedregosa F, Varoquaux G, Gramfort A, Michel V, Thirion B, Grisel O, Blondel M, Prettenhofer P, Weiss R, Dubourg V, Vanderplas J, Passos A, Cournapeau D, Brucher M, Perrot M, Duchesnay E (2011) Scikit-learn: Machine learning in Python. Journal of Machine Learning Research 12:2825–2830

Peherstorfer B, Willcox K, Gunzburger M (2018) Survey of multifidelity methods in uncertainty propagation, inference, and optimization. SIAM Review 60(3):550–591, DOI: 10.1137/16m1082469

Pei P, Quek ST, Peng Y (2023) Enriched global–local multi-objective optimization scheme for fuzzy logic controller-driven magnetorheological damper-based structural system. Mechanical Systems and Signal Processing 193:110,267, DOI: 10.1016/j.ymssp.2023.110267

Perdikaris P, Raissi M, Damianou A, Lawrence ND, Karniadakis GE (2017) Nonlinear information fusion algorithms for data-efficient multi-fidelity modelling. Proceedings of the Royal Society A: Mathematical, Physical and Engineering Sciences 473(2198):20160,751, DOI: 10.1098/rspa.2016.0751

Pifko A, Winter R (1981) Theory and application of finite element analysis to structural crash simulation, Elsevier, pp 277–285. DOI: 10.1016/b978-0-08-027299-3.50036-4

Ponweiser W, Wagner T, Vincze M (2008) Clustered multiple generalized expected improvement: A novel infill sampling criterion for surrogate models. In: 2008 IEEE Congress on Evolutionary Computation (IEEE World Congress on Computational Intelligence), IEEE, DOI: 10.1109/cec.2008.4631273

Pronzato L, Müller WG (2011) Design of computer experiments: space filling and beyond. Statistics and Computing 22(3):681–701, DOI: 10.1007/s11222-011-9242-3

Qian PZG, Wu CFJ (2008) Bayesian hierarchical modeling for integrating low-accuracy and high-accuracy experiments. Technometrics 50(2):192–204, DOI: 10.1198/004017008000000082

Rajabi MM, Ataie-Ashtiani B, Janssen H (2015) Efficiency enhancement of optimized Latin hypercube sampling strategies: Application to Monte Carlo uncertainty analysis and meta-modeling. Advances in Water Resources 76:127–139, DOI: 10.1016/j.advwatres.2014.12.008

Ranjan P, Haynes R, Karsten R (2011) A computationally stable approach to Gaussian process interpolation of deterministic computer simulation data. Technometrics 53(4):366–378, DOI: 10.1198/tech.2011.09141

Rao SS (2019) Engineering Optimization: Theory and Practice. Wiley Online Library, John Wiley & Sons, Hoboken, NJ, USA, DOI: 10.1002/9781119454816

Raponi E, Wang H, Bujny M, Boria S, Doerr C (2020) High dimensional Bayesian optimization assisted by principal component analysis. In: International Conference on Parallel Problem Solving from Nature, Springer, pp 169–183, DOI: 10.1007/978-3-030-58112-1_12

Rasmussen CE, Williams CKI (2005) Gaussian Processes for Machine Learning. MIT Press Ltd, DOI: 10.7551/mitpress/3206.001.0001

Rayas-Sanchez JE (2016) Power in simplicity with ASM: Tracing the aggressive space mapping algorithm over two decades of development and engineering applications. IEEE Microwave Magazine 17(4):64–76, DOI: 10.1109/mmm.2015.2514188

Reisenthel PH, Allen TT (2014) Application of multifidelity expected improvement algorithms to aeroelastic design optimization. In: 10th AIAA Multidisciplinary Design Optimization Conference, American Institute of Aeronautics and Astronautics, National Harbor, MD, USA, DOI: 10.2514/6.2014-1490

Ribeiro LG, Parente E, de Melo AMC (2023) Alternative variable-fidelity acquisition functions for efficient global optimization of black-box functions. Structural and Multidisciplinary Optimization 66(7), DOI: 10.1007/s00158-023-03607-8

Ruan X, Jiang P, Zhou Q, Hu J, Shu L (2020) Variable-fidelity probability of improvement method for efficient global optimization of expensive black-box problems. Structural and Multidisciplinary Optimization 62(6):3021–3052, DOI: 10.1007/s00158-020-02646-9

Rutzmoser J (2018) Model order reduction for nonlinear structural dynamics. PhD thesis, Technical University of Munich, Munich, Germany, URL: http://nbn-resolving.de/urn/resolver.pl?urn:nbn:de:bvb:91-diss-20180313-1381943-1-3

Sacks J, Welch WJ, Mitchell TJ, Wynn HP (1989) Design and analysis of computer experiments. Statistical Science 4(4):409–423, DOI: 10.1214/ss/1177012413

Saltelli A, Ratto M, Andres T, Campolongo F, Cariboni J, Gatelli D, Saisana M, Tarantola S (2007) Global Sensitivity Analysis. The Primer. John Wiley & Sons, Ltd, DOI: 10.1002/9780470725184

Santner TJ, Williams BJ, Notz WI (2003) The Design and Analysis of Computer Experiments. Springer New York, DOI: 10.1007/978-1-4757-3799-8

Sasena M, Papalambros P, Goovaerts P (2002) Global optimization of problems with disconnected feasible regions via surrogate modeling. In: 9th AIAA/ISSMO Symposium on Multidisciplinary Analysis and Optimization, American Institute of Aeronautics and Astronautics, Atlanta, GA, USA, DOI: 10.2514/6.2002-5573

Sattari H, Sedaghati R, Ganesan R (2007) Analysis and design optimization of deep drawing process. Journal of Materials Processing Technology 184(1-3):84–92, DOI: 10.1016/j.jmatprotec.2006.11.008

Schonlau M (1997) Computer experiments and global optimization. PhD thesis, University of Waterloo, Waterloo, Ontario, Canada, iSBN: 978-0-612-22234-2

Schonlau M, Welch WJ, Jones DR (1998) Global versus local search in constrained optimization of computer models. In: New Developments and Applications in Experimental Design, vol 34, Institute of Mathematical Statistics, pp 11–25, URL: http://www.jstor.org/stable/4356058

Siegert K (2015) Blechumformung: Verfahren, Werkzeuge und Maschinen. Springer Berlin Heidelberg, DOI: 10.1007/978-3-540-68418-3

Sóbester A, Leary SJ, Keane AJ (2005) On the design of optimization strategies based on global response surface approximation models. Journal of Global Optimization 33(1):31–59, DOI: 10.1007/s10898-004-6733-1

Sobol' I (1967) On the distribution of points in a cube and the approximate evaluation of integrals. USSR Computational Mathematics and Mathematical Physics 7(4):86–112, DOI: 10.1016/0041-5553(67)90144-9

Storn R, Price K (1997) Differential evolution – a simple and efficient heuristic for global optimization over continuous spaces. Journal of Global Optimization 11(4):341–359, DOI: 10.1023/a:1008202821328

Stoughton TB, Zhu X (2004) Review of theoretical models of the strain-based FLD and their relevance to the stress-based FLD. International Journal of Plasticity 20(8–9):1463–1486, DOI: 10.1016/j.ijplas.2003.11.004

Sun G, Li G, Stone M, Li Q (2010a) A two-stage multi-fidelity optimization procedure for honeycomb-type cellular materials. Computational Materials Science 49(3):500–511, DOI: 10.1016/j.commatsci.2010.05.041

Sun G, Li G, Zhou S, Xu W, Yang X, Li Q (2010b) Multi-fidelity optimization for sheet metal forming process. Structural and Multidisciplinary Optimization 44(1):111–124, DOI: 10.1007/s00158-010-0596-5

Sun G, Li G, Li Q (2012) Variable fidelity design based surrogate and artificial bee colony algorithm for sheet metal forming process. Finite Elements in Analysis and Design 59:76–90, DOI: 10.1016/j.finel.2012.04.012

Swischuk R, Mainini L, Peherstorfer B, Willcox K (2019) Projection-based model reduction: Formulations for physics-based machine learning. Computers & Fluids 179:704–717, DOI: 10.1016/j.compfluid.2018.07.021

Takalkar AS, Chinnapandi LBM (2018) A review on effect of thinning, wrinkling and spring-back on deep drawing process. Proceedings of the Institution of Mechanical Engineers, Part B: Journal of Engineering Manufacture 233(4):1011–1036, DOI: 10.1177/0954405417752509

Tiwari PR, Rathore A, Bodkhe MG (2022) Factors affecting the deep drawing process – a review. Materials Today: Proceedings 56:2902–2908, DOI: 10.1016/j.matpr.2021.10.189

Toal DJJ, Bressloff NW, Keane AJ (2008) Kriging hyperparameter tuning strategies. AIAA Journal 46(5):1240–1252, DOI: 10.2514/1.34822

Tschaetsch H (2006) Metal Forming Practise. Springer Berlin Heidelberg, DOI: 10.1007/3-540-33217-0

Viana FAC (2015) A tutorial on Latin hypercube design of experiments. Quality and Reliability Engineering International 32(5):1975–1985, DOI: 10.1002/qre.1924

Viana FAC, Simpson TW, Balabanov V, Toropov V (2014) Special section on multidisciplinary design optimization: Metamodeling in multidisciplinary design optimization: How far have we really come? AIAA Journal 52(4):670–690, DOI: 10.2514/1.j052375

Volk W, Suh J (2013) Prediction of formability for non-linear deformation history using generalized forming limit concept (GFLC). In: AIP Conference Proceedings, American Institute of Physics, vol 1567, pp 556–561, DOI: 10.1063/1.4850035

Vořechovský M, Novák D (2009) Correlation control in small-sample Monte Carlo type simulations I: A simulated annealing approach. Probabilistic Engineering Mechanics 24(3):452–462, DOI: 10.1016/j.probengmech.2009.01.004

Wang X (2022) Investigation of multi-fidelity design of experiments in the context of multi-fidelity optimization. Master's thesis, Technical University of Munich, Munich, Germany

Wifi AS, Abdelmaguid TF, El-Ghandour AI (2007) A review of the optimization techniques applied to the deep drawing process. In: Proceedings of the 37th international conference on computers and industrial engineering, Alexandria, Egypt, pp 1111–1121

Yao R, Pang T, Zhang B, Fang J, Li Q, Sun G (2023) On the crashworthiness of thin-walled multi-cell structures and materials: State of the art and prospects. Thin-Walled Structures 189:110,734, DOI: 10.1016/j.tws.2023.110734

Ye KQ (1998) Orthogonal column Latin hypercubes and their application in computer experiments. Journal of the American Statistical Association 93(444):1430–1439, DOI: 10.1080/01621459.1998.10473803

Ye KQ, Li W, Sudjianto A (2000) Algorithmic construction of optimal symmetric Latin hypercube designs. Journal of Statistical Planning and Inference 90(1):145–159, DOI: 10.1016/S0378-3758(00)00105-1

Yi J, Wu F, Zhou Q, Cheng Y, Ling H, Liu J (2020) An active-learning method based on multi-fidelity kriging model for structural reliability analysis. Structural and Multidisciplinary Optimization 63(1):173–195, DOI: 10.1007/s00158-020-02678-1

Yu J, Yan C, Guo M (2019) Non-intrusive reduced-order modeling for fluid problems: A brief review. Proceedings of the Institution of Mechanical Engineers, Part G: Journal of Aerospace Engineering 233(16):5896–5912, DOI: 10.1177/0954410019890721

Zhan D, Xing H (2020) Expected improvement for expensive optimization: a review. Journal of Global Optimization 78(3):507–544, DOI: 10.1007/s10898-020-00923-x

Zhang C, Song C, Shafieezadeh A (2022) Adaptive reliability analysis for multi-fidelity models using a collective learning strategy. Structural Safety 94:102,141, DOI: 10.1016/j.strusafe.2021.102141

Zhang Y, Han ZH, Zhang KS (2018a) Variable-fidelity expected improvement method for efficient global optimization of expensive functions. Structural and Multidisciplinary Optimization 58(4):1431–1451, DOI: 10.1007/s00158-018-1971-x

Zhang Y, Kim NH, Park C, Haftka RT (2018b) Multifidelity surrogate based on single linear regression. AIAA Journal 56(12):4944–4952, DOI: 10.2514/1.J057299

Zhou Q, Zhao M, Hu J, Ma M (2023) Multi-fidelity Surrogates. Springer Nature Singapore, DOI: 10.1007/978-981-19-7210-2

Appendix A

Appended publications

A.1 Publication I

Kaps A., Czech C., Duddeck F.: A hierarchical kriging approach for multi-fidelity optimization of automotive crashworthiness problems. Structural and Multidisciplinary Optimization 65(4), 2022. DOI: https://doi.org/10.1007/s00158-022-03211-2

Structural and Multidisciplinary Optimization (2022) 65:114
https://doi.org/10.1007/s00158-022-03211-2

RESEARCH PAPER

A hierarchical kriging approach for multi-fidelity optimization of automotive crashworthiness problems

Arne Kaps[1] · **Catharina Czech**[1] · **Fabian Duddeck**[1]

Received: 18 November 2021 / Revised: 21 January 2022 / Accepted: 21 February 2022 / Published online: 18 March 2022

Abstract
Multi-fidelity optimization schemes enriching expensive high-fidelity functions with cheap-to-evaluate low-fidelity functions have gained popularity in recent years. In the present work, an optimization scheme based on a hierarchical kriging is proposed for large-scale and highly non-linear crashworthiness problems. After comparison to other multi-fidelity techniques an infill criterion called variable-fidelity expected improvement is applied and evaluated. This is complemented by two innovative techniques, a new approach regarding initial sampling and a novel way to generate the low-fidelity model for crash problems are suggested. For the former, a modified Latin hypercube sampling, pushing samples more towards design space boundaries, increases the quality of sampling selection. For the latter, a projection-based non-intrusive model order reduction technique accelerates and simplifies the low-fidelity model evaluation. The proposed techniques are investigated with two application problems from the field of automotive crashworthiness—a size optimization problem for lateral impact and a shape optimization problem for frontal impact. The use of a multi-fidelity scheme compared to baseline single-fidelity optimization saves computational effort while keeping an acceptable level of accuracy. Both suggested modifications, independently and especially combined, increase computational performance and result quality in the presented examples.

Keywords Kriging · Efficient global optimization · Multi-fidelity optimization · Crashworthiness · Model order reduction · Isovolumetric Latin hypercube

1 Introduction

As computational power has increased exponentially in recent years, also Finite Element (FE) models reached a higher level of detail and complexity—e.g. modern day car models for crash simulations may contain more than ten million elements. This balances out such that simulation times are not significantly decreasing. Especially in multi-query analysis such as optimization or robustness applications a high number of evaluations is required, which increases the computational effort to an infeasible level.

One possible remedy is the use of specifically designed optimization approaches such as Efficient Global Optimization (EGO) that was first proposed by Jones et al. (1998). The idea is to build a surrogate model from an initial design of experiments (DoE) and adaptively improve it utilizing a so-called infill criterion (Jones 2001; Forrester and Keane 2009). In this context, mostly kriging models (Krige 1951; Matheron 1963; Sacks et al. 1989) are exploited as surrogate models as their inherent error approximation features are especially beneficial.

More recently, these types of surrogate models were integrated in a multi-fidelity scheme, whereby the high-fidelity FE-analysis is complemented with an additional low-fidelity model: The corresponding multi-fidelity kriging schemes can be categorized into two variants. One class of techniques considers correction-based methods, where a "bridge function" or "scaling function" models the differences between high- and low-fidelity models (Chang et al. 1993; Gano et al. 2006; Han et al. 2013). The second type of multi-fidelity approaches are named cokriging. The idea of the latter is to enhance the low-fidelity surrogate model by utilizing the covariance matrix between low- and high-fidelity model. Originally proposed in the geostatistics community (Journel and Huijbregts 1978), this approach was extended to

Responsible Editor: Shikui Chen

✉ Arne Kaps
arne.kaps@tum.de

[1] TUM School of Engineering and Design, Technical University of Munich, Arcisstr. 21, 80333 Munich, Germany

computer experiments by Kennedy and O'Hagan (2000) and called KOH autoregressive model. Due to its success, numerous extensions and modifications have been added to cokriging since its introduction: Han et al. (2012) proposed an alternative approach for creation of the covariance matrix between low- and high-fidelity models. Moreover, Gratiet and Garnier (2014) reformulated the cokriging algorithm in a recursive manner to reduce computational complexity. An extension considering complex cross-correlations between varying fidelity models can be found in Perdikaris and Karniadakis (2016). The present work is based on hierarchical kriging (HK), suggested by Han and Görtz (2012), whereby the low-fidelity surrogate model represents the trend term in the multi-fidelity predictor. It is beneficial in the context of multi-fidelity optimization as it provides better error estimation capabilities compared to other cokriging models.

As surrogate models were adapted to multi-fidelity applications, so were infill criteria. A criterion named Augmented EI, capable of adaptively sampling low- and high-fidelity models by considering coefficients for cross-correlations and cost ratios between models was suggested by Huang et al. (2006). Moreover, Zhang et al. (2018a) proposed the variable-fidelity expected improvement (VF-EI) criterion that implements a similar idea but with an analytical derivation and free from external coefficients. Therefore, the latter is used in the present work.

A common approach in multi-fidelity optimization is to combine FE models with varying levels of mesh sizes for high and low-fidelity models, such as realized by Zhang et al. (2018a) for an airfoil shape optimization. In combination with a cokriging adaptation presented by Gratiet and Garnier (2014), a hydrofoil shape optimization with varying mesh size levels was performed by Bonfiglio et al. (2018). Similar approaches are investigated in the applications of crashworthiness for honeycomb structures and sheet metal forming in Sun et al. (2010) and Sun et al. (2010), respectively. Alaimo et al. (2018) proposed a multi-fidelity approach where an adaptive functional principal component analysis (PCA) model is utilized with a simulated annealing (SA) algorithm applied to linear elastic structural topology optimization. Anselma et al. (2020) published a multi-fidelity scheme for the crashworthiness discipline inside a multidisciplinary optimization. The authors use analytical equations as a low-fidelity model and propose to only evaluate the FE high-fidelity model if the former predicts infeasible results. Also a cokriging-based multi-fidelity version of EGO was exploited for inverse problems in haemodynamics (Perdikaris and Karniadakis 2016).

In automotive crashworthiness, optimization has been performed for many years (Redhe et al. 2004; Duddeck 2008; Hunkeler et al. 2013). More recently, multi-fidelity schemes have also been applied in this field (Sun et al. 2010). Acar et al. (2020) investigated a multi-fidelity optimization for a frontal impact problem of a bumper system with the multi-fidelity surrogate modeling approach suggested by Zhang et al. (2018b). Results show that multi-fidelity approaches are capable of yielding significant time-savings while maintaining acceptable accuracy. Other mechanics-based low-fidelity models available for crashworthiness applications are listed in Lange et al. (2018). The authors begin with lumped mass-spring models and subsequently motivate the introduction of the so-called component solution space approach that can be applied in early phase component development for crashworthiness analyses.

Recently, model order reduction (MOR) techniques have been introduced also for non-linear problems (Guo and Hesthaven 2017; Swischuk et al. 2019) and applied in crashworthiness (Kneifl et al. 2021). The non-intrusive approaches are based on the results of training simulations—here named snapshots—which are utilized to compute a reduced subspace. In addition, a regression model is trained that combines the basis vectors of the subspace to represent the physical behavior of the system (Guo and Hesthaven 2019). The non-intrusive MOR has been integrated into a multi-fidelity training scheme by Kast et al. (2020) and related projection-based approaches for crashworthiness applications and optimization have been conducted (Le Guennec et al. 2018; Assou et al. 2019; Gstalter et al. 2020; Ren et al. 2020). A summary of recent developments in the field of non-intrusive MOR is presented in Yu et al. (2019) for fluid mechanics application. Moreover, principal component-based surrogate models can also be found in the field of structural topology optimization (Alaimo et al. 2018; Xiao et al. 2020; Choi et al. 2019).

In the present work we aim to develop enhanced multi-fidelity optimization schemes in crashworthiness applications. To that end, we propose to integrate an incremental projection-based MOR approach as low-fidelity model into a multi-fidelity EGO algorithm. In a second step to reduce computational effort, our recently developed isovolumetric sampling approach placing samples closer to design space boundaries is adapted (Kaps et al. 2021). When assessing algorithm performance, two main criteria can be established. The primary goal is to find an optimization approach with reduced computational effort produced by the high number of expensive evaluations of the objective function during the optimization. Secondly, an acceptable level of accuracy must be maintained; i.e. a multi-fidelity optimization scheme should not lead to inferior results compared to an optimization based using only high-fidelity simulations.

This work is structured as follows. Initially, the novel design of experiments approach is introduced in Sect. 2, followed by the optimization scheme based on HK and VF-EI in Sect. 3. The MOR approach used for low-fidelity model generations is presented in Sect. 4. Subsequently, the proposed optimization scheme and its implementation

are explained in Sect. 5. The performance of the complete set of methods is illustrated by a lateral impact example and a crashbox design problem in Sect. 6, and final results are summarized together with an outlook into future work in Sect. 7.

2 Isovolumetric design of experiments

The first step of any population-based optimization is to determine an initial set of sample points by means of DoE. Covering the full design space with a small amount of samples is the general aim. As there is no unique criterion for this vaguely formulated goal, DoE is still an active field of research. An overview of popular criteria and approaches is given in Garud et al. (2017).

In the present work, a modified optimal Latin hypercube (OLH) approach is used. The standard construction of a Latin hypercube design (LHD) for N samples in d dimensions is described in the following. In each dimension the space is divided into N strata of equal probability, i.e. the design space then consists of N^d cells. Randomly, N cells are selected such that each stratum of a dimension may only contain a single sample. Each sample can be placed in the center of its cell or randomly located within it (Rajabi et al. 2015), whereby the centered case is considered in the present work.

Initial Latin hypercube samples are incrementally optimized with a Simulated Annealing algorithm that consists of random pairwise- and coordinate-wise swaps. In an iterative process new samples are accepted if they improve a space-filling criterion or accepted with a certain probability if they do not bring an improvement (Morris and Mitchell 1995). Other approaches with deterministic sample selection, e.g. (Ye et al. 2000) or more elaborate optimization schemes such as the Enhanced Stochastic Evolutionary algorithm (Jin et al. 2003) have been suggested.

Recently, we proposed an adaptation to Latin hypercube sampling, named isovolumetric LHD, that places samples closer to design space boundaries (Kaps et al. 2021). The idea is to rethink the uniform strata that are created in each coordinate dimension for standard Latin hypercube sampling as nested hypervolume shells in the design space. These are created as shown with the colored regions in Fig. 1. Here, all shells are required to have identical volume, which is especially advantageous for higher dimensions, i.e. higher number of design variables. Applying this condition to a d-dimensional unit hypercube, with strata boundaries $p_i = \frac{i}{N}$ and sizes $a_j = \frac{1}{N}$ for standard LHS, yields the following new equations

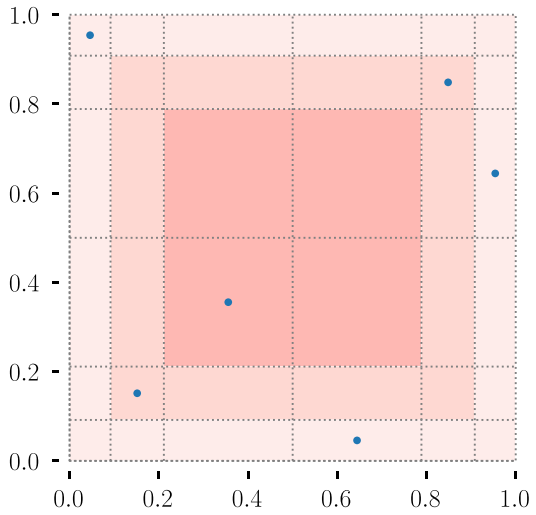

Fig. 1 Exemplary design of experiments for the isovolumetric Latin hypercube adaptation for six samples in two dimensions. Differently colored regions have the same area. (Kaps et al. 2021)

$$p_i = \begin{cases} 0.5\left(1 - \left(\frac{N_v+1-i}{N_v}\right)^{1/d}\right), & i \in \{1, 2, ..., N_v\} \\ 0.5\left(1 + \left(\frac{i-(N_v+1)}{N_v}\right)^{1/d}\right), & i \in \{N_v + 1, ..., N + 1\} \end{cases} \tag{1}$$

$$a_j = p_{j+1} - p_j, \quad j \in \{1, 2, ..., N\}. \tag{2}$$

Here, N is the number of samples to be drawn and $N_v = \frac{N}{2}$ the number of nested hypervolume shells. An exemplary isovolumetric Latin hypercube design for six samples in two dimensions is depicted in Fig. 1. The adaptation is easy to implement and does not increase computational requirements; however, it has been shown to increase the quality of DoEs in popular space-filling criteria such as potential energy (Audze and Eglais 1977) in mid- to high-dimensional situations, i.e. five and more dimensions (Kaps et al. 2021). One expected advantage in the current application is that training points associated to the surrogate models are closer to the design space boundaries. Thereby, the prediction of surrogate models will be more based on interpolation of samples as opposed to extrapolation.

This approach, named optimal isovolumetric Latin hypercube (OIVLH), is transferred to the context of optimization in crashworthiness applications in the present work.

3 Multi-fidelity efficient global optimization

In the following, a multi-fidelity EGO approach is introduced. In general, EGO techniques are based on kriging models, which have first been introduced by (Krige 1951;

Matheron 1963; Sacks et al. 1989) and are nowadays a popular choice for surrogate models. The idea of adaptively improving an initially created kriging model by means of an infill criterion was proposed by Jones et al. (1998). Common early variants of the approach are compared in Jones (2001).

Over the years, many surrogate models of variable fidelity have been suggested. Overviews can be found for example in Forrester et al. (2007) or Park et al. (2016). In the present work, hierarchical kriging is applied as the approach has been shown to yield better error estimations than other cokriging methods (Han and Görtz 2012). The relevant aspects of creating an HK model are summarized below, readers are referred to the original publication for detailed derivations (Han and Görtz 2012).

The idea is to first create a kriging model of the low-fidelity function that is subsequently used in the hierarchical kriging model for high-fidelity prediction. Based on these surrogate models, new sample points can be evaluated. The models are then adaptively improved. To that end, an infill criterion is introduced that can be maximized to determine the best location and fidelity level for a new adaptive sample.

Following, all steps of the outlined process are explained in details. The low-fidelity function is represented by a normal kriging model. Consider a random process for the low-fidelity (LF) function

$$Y_{lf}(\boldsymbol{x}) = \beta_{0,lf} + Z_{lf}(\boldsymbol{x}), \tag{3}$$

with $\beta_{0,lf}$ an unknown constant and $Z_{lf}(\boldsymbol{x})$ a stationary random process. For a d-dimensional problem, the low-fidelity kriging model is based on a set of sampling data $(\boldsymbol{S}_{lf}, \boldsymbol{y}_{S,lf})$ consisting of m_{lf} samples with input variable data $\boldsymbol{S}_{lf} \in \mathbb{R}^{m_{lf} \times d}$ and corresponding output $\boldsymbol{y}_{S,lf} \in \mathbb{R}^{m_{lf}}$.

To be able to construct the kriging predictor for new points, a correlation function, also named kernel, is needed to model the correlation between given sample points and new points. An overview of popular choices is for example given in Rasmussen and Williams (2005). In the present work, a squared-exponential kernel, also called Gaussian radial-basis function (RBF) kernel is utilized due to its smoothness and infinite differentiability:

$$R(\boldsymbol{x}^{(i)}, \boldsymbol{x}^{(j)}) = \prod_{k=1}^{d} \exp\left(-\theta_k |x_k^{(i)} - x_k^{(j)}|^2\right). \tag{4}$$

Here, θ_k denotes the kernel length scale. The kernel is called anisotropic, if there is a separate length scale for each design space dimension as in the equation above. In the present work, an isotropic kernel is chosen, where the hyperparameter $\theta_k = \theta$ is a scalar, i.e. independent of coordinate dimension. In fact, many different RBF kernels with similar properties than the Gaussian kernel exist. The focus in the present work lies solely on the latter for the sake of clarity.

The low-fidelity predictor for a new point $\boldsymbol{x}$ can then be written as

$$\begin{aligned} &\hat{y}_{lf}(\boldsymbol{x}) = \beta_{0,lf} + \boldsymbol{r}_{lf}^T(\boldsymbol{x}) \boldsymbol{R}_{lf}^{-1} (\boldsymbol{y}_{S,lf} - \beta_{0,lf} \boldsymbol{1}), \\ &\text{with} \quad \beta_{0,lf} = (\boldsymbol{1}^T \boldsymbol{R}_{lf}^{-1} \boldsymbol{1})^{-1} \boldsymbol{1}^T \boldsymbol{R}_{lf}^{-1} \boldsymbol{y}_{S,lf}, \\ &\text{and} \quad \boldsymbol{r}_{lf} = [R(\boldsymbol{x}, \boldsymbol{x}^{(1)}), ..., R(\boldsymbol{x}, \boldsymbol{x}^{(m)})] \in \mathbb{R}^{m_{lf}} \end{aligned} \tag{5}$$

where $\boldsymbol{r}_{lf}$ is the correlation vector between the sample data and the new point, $\boldsymbol{R}_{lf} \in \mathbb{R}^{m_{lf} \times m_{lf}}$ the correlation matrix representing correlation between sample data points and $\boldsymbol{1} \in \mathbb{R}^{m_{lf}}$ a column vector filled with ones.

Following the calculation of the initial sample data set, the kriging model is fitted by separately optimizing the kernel hyperparameter θ. Differential evolution (Storn and Price 1997) is selected for the optimization of the hyperparameters in the present work due to its simplicity and its good global search characteristics. More on hyperparameter optimizations can be found in Toal et al. (2008).

Next, the hierarchical kriging model can be constructed including the predictor of the low-fidelity model. Therefore, consider a random process corresponding to the high-fidelity function

$$Y(\boldsymbol{x}) = \beta_0 \hat{y}_{lf}(\boldsymbol{x}) + Z(\boldsymbol{x}). \tag{6}$$

Here, the low-fidelity predictor scaled by an unknown constant β_0 is a trend term and $Z(\boldsymbol{x})$ is a stationary random process. Given a d-dimensional sampling data set $(\boldsymbol{S}, y_S)$ containing m samples with input variable data $\boldsymbol{S} \in \mathbb{R}^{m \times d}$ and corresponding output $y_S \in \mathbb{R}^m$, the HK predictor for the high-fidelity function can be written as

$$\begin{aligned} &\hat{y}(\boldsymbol{x}) = \beta_0 \hat{y}_{lf}(\boldsymbol{x}) + \boldsymbol{r}^T(\boldsymbol{x}) \boldsymbol{R}^{-1} (\boldsymbol{y}_S - \beta_0 \boldsymbol{F}) \\ &\text{with} \quad \beta_0 = (\boldsymbol{F}^T \boldsymbol{R}^{-1} \boldsymbol{F})^{-1} \boldsymbol{F}^T \boldsymbol{R}^{-1} \boldsymbol{y}_S, \end{aligned} \tag{7}$$

where β_0 is a scaling factor indicating the correlation between high- and low-fidelity functions and $\boldsymbol{F} = [\hat{y}_{lf}(\boldsymbol{x}^{(1)}) ... \hat{y}_{lf}(\boldsymbol{x}^{(n)})]^T, \forall \boldsymbol{x}^{(i)} \in \boldsymbol{S}$ represents the low-fidelity prediction at high-fidelity sample points. $\boldsymbol{r} \in \mathbb{R}^m$ and $\boldsymbol{R} \in \mathbb{R}^{m \times d}$ are defined the same way as for the low-fidelity predictor above. The factor $\boldsymbol{R}^{-1}(\boldsymbol{y}_S - \beta_0 \boldsymbol{F})$, named $\boldsymbol{V}_{HK}$ in the original publication, does not depend on the untried point $\boldsymbol{x}$ and can thus be calculated at model fitting time. The mean squared error (MSE) of the HK prediction is given with σ^2, the process variance of $Z(\boldsymbol{x})$

$$\text{MSE}(\hat{y}(x)) = \sigma^2 (1.0 - r^T \boldsymbol{R}^{-1} r + \left[r^T \boldsymbol{R}^{-1} \boldsymbol{F} - \hat{y}_{lf}\right]^2 \left(\boldsymbol{F}^T \boldsymbol{R}^{-1} \boldsymbol{F}\right)^{-1}). \tag{8}$$

Once the initial HK model is built, it is adaptively improved using an infill criterion to determine the ideal position of new samples. In multi-fidelity applications two options exist: a 'classic' single-fidelity infill criterion or a multi-fidelity criterion. Among the former, expected improvement

(Jones et al. 1998) is the most popular method. The interested reader is referred to Jones (2001) for other common techniques. The disadvantage of a single-fidelity criterion is that only high-fidelity samples can be considered adaptively. Hence, they are not further discussed here. In the present work, the so-called variable-fidelity expected improvement criterion (Zhang et al. 2018a) is utilized. It is defined at location $\boldsymbol{x}$ and fidelity level L as

$$EI_{vf}(\boldsymbol{x}, L) = \begin{cases} s(\boldsymbol{x}, L)[u\boldsymbol{\Phi}(u) + \phi(u)], & \text{if} \quad s(\boldsymbol{x}, L) > 0 \\ 0, & \text{if} \quad s(\boldsymbol{x}, L) = 0 \end{cases}, \tag{9}$$

where $u = \frac{y_{min} - \hat{y}(\boldsymbol{x})}{s(\boldsymbol{x}, L)}$ and y_{min} as the currently best observed feasible high-fidelity function value. The term $s(\boldsymbol{x}, L)$ denotes the uncertainty of the HK model. The previously introduced scaling factor between fidelity levels β_0 is used here to model the uncertainty in high-fidelity prediction caused by the low-fidelity predictor

$$s^2(\boldsymbol{x}, L) = \begin{cases} \beta_0^2 \cdot \text{MSE}(\hat{y}_{lf}(\boldsymbol{x})), & L = 0 \text{ low-fidelity} \\ \text{MSE}(\hat{y}(\boldsymbol{x})), & L = 1 \text{ high-fidelity} \end{cases}. \tag{10}$$

Here, $\text{MSE}(\hat{y}(\boldsymbol{x}))$ and $\text{MSE}(\hat{y}_{lf}(\boldsymbol{x}))$ are the MSEs of the high- and low-fidelity kriging predictors, respectively. $\boldsymbol{\Phi}(\bullet)$ and $\phi(\bullet)$ in Eq. (9) represent the cumulative distribution and probability density functions of the standard normal distribution, respectively. The two summands in Eq. (9) can be identified with exploration and exploitation. The first term $\big(y_{min} - \hat{y}(\boldsymbol{x})\big)\boldsymbol{\Phi}(u)$ is dominated by improving the solution $\hat{y}(\boldsymbol{x})$ and thus represents exploitation, while the second term $s(\boldsymbol{x}, L)\phi(u)$ represents exploration because it is dominated by the solution uncertainty $s(\boldsymbol{x}, L)$.

Due to the highly multi-modal nature of the EI functions, differential evolution (Storn and Price 1997) is selected for optimization of the infill criterion in the present work.

Notably, the VF-EI formulation is similar to the original EI definition (Jones et al. 1998); however, in addition the dependency on the fidelity level is introduced. In terms of multi-fidelity optimization the VF-EI criterion is comparable to the augmented EI criterion proposed by Huang et al. (2006). Both describe the expected improvement of the high-fidelity function with respect to adaptive samples on both fidelity levels. To that end, augmented EI contains two factors that are multiplied with a standard EI for the high-fidelity function. A more detailed discussion about the differences between VF-EI and augmented EI can be found in Zhang et al. (2018a). Here, we use VF-EI as it is free of empirical parameters and is as such more intuitive.

4 Model order reduction

The proposed multi-fidelity approach exploits a data-driven model order reduction (MOR) technique to create the low-fidelity model. As an analytical simplification is not available for non-linear problems, a data-driven approach is commonly used (Sirovich 1987). Therefore, an online and offline phase are introduced, whereby the offline phase can be understood as the counter part to the DoE. In particular, the surrogate model is created during the offline, also called training phase. Afterwards the simplified model can be evaluated for multi-fidelity analysis in the online phase.

4.1 Training phase

Within the training phase, a set of full order simulations is created, whereby all resultants are stored as snapshots $x_i \in \mathbb{R}^N$ with N degrees of freedom. Combining the training simulations to a so-called snapshot matrix $\boldsymbol{A} \in \mathbb{R}^{N \times n}$, with n the number of collected snapshots, a reduced subspace and its projection matrix can be computed. Through the Singular Value Decomposition (SVD), also referred to as thin SVD (Golub and Van Loan 2013) the snapshot matrix $\boldsymbol{A}$ can be represented by the left-singular vectors $\boldsymbol{U} \in \mathbb{R}^{N \times n}$, the diagonal matrix $\Sigma \in \mathbb{R}^{n \times n}$ containing non-negative singular values σ_i in descending order and the right-singular matrix $\boldsymbol{Z} \in \mathbb{R}^{n \times n}$. Thus, the columns of the matrix $\boldsymbol{U}$ are the eigenvectors of $\boldsymbol{A}\boldsymbol{A}^T$.

$$\boldsymbol{A} = \boldsymbol{U}\Sigma\boldsymbol{Z}^T \approx \boldsymbol{U}_k\Sigma_k\boldsymbol{Z}_k^T = \boldsymbol{V}\Sigma_k\boldsymbol{Z}_k^T. \tag{11}$$

Moreover, the matrix $\boldsymbol{A}$ is approximated by truncating its parts to a rank $k \leq n, m$, such that $\boldsymbol{U}_k \in \mathbb{R}^{N \times k}$, $\Sigma_k \in \mathbb{R}^{k \times k}$ and $\boldsymbol{Z}_k \in \mathbb{R}^{k \times N}$, respectively. To define the reduced basis of the subspace, $\boldsymbol{V} := \boldsymbol{U}_k \in \mathbb{R}^{N \times k}$ is further utilized as the projection matrix. In practice, the optimal rank k is not known beforehand and $k = \min \tilde{k}$ with

$$\frac{\|\boldsymbol{A} - \boldsymbol{U}_{\tilde{k}}\Sigma_{\tilde{k}}\boldsymbol{Z}_{\tilde{k}}^T\|_F}{\|\boldsymbol{A}\|_F} = \sqrt{\frac{\sum_{i=\tilde{k}+1}^{k} \sigma_i^2}{\sum_{i=1}^{k} \sigma_i^2}} \leq \epsilon \tag{12}$$

can be found for an error threshold ϵ. In other words, the matrices are truncated by $\tilde{k}$ such that an energy cutoff ratio μ is maintained:

$$\mu = \frac{\sum_{i=1}^{k} \sigma_i^2}{\sum_{i=1}^{n} \sigma_i^2}. \tag{13}$$

For large-scale matrices the evaluation of the full SVD is cost intensive as its complexity is in the range $O(n^2)$ with n as the number of snapshots. Therefore, multiple approaches (Bach et al. 2019; Phalippou et al. 2020) to efficiently

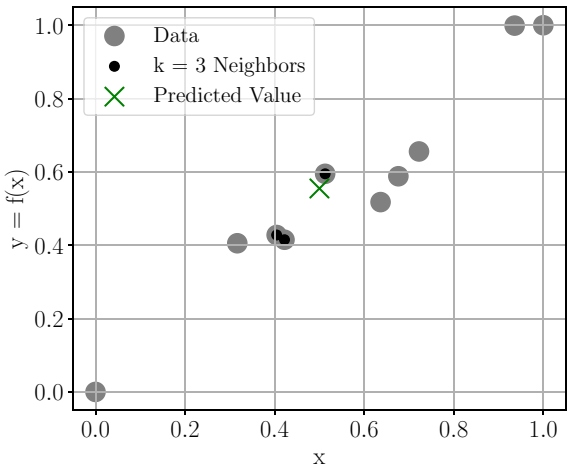

Fig. 2 One-dimensional example of regression based on k-nearest neighbors with k = 3. The 'X' marks the prediction at $x = 0.5$ according to the three nearest previously known points marked with black dots

compute the truncated projection matrix, such as randomized or incremental SVD techniques, e.g. (Oxberry et al. 2017), can be applied. Here, an incremental SVD algorithm (Baker et al. 2012)[1] is utilized. To save computational resources, the snapshot matrix $\boldsymbol{A}$ is built up incrementally. Therefore, $\boldsymbol{A}$ is divided into batches, which are added to the projection matrix $\boldsymbol{V}$. The SVD is computed within every iteration via QR decomposition and its truncation rank k is evaluated. The batch is added to the global $\boldsymbol{V}$ and Σ before the algorithm steps into the next iteration with new snapshots. Readers are referred to Baker et al. (2012) for a detailed algorithm description. In summary, a complexity of $O(mnk)$ with m full order unknowns can be reached.

After the construction of the reduced subspace a regression or interpolation approach is introduced. The metamodel represents the unknown in the reduced space and is therefore restricted to the physical solution spanned in the subspace. In addition, the number of unknowns n is drastically reduced, as $k << n$. Within this work the k-nearest neighbor (kNN) approach is utilized as an interpolation technique, but any other machine learning approach such as polynomial regression function, Gaussian process regression or neural networks could be used (Swischuk et al. 2019). k-nearest neighbor is mainly known as a classification technique, but can also be applied as a regression model. The function $y = f(x)$ is interpolated by the k-nearest neighbors of x as shown in Fig. 2 for a one-dimensional example. Here, three neighbors of x and their distances are evaluated to estimate $f(x)$.

[1] Implemented in IncPACK library.

4.2 Online phase

After the construction of the low-fidelity model is completed, it is evaluated in the online phase. Recalling the truncated singular value decomposition, the columns of the matrix $\boldsymbol{V} \in \mathbb{R}^{N \times k}$ can be interpreted as the basis vectors $\boldsymbol{v}$ of the subspace.

$$V = \begin{bmatrix} \boldsymbol{v_1} & \boldsymbol{v_2} & \cdots & \boldsymbol{v_k} \end{bmatrix} \tag{14}$$

The full displacement vector is estimated by the linear combination of the basis vectors $\boldsymbol{v}$, whereby every basis is weighted by a scalar value σ_i.

$$\boldsymbol{x} \approx \sum_{i=1}^{k} \boldsymbol{v_i} \sigma_i \tag{15}$$

The kNN approach provides an estimation for each σ_i, the degrees of freedoms of the subspace.

5 Proposed optimization scheme

In the present work the performance of multi-fidelity optimization schemes in crashworthiness applications is investigated. To that end, a multi-fidelity optimization method that integrates a non-intrusive reduced order model into the hierarchical kriging surrogate is proposed. The schematic process of this approach is shown in Fig. 3 following the baseline multi-fidelity scheme proposed by Zhang et al. (2018a). Initially, DoE is performed as described in Sect. 2 on both, the high- and the low-fidelity level separately, usually generating significantly more low- than high-fidelity samples. OLH and OIVLH are both applied in the present work, to assess the impact on optimization performance. All high-fidelity samples are then calculated. For memory efficiency, a reduced order model is incrementally created during the high-fidelity evaluations as introduced in Sect. 4. Following all initial high-fidelity simulations and as the main adaptation to the originally proposed scheme, the reduced basis is evaluated and the k-nearest neighbor regression model is trained for predictions. The reduced order model is evaluated on the initially created low-fidelity DoE points. From the results, the initial low-fidelity kriging model and subsequently the hierarchical kriging model are fitted. For adaptive improvement, the infill criterion (i.e. VF-EI) is maximized separately on both fidelity levels. Depending on which level yields the better results the next adaptive sample can be either low-fidelity (L=0 in Fig. 3) or high-fidelity (L=1). The objective function is evaluated for the respective new adaptive sample and the kriging model(s) are updated. Then, another infill criterion optimization is started and the iterative improvement continues.

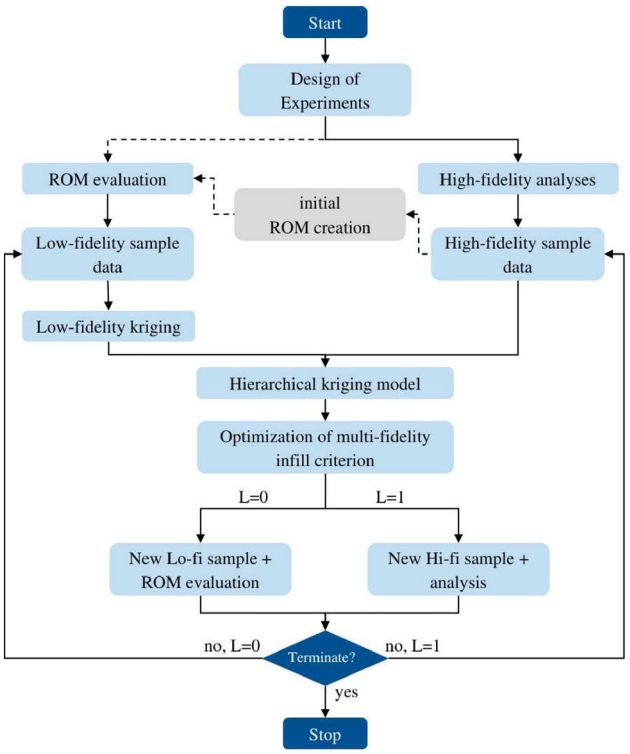

Fig. 3 Schematic representation of the proposed optimization scheme to integrate reduced order model (ROM) into a multi-fidelity optimization based on hierarchical kriging and variable-fidelity expected improvement (compare Fig. 2 in Zhang et al. (2018a)). The main difference to the originally proposed scheme is the utilization of initial high-fidelity sample data for ROM creation (marked by the grey box). Not shown is the varying method of the design of experiment performed in the present work

Three different criteria determine the termination of the algorithm. First, a minimum allowable value for the maximized infill criterion is specified (here $IC_{th} = 10^{-5}$). Second, a maximum number of high-fidelity evaluations is specified. Third, a maximum total number of objective evaluations can be specified, which in single-fidelity optimizations is equivalent to the second criterion. Values specified for the criteria are given in Sect. 6 with the respective examples. The first criterion can be interpreted as convergence of the algorithm to an optimal point with little improvement possibilities. The other two criteria are used to represent time restrictions on the optimization runs, i.e. an estimation of the maximum run time.

The proposed scheme is implemented in an in-house Python code. The DoE part of the algorithm is based on Kaps et al. (2021). The implementation of the incremental SVD technique in the present work is adjusted from Baker et al. (2012) and Bach et al. (2019). HK model generation and kernel implementation are based on the scikit-learn library in Python (Pedregosa et al. 2011).

Table 1 Overview of different optimization schemes applied in the following crashworthiness examples. All techniques are referred to by the abbreviation given in the first column

Method Name	DoE Method	LF Model	Surr. Model	Infill Crit.
SF (base)	OLH	–	Kriging	EI
SF + OIVLH	OIVLH	–	Kriging	EI
MF (base)	OLH	Coarse FE	HK	VF-EI
MF + OIVLH	OIVLH	Coarse FE	HK	VF-EI
MF (MOR)	OLH	ROM	HK	VF-EI
MF (MOR) + OIVLH	OIVLH	ROM	HK	VF-EI

6 Crashworthiness application problems

In the following, the presented optimization scheme is compared to a baseline multi-fidelity scheme proposed by Zhang et al. (2018a) as well as a single-fidelity scheme based on a high-fidelity model and EI. Additionally, each of the techniques is assessed with a standard OLH sampling as well as the OIVLH method that places samples closer to design space boundaries. These overall six approaches are each evaluated for two crashworthiness problems in terms of result quality and computational requirements. Each optimization run is repeated ten times to ensure reliability of the assessment. An overview of the compared methods and nomenclature is given in Table 1. All analyses are performed on the identical hardware using the explicit finite element software LS-Dyna in its MPP version distributed on eight cores. All objective function values referred to below are based on the high-fidelity model unless explicitly stated otherwise.

6.1 Side sill impact problem

The initial problem is a crash model representing the side sill of a car under side pole impact as depicted in Fig. 4. Both ends of the side sill are fixed, and the pole represented by a cylindrical rigid body with radius 35mm has a prescribed initial velocity of 36 km/h and a mass of 86 kg. Further modeling information as well as all material parameters are summarized in "Appendix A". The simulation is terminated when the impactor stops or—as a backup—after 40 ms.

The design variables of the optimization problem are the thicknesses t_i of the five horizontal reinforcement ribs in the interior of the side sill (compare detail in Fig. 4). The objective is to minimize the mass of the side sill, i.e. the mass of the horizontal ribs, while keeping the lateral intrusion below $u_{\text{allow}} = 50$ mm. Applying the penalty method with a penalty factor $p = 3.75$, the deformation constraint is included into the objective function. The complete optimization problem can then be formulated as

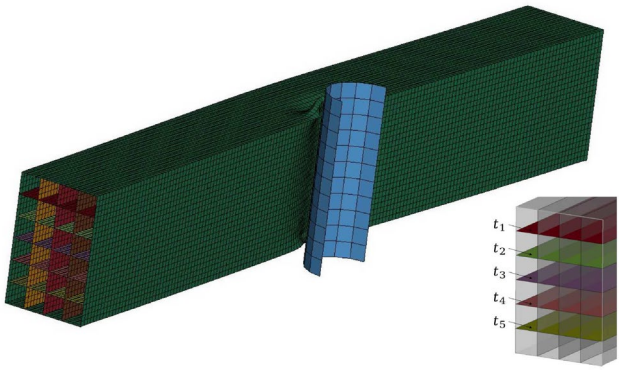

Fig. 4 Side sill impact problem: Both ends of the component are fixed and the impactor represented by a cylindrical rigid body has a prescribed velocity and mass. Detail in the bottom right shows the five design variables of the optimization

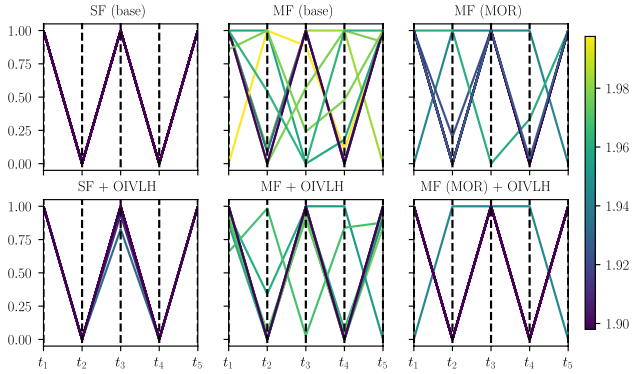

Fig. 5 Side sill impact problem: Parallel coordinates plot comparing results of ten repetitions for six different approaches. Design variable values on the *y*-axis are normalized. The color scale indicates objective value of the respective results (lower is better)

$$\min_{\boldsymbol{t}} \quad f(\boldsymbol{t}) = m_{\text{ribs}} + p \cdot \max(c(\boldsymbol{t}), 0), \quad \text{with } p = 3.75, \tag{16a}$$

$$\text{subj. to} \quad c(\boldsymbol{t}) = \frac{u_{\max}}{u_{\text{allow}}} - 1 \leq 0, \quad u_{\text{allow}} = 50\,\text{mm}, \tag{16b}$$

$$\text{where} \quad 0.5\,\text{mm} \leq t_i \leq 3.0\,\text{mm}, \quad i = 1, ..., 5. \tag{16c}$$

The model depicted in Fig. 4 represents the high-fidelity model with an element size of approximately 5mm in each direction. For comparison, the low-fidelity model with the element size doubled to 10mm is depicted in "Appendix A". Thus, the speed-up factor of the low-fidelity model is about five to six. The number of initial high-fidelity samples for the single-fidelity case is set to 50. For all multi-fidelity approaches, the number of initial samples is 20 and 120 for high- and low-fidelity models, respectively. In this example, the only termination criterion specified is a threshold value for the respective infill criterion, i.e. EI for *SF* methods and VF-EI for *MF* methods, of $IC_{th} = 10^{-5}$.

The reduced order model is constructed with 20 training simulations sampled by the respective method. With the truncation energy of $\mu = 0.9999$ a subspace containing approximately $k = 4$ basis vectors is computed. Moreover, the kNN regressor using 5 neighbors is trained for the unknowns in the reduced subspace. Eventually, a single evaluation of the reduced order model has a speed-up factor of 150 in comparison to the high-fidelity simulation.

In Fig. 5, optimization results for the six different approaches are compared with a parallel coordinates plot. On the x-axes all five design variables are listed while the y-axes represent their normalized ranges. Each curve illustrates an optimized design, whereby the color indicates the respective objective function value. The problem seems to have a clear global optimum with $t_1 = t_3 = t_5 = 3.0$mm and $t_2 = t_4 = 0.5$mm. Distributing three horizontal ribs with the maximum allowable thickness across the whole height of the component and having the two ribs in between vanish results in the best compromise between low weight and sufficiently low impactor intrusion. The respective objective value $f(\boldsymbol{t}) = 1.898$ is found in the majority of single-fidelity and *MF (MOR)* repetitions independent of the chosen DoE method. For this set of input variables, the maximum impactor displacement of the high-fidelity model is $u_{\max} = 50.6$ mm. The specified constraint $u_{\text{allow}} = 50$mm is violated by 1.2%, which is considered acceptable in this exemplary problem. All compared results have a similar level of constraint violation, which is not further investigated to focus on the multi-fidelity optimization itself.

Individual results for single-fidelity, i.e. high-fidelity, EGO show a low variation for different DoE methods and the majority of repetitions terminate at the global optimum. For *MF (base)* and *MF + OIVLH*, results vary quite significantly and only three of the overall 20 runs converge to the global optimum. Many of the evaluations terminate at points rather close to the global optimum so that the objective function value is only a few percents of the optimal value. Notably, more *MF + OIVLH* analyses get close to the global optimum than *MF (base)*. The *MF (MOR)* approaches yield more consistent results than *MF (base)* and *MF + OIVLH*, converging to the optimum for a total of 14 out of 20 assessments across both DoE methods, with two more runs being very close to the optimum. Overall, the OIVLH-based approaches yield a higher consistency within the multi-fidelity schemes. OIVLH places samples significantly closer to design space boundaries. Therefore, the reduced order low-fidelity model being created from the high-fidelity samples is based more on interpolation between samples than on extrapolation.

In a further step, the quality of the two varying types of low-fidelity models is assessed. To that end, the low-fidelity

Table 2 Side sill impact problem: Evaluation of low-fidelity model quality. For all optimization runs, low-fidelity models are evaluated for the respective optimum and maximum impactor displacements are compared to those of the high-fidelity model [see Eqs. (17) and (18)]

Method	e_{abs} [mm]	e_{rel} [%]
MF (base)	3.22	6.3
MF + OIVLH	3.43	6.5
MF (MOR)	2.76	5.3
MF (MOR) + OIVLH	2.15	4.1

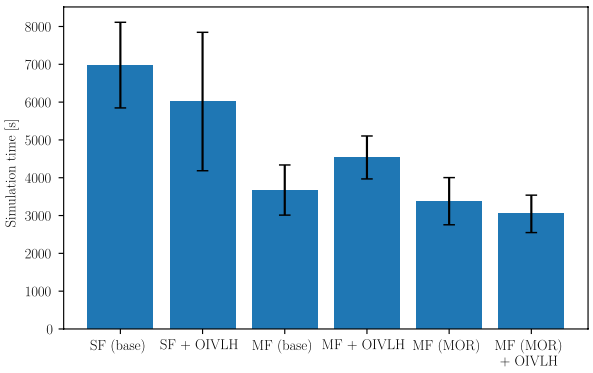

Fig. 6 Side sill impact problem: Average run times for all compared optimization approaches in seconds. Also shown is the standard deviation of the optimization run time

models are evaluated at the respective determined optimum. The maximum displacement of the impactor d_{max} is considered as a metric to compare high- (HF) and low-fidelity (LF) models. This metric is chosen as it directly represents the constraint and—because the mass of the component can analytically be calculated from the given design variables—it also implies the objective function of the optimization problem. As such it estimates the accuracy of the low-fidelity models in the present example. The error metrics are defined as

$$e_{abs} = |d_{max,hf} - d_{max,lf}|, \tag{17}$$

$$e_{rel} = \frac{|d_{max,hf} - d_{max,lf}|}{|d_{max,hf}|}, \tag{18}$$

for the absolute difference e_{abs} and the relative difference e_{rel} between fidelity levels, respectively. Results for all methods are listed in Table 2. Each of the listed values represents the mean value of ten evaluations. For *MF (base)* and *MF + OIVLH* the low-fidelity model is identical for all evaluations, while for the MOR based methods, the low-fidelity model depends on the initial high-fidelity samples (compare Fig. 3). Both types of low-fidelity models approximate the (maximum) impactor displacement sufficiently well with an error of 4-6%. The error indicators for the reduced order low-fidelity models are slightly better, i.e. lower, compared to those of the coarse simulation models. For the latter, the use of OIVLH sampling does not significantly impact the low-fidelity result quality. However, for *MF (MOR) + OIVLH* the low-fidelity model is slightly more accurate than for *MF (MOR)* which may explain the performance difference between the two methods. It also indicates that the increased interpolation share for OIVLH sampling can in fact increase the ROM quality.

Keeping in mind the quality of the results, the computational requirements for all approaches are evaluated. Average run times along with their respective standard deviations are listed in Fig. 6 for all techniques. The larger standard deviations for *SF (base)* and *SF + OIVLH* compared to the other four methods are explained by a single outlier in each of the methods. In both cases, the algorithm finds the global optimum in a reasonable number of iterations but then requires many adaptive samples to reach the specified termination criterion. So both outliers can be explained by the somewhat unrealistic definition of termination criterion here, where no maximum allowed number of iterations was specified. As the standard deviations in all methods are similar apart from that, the following comparisons are focused on the average times. *SF (base)* is taken as a baseline for all comparisons. Without changing the optimization itself, switching the DoE to OIVLH reduces 14% of computation time in this problem, while maintaining result quality.

Using an *MF* approach with a coarser low-fidelity model lowers the computational cost about 47% and 35% for OLH and OIVLH, respectively. In fact, this is the only case in the present work, where OIVLH requires more computational time than OLH. The reason here is the same as for the outliers outlined above. Both *MF (base)* and *MF + OIVLH* find the respective optimum after a similar number of high-fidelity iterations, but the latter variant requires a few more adaptive iterations than the former to reach the termination criterion. The work load to create the low-fidelity model is not considered here, however for complex models this is an additional time intensive step. Especially, when considering that the low-fidelity model may not be needed otherwise. Contrary to that, both *MF (MOR)* options do not require the manual creation of a low-fidelity model. They reduce computation times by about 51% and 56% for *MF (MOR)* and *MF (MOR) + OIVLH*, respectively. The speed-up of *MF (MOR)* compared to the other *MF* techniques can be explained by the significantly faster evaluation times of the reduced order low-fidelity models compared to the coarse simulation model. In comparison the *MF (MOR) + OIVLH* approach yields the best overall improvement for the side sill impact problem. It saves on average more than 50% computation time compared to *SF (base)* while maintaining an acceptable level of accuracy.

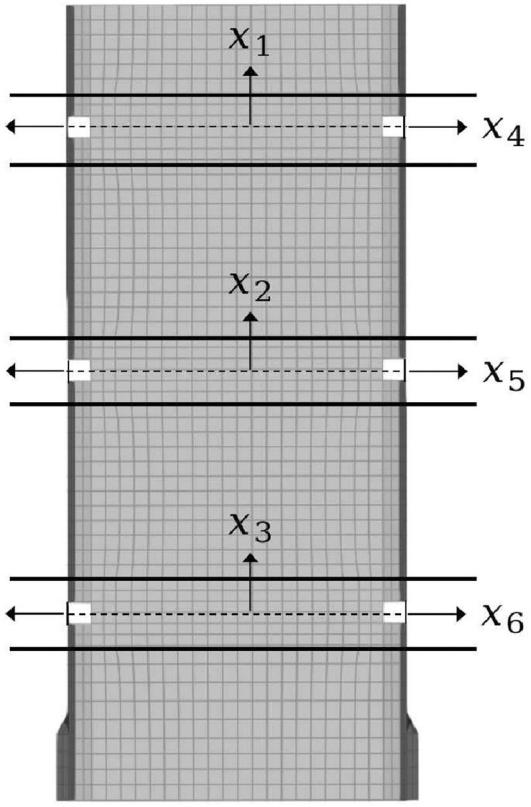

Fig. 7 Frontal impact problem of a crash box impacted by a planar rigid wall: The lower end is fixed, the impactor moving from the top downwards has a prescribed mass and velocity. Design variables are the vertical trigger positions as well as depths of the three triggers in the crashbox. The latter are realized by shifting the respective element rows in or against the direction indicated by the respective arrows next to x_4, x_5 and x_6

6.2 Frontal impact problem

A shape optimization problem of the frontal impact of a crash box, as depicted in Fig. 7 is presented as a second application problem for the suggested multi-fidelity scheme. For the high-fidelity model, an element length of about $4-5$mm is specified, while for the low-fidelity model, the element length is in the region of 10mm. This yields a high-fidelity model with 4,928 elements and a low-fidelity model with 1,296 elements. The planar impactor crushing the component from the top has a prescribed mass of 300kg and an initial velocity of 30 km/h. The impactor is modeled as a rigid body, and the crash box is constructed as a tube with a steel-like material and a piecewise linear plasticity model. Exact material parameters are listed in "Appendix B". For the contact formulation, the LS-Dyna '*CONTACT_AUTOMATIC_SINGLE_SURFACE' is applied. The simulation is terminated when the impactor stops or after 45ms.

The crash box of the optimization study and its design variables are depicted in Fig. 7. The first three design variables are the vertical positions of the triggers in the model. The corner elements of the triggers are deleted to increase numerical stability. Three additional design variables are the depths of the triggers, i.e. the respective element rows are shifted in or against the arrow directions indicated in the figure next to the variables x_4, x_5 and x_6. The configuration depicted in Fig. 7 represents the setup for $\boldsymbol{x} = 0$ for all design variables. Model generation features are realized using ANSA preprocessor.

Throughout the optimization analyses, the mass of the crash box remains approximately constant as the effect of design variables is negligibly small. The objective function is chosen as the load uniformity, also called peak amplification, of the force-displacement curve. It is defined as the peak force F_{max} divided by the mean force F_{mean} of the complete force-displacement curve measured at the rigid body impactor. The optimization problem can then be formulated as

$$\min_{\boldsymbol{x}} \quad f(\boldsymbol{x}) = \frac{F_{\text{max}}}{F_{\text{mean}}}, \tag{19a}$$

$$\text{where} \quad -10\,\text{mm} \le x_i \le 10\,\text{mm}, \quad i = 1,2,3, \tag{19b}$$

$$-4\,\text{mm} \le x_i \le 4\,\text{mm}, \quad i = 4,5,6. \tag{19c}$$

The processing time of the classical low-fidelity model is one fourth of the high-fidelity computation time. The number of initial samples is accordingly set to 60 in single-fidelity analysis, and 30/90 for high-/low-fidelity samples in the multi-fidelity methods. For this problem, all possible termination criteria presented in Sect. 5 are specified and respective values are listed in Appendix Table 7. To construct the snapshot matrix for the reduced order model, 30 initial high-fidelity samples are utilized. With the truncation energy of $\mu = 0.9999$, a subspace with approximately $k = 15$ bases is computed. Moreover, the kNN regressor using 5 neighbors is trained for the unknowns in the reduced subspace. A single evaluation of the reduced order model has a speed-up factor of 50 to 100 in comparison to the high-fidelity simulation.

To investigate the convergence of the optimization schemes, Fig. 8 shows the best current objective values in each iteration for all (high-fidelity) evaluations of *SF (base)* (grey lines) and *MF (MOR) + OIVLH* (black lines). These two methods are representatively chosen from all investigated methods for the purpose of clarity. The adaptive phase of the algorithm starts after 60 evaluations for the single-fidelity case and 30 evaluations for the multi-fidelity case. Both approaches reach objective values below 3.4, i.e. close to the final optimum, mostly within ten adaptive high-fidelity evaluations. Afterwards only slight improvements are achieved.

In addition, the termination criteria can give valuable insights to the performed optimization studies. Here, the observations are contrary to those of the previous lateral impact example, where all optimization analyses are

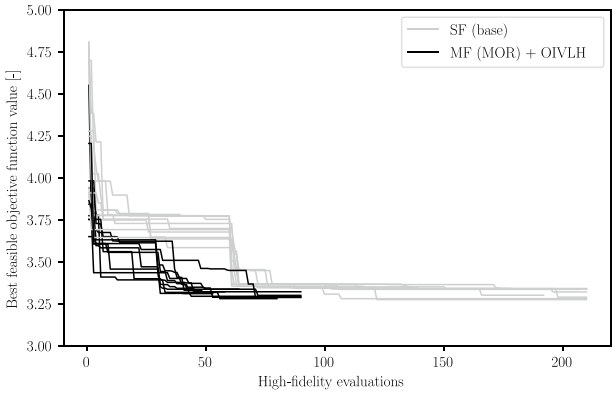

Fig. 8 Frontal impact problem: Convergence comparison for *SF (base)* and *MF (MOR) + OIVLH*. Depicted is the best current objective function value over the number of high-fidelity evaluations for each separate optimization run. Grey and black lines represent *SF (base)* and *MF (MOR) + OIVLH* versions, respectively

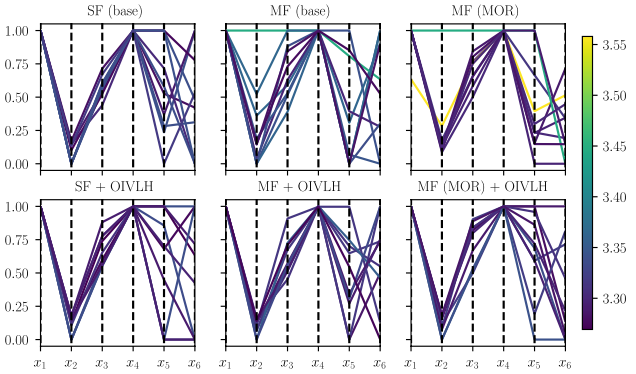

Fig. 9 Frontal impact problem: Parallel coordinates plot comparing results of ten repetitions for six different approaches. Design variable values on the *y*-axis are normalized. The color scale indicates objective value of the respective results (lower is better)

terminated by the threshold infill criterion. A majority of analyses for the crash box example terminate after reaching the maximum number of allowed iterations. Of course, there is an argument to be made that these optimization runs may not be fully converged. However, as seen in Fig. 8 and because some runs do actually terminate due to IC_{th}, the authors believe that this is not the case. A maximum allowable number of iterations also represents a situation more akin to a practical application case. It matters more to find an acceptable result in a given time as opposed to the best result in as much time as necessary.

A comparison of the optimization results for the presented methods is depicted in Fig. 9. Low objective function values of slightly below 3.3 depend on x_1 on its upper limit of 10mm, x_2 around its lower limit of −10mm and x_3 in a mid region albeit slightly above 0mm. Only the first of the trigger depths x_4, x_5 and x_6, which is found close the maximum of 4mm throughout all methods, seems to significantly impact the optimization results. A significant share of the crash energy is absorbed in the first fold, i.e. the one controlled by x_1 and x_4. It usually also contains the total maximum in the force-displacement curve $F_{\max}$. To that end, it appears reasonable that those two design variables appear to always converge to similar values, while the others, especially x_5 and x_6, may vary between optimizations.

All compared methods yield rather similar results in terms of objective function values except for a total of three runs in *MF (base)* and *MF (MOR)*. In these, the best objective value is up to 10% off the best overall result because the algorithm terminates in a local optimum. For the *SF* approaches, OIVLH appears to not affect result quality or consistency. In the multi-fidelity setups however, OIVLH sampling reduces the number of outliers compared to *MF (base)* and *MF (MOR)*, respectively. All variants utilizing OIVLH sampling as well as the baseline single-fidelity EGO yield very similar results.

Table 3 Frontal impact problem: Evaluation of low-fidelity model quality. For all optimization runs, low-fidelity models are evaluated for the respective optimum and maximum impactor displacements are compared to the high-fidelity model [see Eqs. (17) and (18)]

Method	e_{abs} [mm]	e_{rel} [%]
MF (base)	16.03	11.0
MF + OIVLH	22.28	15.4
MF (MOR)	8.72	6.0
MF (MOR) + OIVLH	4.29	3.0

In a further step the quality of low-fidelity models is evaluated as done for the previous example. Here the same error metric is chosen mainly for two reasons. First, as the impactor kinetic energy remains constant, the maximum impactor displacement is directly related to the mean force F_{mean} which is part of the objective function. Second, having the same comparison metric as in the previous example allows for comparisons of low-fidelity model accuracy between the two examples. Table 3 lists mean values for the differences in maximum impactor displacement between low- and high-fidelity models in the different methods [compare Eqs. (17) and (18)]. In this example, the coarse simulation model of *MF (base)* and *MF + OIVLH* has a significantly larger error value compared to the ROMs. Due to the highly nonlinear nature of frontal impact simulation, the mesh size has a high impact on the crushing behaviour of the component. As the ROM-based low-fidelity models utilize the high-fidelity model mesh for learning and predictions, they are not affected and show better accuracy compared to the coarse low-fidelity model. The present example confirms that the application of OIVLH for reduced order models increases the prediction accuracy. The results of *MF (base)* and *MF + OIVLH*, as listed in Table 3 differ mainly due

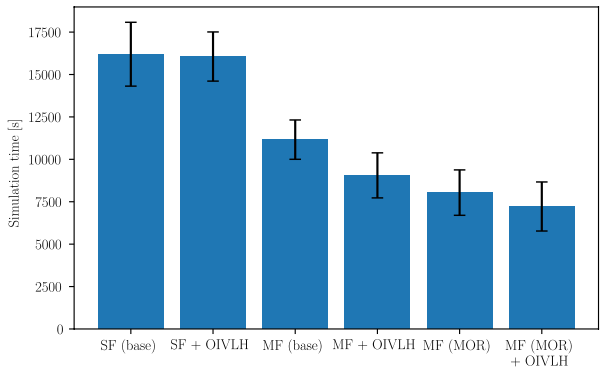

Fig. 10 Frontal impact problem: Average run times for all compared optimization approaches in seconds. Also shown is the standard deviation of the optimization run time

to one single outlier in *MF + OIVLH*, where the low-fidelity model predicts a significantly earlier stop of the impactor, thus inflating the error measure. Overall, the low-fidelity accuracy of the two methods is similar, which is expected as the choice of DoE should not have an impact on the simulation model.

Computational requirements are again compared for all different methods using the mean run time of each optimization. The averaged processing times for all techniques are plotted in Fig. 10. Regarding the varying EGO approaches, the findings here are highly similar to those of the previous problem. Compared to *SF (base)*, *MF (base)* and *MF + OIVLH* yield about 30-45% speed-up while *MF (MOR)* and *MF (MOR) + OIVLH* result in 50-55% time reduction. Here, the use of OIVLH over OLH shows slight time benefits across all variants. Notably, the time benefit *SF + OIVLH* yields over *SF (base)* is significantly smaller than for the previous example (compare Fig. 6). This is due to the difference in applied termination criterion between the examples.

Overall, results for the present application example closely match those for the side sill impact example presented above. The *MF (MOR) + OIVLH* scheme performs best with time-savings of more than 50% compared to *SF (base)*. Here, all approaches utilizing OIVLH perform better than respective OLH variants.

7 Conclusions

In the present work, a multi-fidelity efficient global optimization based on recently proposed hierarchical kriging and variable-fidelity expected improvement is applied to crashworthiness examples and its performance is investigated. Additionally, two adaptations to the scheme regarding initial design of experiments and the choice of low-fidelity model are proposed. For the former, a recently developed variant of Latin hypercube sampling is chosen that places samples closer to design space boundaries and thus allows for more interpolation instead of extrapolation in surrogate models. For the latter, a non-intrusive model order reduction scheme is applied as low-fidelity model as it integrates nicely into the existing multi-fidelity optimization scheme. All different optimization schemes are investigated on two crashworthiness application examples: one side sill impact size optimization and one frontal impact shape optimization. Already with the rather small problems presented here, results show that multi-fidelity optimization is capable of reducing computational costs of the optimizations significantly while not compromising result quality. Both proposed adaptations independently and especially combined further reduce computation times and also increase result quality compared to the baseline multi-fidelity optimization. Especially the use of non-intrusive reduced order modeling techniques is promising as it removes the need to (manually) create an additional low-fidelity model. Together, a speed-up factor of two in the optimization with next to no influence on result quality is observed.

The problems shown in the present work represent rather small examples with a low number of design variables. Based on the works introducing OIVLH (Kaps et al. 2021) and previous investigations on the projection of large-scale systems (Bach et al. 2019), it seems reasonable to assume that the advantages of the proposed schemes grow as the model size and number of design variables increase.

Multi-fidelity optimization is a wide topic with a variety of different applications and many imaginable adjustments to be explored. Based on the promising results of the present work we have collected some topics and questions that we believe to be interesting for future work:

- In the present work all DoEs are performed separately for different fidelity levels and with no connection between levels. It seems only reasonable to use a multi-fidelity DoE scheme if the initial samples are combined into a multi-fidelity surrogate. Multi-fidelity sampling approaches proposed so far, require the high-fidelity DoE to be a subset of the low-fidelity DoE. It could be investigated, how these approaches perform for multi-fidelity optimizations shown here and if methodological improvements can be achieved.
- We believe the potential of the proposed multi-fidelity scheme(s) should be confirmed in further studies on more complex larger crashworthiness application problems and other fields of applications.
- A big challenge in practical applications is robustness with regards to both the method as well as the objective function. An optimization method should produce consistent results for given inputs, as in practice, repeating runs is often infeasible. Moreover, an optimum highly sensitive to small perturbations of the inputs is also not

desirable. To that end, an effort has to be made to integrate robustness into the optimization framework seamlessly.

Appendix A

See Tables 4 and 5 (Figs. 11, 12).

Table 4 Side sill impact problem: general modeling properties

Parameter	Value
Component width	800 mm
Component height	120 mm
Component depth	80 mm
No. vertical ribs	3 (evenly distributed)
No. horizontal ribs	5 (evenly distributed)
Element formulation	Belytschko-Lin-Tsay
Contact formulation (LS-Dyna)	*CONTACT_AUTOMATIC_SURFACE_TO_SURFACE

Table 5 Side sill impact problem: material properties used for modeling the aluminum component

Parameter	Symbol	Value
Young's modulus	E	70GPa
Poisson's ratio	ν	0.33
mass density	ρ	$2700\frac{\text{kg}}{\text{m}^3}$
yield strength	σ_y	180MPa
plasticity	See Figs. 11, 12 below	

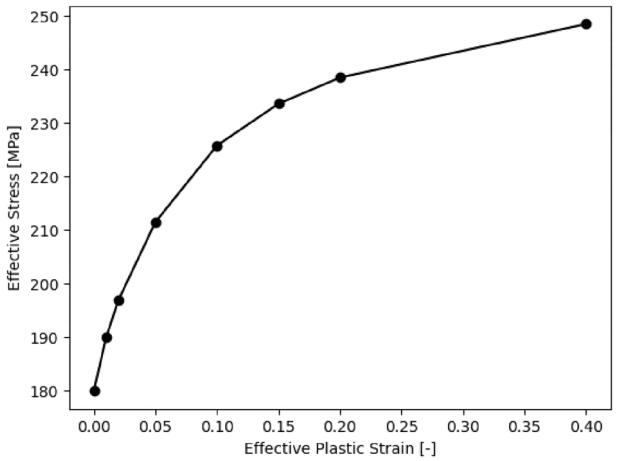

Fig. 11 Side sill impact problem: Piecewise linear plasticity curve used in the aluminum material model

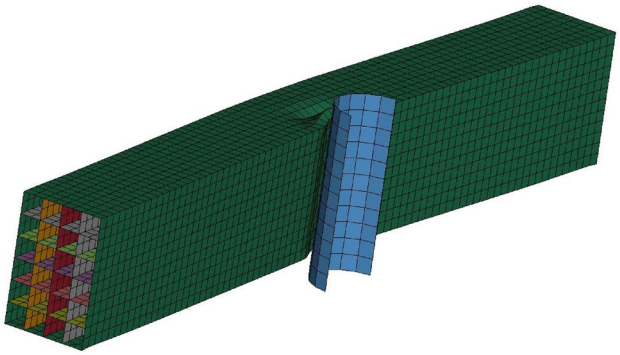

Fig. 12 Low-fidelity model for side sill impact problem with a cylindrical rigid body representing a pole. Both ends are fixed, the impactor has a prescribed velocity

Appendix B

See Tables 6 and 7.

Table 6 Frontal impact problem: material properties used for modeling the steel component

Parameter	Symbol	Value
Young's modulus	E	200 GPa
Poisson's ratio	ν	0.3
Mass density	ρ	$7830\frac{kg}{m^3}$
Yield strength	σ_y	360 MPa
Strainrate model	Cowper-Symmonds	
Strainrate parameters	C	40
	p	5
Plasticity	See Fig. 13 below	

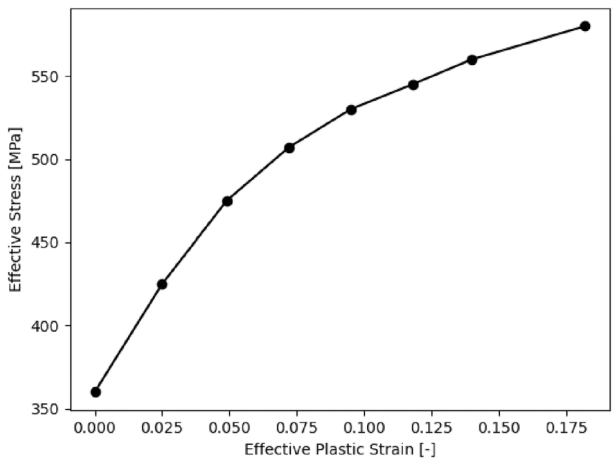

Fig. 13 Frontal impact problem: Piecewise linear plasticity curve used in the steel material model

Table 7 Table caption

Criterion	SF	MF	MF (MOR)
IC_{th}	10^{-5}	10^{-5}	10^{-5}
Max. *HF* it.	–	60	60
Max. it	150	150	150

Acknowledgements The authors would like to thank Koushyar Komeilizadeh for valuable insights and discussions.

Author contributions AK: conceptualization, AK, CC: methodology, AK: software, AK: formal analysis and investigation, AK, CC: writing—original draft preparation, AK, CC, FD: writing—review and editing, FD: supervision.

Funding Open Access funding enabled and organized by Projekt DEAL.

Declarations

Conflict of interest The authors declare that they have no conflict of interest.

Replication of results The detailed information of the proposed methods and the corresponding software employed in this paper can be found in respective sections. This includes algorithms and the used hyper-parameters. A detailed discussion about the implementation can also be found at the end of Sect. 5. The self-implemented parts of the in-house Python code can be obtained from the corresponding author on reasonable request.

References

Acar E, Yilmaz B, Güler MA, Altin M (2020) Multi-fidelity crashworthiness optimization of a bus bumper system under frontal impact. J Braz Soc Mech Sci Eng 42(9):1–17. https://doi.org/10.1007/s40430-020-02572-3

Alaimo G, Auricchio F, Bianchini I, Lanzarone E (2018) Applying functional principal components to structural topology optimization. Int J Numer Methods Eng 115(2):189–208. https://doi.org/10.1002/nme.5801

Anselma PG, Niutta CB, Mainini L, Belingardi G (2020) Multidisciplinary design optimization for hybrid electric vehicles: component sizing and multi-fidelity frontal crashworthiness. Struct Multidisc Optim 62(4):2149–2166. https://doi.org/10.1007/s00158-020-02603-6

Assou S, Tourbier Y, Gstalter E, Charrier M, Dessombz O, Jézéquel L (2019) A reduced model using random forest: application on car crash optimization. SeMA J. https://doi.org/10.1007/s40324-019-00208-8

Audze P, Eglais V (1977) New approach to the design of experiments. Probl Dyn Strength 35:104–107

Bach C, Ceglia D, Song L, Duddeck F (2019) Randomized low-rank approximation methods for projection-based model order reduction of large nonlinear dynamical problems. Int J Numer Methods Eng 118(4):209–241. https://doi.org/10.1002/nme.6009

Baker CG, Gallivan KA, Dooren PV (2012) Low-rank incremental methods for computing dominant singular subspaces. Linear Algebra Appl 436(8):2866–2888. https://doi.org/10.1016/j.laa.2011.07.018

Bonfiglio L, Perdikaris P, Brizzolara S, Karniadakis G (2018) Multi-fidelity optimization of super-cavitating hydrofoils. Comput Methods Appl Mech Eng 332:63–85. https://doi.org/10.1016/j.cma.2017.12.009

Chang KJ, Haftka RT, Giles GL, Kao PJ (1993) Sensitivity-based scaling for approximating structural response. J Aircr 30(2):283–288. https://doi.org/10.2514/3.48278

Choi Y, Oxberry G, White D, Kirchdoerfer T (2019) Accelerating design optimization using reduced order models. pp 1–20. https://doi.org/10.13140/rg.2.2.16056.08965

Duddeck F (2008) Multidisciplinary optimization of car bodies. Struct Multidisc Optimi 35(4):375–389. https://doi.org/10.1007/s00158-007-0130-6

Forrester AI, Keane AJ (2009) Recent advances in surrogate-based optimization. Prog Aerosp Sci 45(1–3):50–79. https://doi.org/10.1016/j.paerosci.2008.11.001

Forrester AI, Sóbester A, Keane AJ (2007) Multi-fidelity optimization via surrogate modelling. Proc R Soc: Mathe Phys Eng Sci 463(2088):3251–3269. https://doi.org/10.1098/rspa.2007.1900

Gano SE, Renaud JE, Martin JD, Simpson TW (2006) Update strategies for kriging models used in variable fidelity optimization. Struct Multidisc Optim 32(4):287–298. https://doi.org/10.1007/s00158-006-0025-y

Garud SS, Karimi IA, Kraft M (2017) Design of computer experiments: a review. Comput Chem Eng 106:71–95. https://doi.org/10.1016/j.compchemeng.2017.05.010

Golub GH, Van Loan CFCF (2013) Matrix computations, 4th edn. The Johns Hopkins University Press, Baltimore

Gratiet LL, Garnier J (2014) Recursive co-kriging model for design of computer experiments with multiple levels of fidelity. Int J Uncertain Quantif 4(5):365–386. https://doi.org/10.1615/int.j.uncertaintyquantification.2014006914

Gstalter E, Assou S, Tourbier Y, De Vuyst F (2020) Toward new methods for optimization study in automotive industry including recent reduction techniques. Adv Model Simul Eng Sci 7(1):1–16. https://doi.org/10.1186/s40323-020-00151-8

Guo M, Hesthaven JS (2017) Reduced order modeling for nonlinear structural analysis using Gaussian process regression. Comput Methods Appl Mech Eng 341:807–826. https://doi.org/10.1016/j.cma.2018.07.017

Guo M, Hesthaven JS (2019) Data-driven reduced order modeling for time-dependent problems. Comput Methods Appl Mech Eng 345:75–99. https://doi.org/10.1016/j.cma.2018.10.029

Han ZH, Görtz S (2012) Hierarchical kriging model for variable-fidelity surrogate modeling. AIAA J 50(9):1885–1896. https://doi.org/10.2514/1.J051354

Han ZH, Zimmermann R, Görtz S (2012) Alternative cokriging method for variable-fidelity surrogate modeling. AIAA J 50(5):1205–1210. https://doi.org/10.2514/1.j051243

Han ZH, Görtz S, Zimmermann R (2013) Improving variable-fidelity surrogate modeling via gradient-enhanced kriging and a generalized hybrid bridge function. Aerosp Sci Technol 25(1):177–189. https://doi.org/10.1016/j.ast.2012.01.006

Huang D, Allen TT, Notz WI, Miller RA (2006) Sequential kriging optimization using multiple-fidelity evaluations. Struct Multidisc Optim 32(5):369–382. https://doi.org/10.1007/s00158-005-0587-0

Hunkeler S, Duddeck F, Rayamajhi M, Zimmer H (2013) Shape optimisation for crashworthiness followed by a robustness analysis with respect to shape variables. Struct Multidisc Optim 48(2):367–378. https://doi.org/10.1007/s00158-013-0903-z

Jin R, Chen W, Sudjianto A (2003) An efficient algorithm for constructing optimal design of computer experiments. international design engineering technical conferences and computers and information in engineering conference, Chicago, IL, USA, vol 37009. pp 545–554

Jones DR (2001) A taxonomy of global optimization methods based on response surfaces. J Glob Optim 21(4):345–383. https://doi.org/10.1023/A:1012771025575

Jones DR, Schonlau M, Welch WJ (1998) Efficient global optimization of expensive black-box functions. J Glob Optim 13(4):455–492. https://doi.org/10.1023/A:1008306431147

Journel AG, Huijbregts C (1978) Mining geostatistics. Academic Press, New York. https://doi.org/10.1180/minmag.1979.043.328.34

Kaps A, Komeilizadeh K, Duddeck F (2021) An ISO-volumetric weighting approach to increase efficiency of stratified samplings. In: 14th world congress of structural and multidisciplinary optimization, Boulder, CO, USA.

Kast M, Guo M, Hesthaven JS (2020) A non-intrusive multifidelity method for the reduced order modeling of nonlinear problems. Comput Methods Appl Mech Eng 364:112947. https://doi.org/10.1016/j.cma.2020.112947

Kennedy MC, O'Hagan A (2000) Predicting the output from a complex computer code when fast approximations are available. Biometrika 87(1):1–13. https://doi.org/10.1093/biomet/87.1.1

Kneifl J, Grunert D, Fehr J (2021) A nonintrusive nonlinear model reduction method for structural dynamical problems based on machine learning. Int J Numer Methods Eng 122(17):1–13. https://doi.org/10.1002/nme.6712

Krige DG (1951) A statistical approach to some basic mine valuation problems on the Witwatersrand. J South Afr Inst Min Metall 52(6):119–139

Lange VA, Fender J, Song L, Duddeck F (2018) Early phase modeling of frontal impacts for crashworthiness: from lumped mass-spring models to deformation space models. Proc Inst Mech Eng D 233(12):3000–3015. https://doi.org/10.1177/0954407018814034

Le Guennec Y, Brunet JP, Daim FZ, Chau M, Tourbier Y (2018) A parametric and non-intrusive reduced order model of car crash simulation. Comput Methods Appl Mech Eng 338:186–207. https://doi.org/10.1016/j.cma.2018.03.005

Matheron G (1963) Principles of geostatistics. Econ Geol 58(8):1246–1266. https://doi.org/10.2113/gsecongeo.58.8.1246

Morris MD, Mitchell TJ (1995) Exploratory designs for computational experiments. J Stat Plan Inference 43(3):381–402. https://doi.org/10.1016/0378-3758(94)00035-T

Oxberry GM, Kostova-Vassilevska T, Arrighi W, Chand K (2017) Limited-memory adaptive snapshot selection for proper orthogonal decomposition. Int J Numer Methods Eng 109(2):198–217. https://doi.org/10.1002/nme.5283

Park C, Haftka RT, Kim NH (2016) Remarks on multi-fidelity surrogates. Struct Multidisc Optim 55(3):1029–1050. https://doi.org/10.1007/s00158-016-1550-y

Pedregosa F, Varoquaux G, Gramfort A, Michel V, Thirion B, Grisel O, Blondel M, Prettenhofer P, Weiss R, Dubourg V, Vanderplas J, Passos A, Cournapeau D, Brucher M, Perrot M, Duchesnay E (2011) Scikit-learn: machine learning in Python. J Mach Learn Res 12:2825–2830

Perdikaris P, Karniadakis GE (2016) Model inversion via multi-fidelity Bayesian optimization: a new paradigm for parameter estimation in haemodynamics, and beyond. J R Soc Interface 13(118):20151107. https://doi.org/10.1098/rsif.2015.1107

Phalippou P, Bouabdallah S, Breitkopf P, Villon P, Zarroug M (2020) 'On-the-fly' snapshots selection for proper orthogonal decomposition with application to nonlinear dynamics. Comput Methods Appl Mech Eng 367:113120. https://doi.org/10.1016/j.cma.2020.113120

Rajabi MM, Ataie-Ashtiani B, Janssen H (2015) Efficiency enhancement of optimized Latin hypercube sampling strategies: application to Monte Carlo uncertainty analysis and meta-modeling. Adv Water Resour 76:127–139. https://doi.org/10.1016/j.advwatres.2014.12.008

Rasmussen CE, Williams CKI (2005) Gaussian processes for machine learning. MIT Press Ltd, Cambridge

Redhe M, Giger M, Nilsson L (2004) An investigation of structural optimization in crashworthiness design using a stochastic approach. Struct Multidisc Optim 27(6):446–459. https://doi.org/10.1007/s00158-004-0400-5

Ren C, Min H, Ma T, Wang F (2020) Efficient structure crash topology optimization strategy using a model order reduction method combined with equivalent static loads. Proc Inst Mech Eng D 234(7):1897–1911. https://doi.org/10.1177/0954407019893841

Sacks J, Welch WJ, Mitchell TJ, Wynn HP (1989) Design and analysis of computer experiments. Stat Sci 4(4):409–423. https://doi.org/10.1214/ss/1177012413

Sirovich L (1987) Turbulence and the dynamics of coherent structures. I. Coherent structures. Q Appl Math 45(10):561–571. https://doi.org/10.1090/qam/910462

Storn R, Price K (1997) Differential evolution—a simple and efficient heuristic for global optimization over continuous spaces. J Glob Optim 11(4):341–359. https://doi.org/10.1023/a:1008202821328

Sun G, Li G, Stone M, Li Q (2010) A two-stage multi-fidelity optimization procedure for honeycomb-type cellular materials. Comput Mater Sci 49(3):500–511. https://doi.org/10.1016/j.commatsci.2010.05.041

Sun G, Li G, Zhou S, Xu W, Yang X, Li Q (2010) Multi-fidelity optimization for sheet metal forming process. Struct Multidisc Optim 44(1):111–124. https://doi.org/10.1007/s00158-010-0596-5

Swischuk R, Mainini L, Peherstorfer B, Willcox K (2019) Projection-based model reduction: formulations for physics-based machine learning. Comput Fluids 179:704–717. https://doi.org/10.1016/j.compfluid.2018.07.021

Toal DJJ, Bressloff NW, Keane AJ (2008) Kriging hyperparameter tuning strategies. AIAA J 46(5):1240–1252. https://doi.org/10.2514/1.34822

Xiao M, Lu D, Breitkopf P, Raghavan B, Dutta S, Zhang W (2020) On-the-fly model reduction for large-scale structural topology optimization using principal components analysis. Struct Multidisc Optim 62:209–230. https://doi.org/10.1007/s00158-019-02485-3

Ye KQ, Li W, Sudjianto A (2000) Algorithmic construction of optimal symmetric Latin hypercube designs. J Stat Plan Inference 90(1):145–159. https://doi.org/10.1016/S0378-3758(00)00105-1

Yu J, Yan C, Guo M (2019) Non-intrusive reduced-order modeling for fluid problems: a brief review. Proc Inst Mech Eng G 233(16):5896–5912. https://doi.org/10.1177/0954410019890721

Zhang Y, Han ZH, Zhang KS (2018a) Variable-fidelity expected improvement method for efficient global optimization of expensive functions. Struct Multidisc Optim 58(4):1431–1451. https://doi.org/10.1007/s00158-018-1971-x

Zhang Y, Kim NH, Park C, Haftka RT (2018b) Multifidelity surrogate based on single linear regression. AIAA J 56(12):4944–4952. https://doi.org/10.2514/1.J057299

A.2 Publication II

Kaps A., Lehrer T., Lepenies I., Wagner M., Duddeck F.: Multi-fidelity optimization of metal sheets concerning manufacturability in deep-drawing processes. Structural and Multidisciplinary Optimization 66(8), 2023. DOI: https://doi.org/10.1007/s00158-023-03631-8

Structural and Multidisciplinary Optimization (2023) 66:175
https://doi.org/10.1007/s00158-023-03631-8

RESEARCH PAPER

Multi-fidelity optimization of metal sheets concerning manufacturability in deep-drawing processes

Arne Kaps[1] · Tobias Lehrer[1,2] · Ingolf Lepenies[3] · Marcus Wagner[2] · Fabian Duddeck[1]

Received: 8 March 2023 / Revised: 29 June 2023 / Accepted: 1 July 2023

Abstract
Multi-fidelity optimization, which complements an expensive high-fidelity function with cheaper low-fidelity functions, has been successfully applied in many fields of structural optimization. In the present work, an exemplary cross-die deep-drawing optimization problem is investigated to compare different objective functions and to assess the performance of a multi-fidelity efficient global optimization technique. To that end, hierarchical kriging is combined with an infill criterion called variable-fidelity expected improvement. Findings depend significantly on the choice of objective function, highlighting the importance of careful consideration when defining an objective function. We show that one function based on the share of bad elements in a forming limit diagram is not well suited to optimize the example problem. In contrast, two other definitions of objective functions, the average sheet thickness reduction and an averaged limit violation in the forming limit diagram, confirm the potential of a multi-fidelity approach. They significantly reduce computational cost at comparable result quality or even improve result quality compared to a single-fidelity optimization.

Keywords Multi-fidelity optimization · Efficient global optimization · Sheet metal forming · Deep drawing

1 Introduction

Sheet-metal forming is one of the essential manufacturing processes for structural and body parts in various industries, for example, the automotive industry. Essentially, a thin metal sheet is plastically deformed into its desired shape by means of forming tools. Not only the process of forming itself is subject to a number of process parameters, but also material and shape parameters of the component influence the success of the forming process. Numerical methods such as finite element (FE) methods have been developed since the 1960s and have been applied in industrial use since about the 1980s. An early overview can, for example, be found in Makinouchi (1996). More recently, inverse methods have been proposed to save computational resources while still being able to predict the manufacturability of components (Lee and Huh 1997, 1998; Guo et al. 2000). For an overview of more recent developments in simulation methods for sheet metal forming, interested readers are referred to some of the nice review articles on the topic, such as by Ablat and Qattawi (2016) or by Andrade-Campos et al. (2022).

Along with the development of improved simulation methods, new optimization methods for structural problems were suggested. One common challenge in applying such multi-query algorithms to structural problems is the often infeasible amount of computational resources required for running an FE simulation with every evaluation. Modern optimization approaches, such as efficient global optimization [EGO; Jones et al. (1998)], which were specifically designed to reduce the required evaluations, can partially solve this problem. The idea of EGO is to first fit a surrogate model from the initial design of experiments (DoE). Typically, a kriging model (Krige 1951; Matheron 1963; Sacks et al. 1989) is used due to its inherent error approximation. Subsequently, this surrogate model is iteratively improved using an infill criterion that determines new sample locations. The most popular criterion is the originally proposed

Responsible Editor: Lei Wang.

✉ Arne Kaps
arne.kaps@tum.de

[1] TUM School of Engineering and Design, Technical University of Munich, Arcisstr. 21, 80333 Munich, Germany

[2] Department of Mechanical Engineering, Ostbayerische Technische Hochschule Regensburg, Galgenbergstr. 30, 93053 Regensburg, Germany

[3] SCALE GmbH, Dresden, Germany

Published online: 12 July 2023

expected improvement [EI; Jones et al. (1998)], while several other options can be found, for example, in Jones (2001). A more detailed review of this type of surrogate-based optimization is given in Forrester and Keane (2009).

More recently, in an effort to further reduce computational requirements on the optimization scheme, EGO and kriging were extended to so-called multi-fidelity schemes. Here, the accurate, high-fidelity simulation model is complemented by some form of low-fidelity model, which is usually less accurate but significantly cheaper to calculate. In the present work, a multi-fidelity variant of EGO based on hierarchical kriging (HK), a multi-fidelity extension to kriging suggested by Han and Görtz (2012) and an infill criterion called variable-fidelity expected improvement (VF-EI; Zhang et al. (2018)) is utilized. Interested readers are referred to previous work on multi-fidelity surrogate models as well as optimization for more information [e.g., Forrester et al. (2007); Park et al. (2016)].

Since the 1990s, different optimization approaches have also been applied to sheet metal forming. Ohata et al. (1998) optimized a two-stage deep-drawing process using three design variables in incremental forming simulations. Guo et al. (2000) utilized an inverse approach to optimize the blank shape for manufacturability. A surrogate-based optimization approach was suggested by Jansson et al. (2005) for the design of drawbeads and validated with experimental data. Different surrogate-based schemes, including kriging, were used to optimize a time-dependent blankholder force curve by Jakumeit et al. (2005). An overview of some of the earlier applications of optimization schemes to sheet-metal-forming problems is given by Wifi et al. (2007). More recently, a multi-fidelity optimization scheme for drawbead design combining both incremental high-fidelity forming simulations and a more efficient low-fidelity simulation has been proposed by Sun et al. (2010). Although the initial work is based on polynomial regression, the authors later extended the approach to other metamodels such as kriging using an artificial bee colony optimization algorithm (Sun et al. 2012).

In the present work, we apply a modern HK-based multi-fidelity optimization approach to an exemplary problem on the manufacturability of a deep-drawn cross-die component. We compare three different objective functions, which have all been proposed in the literature in a similar form. There are two main goals when comparing the performance of multi-fidelity algorithms in the context of this work. First, the multi-fidelity approach should reduce the overall computational effort of the optimization process. Second, it should not lead to significantly worse results compared to optimization using only high-fidelity simulations. We aim to establish the applicability of a modern multi-fidelity optimization approach to sheet metal forming and work out possible differences between the objective functions.

The present work is structured as follows. In Sect. 2, the multi-fidelity optimization approach utilizing HK and VF-EI is introduced. In Sect. 3, the numerical example studied here is presented. The objective functions compared here are introduced in Sect. 4 along with the definition of the optimization problem. The performance of the algorithms is compared and discussed in Sect. 5. Finally, all findings are summarized, and an outlook into possible future work is given in Sect. 6.

2 Multi-fidelity optimization

In the following, the multi-fidelity EGO approach based on HK and VF-EI is introduced, which will be used in this work. At the top level, this surrogate-based optimization scheme can be divided into two parts. First, a design of experiments is used to generate design samples to subsequently fit the surrogate model. Here, HK is utilized because it has been shown to yield better error approximations compared to other multi-fidelity kriging approaches (Han and Görtz 2012). Subsequently, adaptive samples are added, whereby their location is determined through maximization of an infill criterion on the previously created surrogate model. Here, VF-EI is applied because it has been shown to perform very well in application problems [see, for example, Zhang et al. (2018); Ruan et al. (2020)]. A schematic representation of the optimization scheme applied here is depicted in Fig. 1.

All steps of the outlined process are now explained in more detail. The first step as in any population-based optimization scheme is DoE. DoE is an active field of research, as there is no unique ‘best’ way to distribute these initial samples apart from the rather vague goal of good coverage of the design space. Interested readers are referred to one of the review articles such as Garud et al. (2017) for more information on different DoE methods and quality criteria for DoE.

In the present work, an optimal Latin hypercube (OLH) approach is used as it shows great performance in lower-dimensional applications. A Latin hypercube design (LHD) is commonly constructed as follows. When looking for N samples in d dimensions, each dimension of the design space is divided into N bins of equal probability. N cells of the total N^d created cells are then randomly selected so that each bin of each dimension only contains a single selected cell (McKay et al. 1979). Within each selected cell, a single sample is placed either in the center or randomly located [compare Rajabi et al. (2015)], whereby the former case is used here.

Initial Latin hypercube designs may still suffer from problems, such as correlations. Optimal Latin hypercube (OLH) provides a remedy by incrementally improving DoE quality

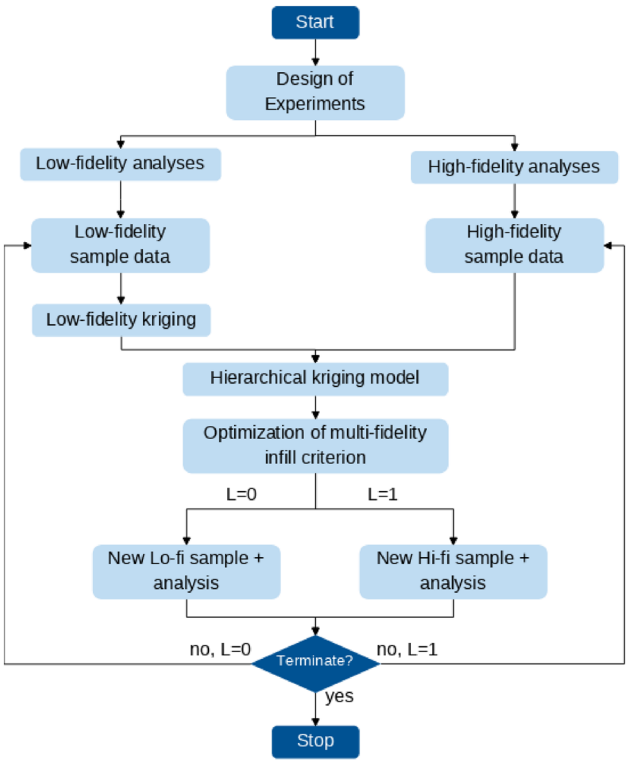

Fig. 1 Schematic representation of the optimization scheme applied in the present work [adapted from Zhang et al. (2018)]

according to a space-filling criterion. In the present work, a simulated annealing algorithm consisting of random pairwise and coordinate-wise swaps is utilized. New samples are always accepted if they improve the space-filling criterion and are accepted with a certain probability if they do not offer an improvement (Morris and Mitchell 1995). Other optimization approaches for OLH include deterministic sample selection (Ye et al. 2000) and Enhanced Stochastic Evolutionary algorithm as suggested by Jin et al. (2003). An overview of more recent developments around OLH can also be found in Viana (2015).

The second step of EGO is to fit an initial HK model to the d-dimensional objective functions based on the calculated sampling data. Readers are referred to the original publications (Krige 1951; Matheron 1963; Sacks et al. 1989) as well as more recent textbooks [such as Rasmussen and Williams (2005)] for more information on kriging in general and the original publication for a detailed derivation of the HK predictor (Han and Görtz 2012). The idea of HK is to first create a kriging model for the low-fidelity function. Therefore, consider a random process for the low-fidelity (LF) function

$$Y_{\mathrm{LF}}(\boldsymbol{x}) = \beta_{0,\mathrm{LF}} + Z_{\mathrm{LF}}(\boldsymbol{x}), \tag{1}$$

where $\beta_{0,\mathrm{LF}}$ is an unknown constant and $Z_{\mathrm{LF}}(\boldsymbol{x})$ is a stationary random process. Furthermore, a sample dataset $(\boldsymbol{S}_{\mathrm{LF}}, \boldsymbol{y}_{S,\mathrm{LF}})$ consisting of m_{LF} samples with input variable data $\boldsymbol{S}_{\mathrm{LF}} \in \mathbb{R}^{m_{\mathrm{LF}} \times d}$ and the corresponding output $\boldsymbol{y}_{S,\mathrm{LF}} \in \mathbb{R}^{m_{\mathrm{LF}}}$ is required.

To predict points based on the random process and the sampling dataset, the correlation between sample points is modeled through a so-called kernel. Over the years, many different kernel functions with varying properties have been suggested. Here, a squared-exponential kernel, also called a Gaussian radial-basis function (RBF) kernel, is utilized due to its smoothness and infinite differentiability:

$$R\left(\boldsymbol{x}^{(i)}, \boldsymbol{x}^{(j)}\right) = \prod_{k=1}^{d} \exp\left(-\theta_k \left| x_k^{(i)} - x_k^{(j)} \right|^2\right), \tag{2}$$

where θ_k denotes the kernel length scale that represents the hyperparameter(s) of the kriging surrogate model. The kernel function depicted above is called anisotropic because there is a separate length scale parameter for each design space dimension. In the present work, an isotropic kernel is chosen, where the hyperparameter $\theta_k = \theta$ is a scalar, that is, independent of coordinate dimension. Other popular kernel function choices can be found in textbooks such as Rasmussen and Williams (2005) or in popular software implementations of kriging [for example, Pedregosa et al. (2011) or GPy (2012)]. Given the sample dataset, the kriging model is fitted by running a separate optimization for the kernel hyperparameter θ. Here, differential evolution (Storn and Price 1997) is used due to its simplicity and good global search characteristics. However, more advanced approaches for hyperparameter optimization have been suggested [see, for example, Toal et al. (2008) for more information].

With the representation of the random process, the sampling data, and the kernel function, the low-fidelity predictor for a new point $\boldsymbol{x}$ can be written as follows:

$$\begin{aligned} &\hat{y}_{\mathrm{LF}}(\boldsymbol{x}) = \beta_{0,\mathrm{LF}} + \boldsymbol{r}_{\mathrm{LF}}^T(\boldsymbol{x}) \boldsymbol{R}_{\mathrm{LF}}^{-1} (\boldsymbol{y}_{S,\mathrm{LF}} - \beta_{0,\mathrm{LF}} \boldsymbol{1}), \\ &\text{with} \quad \beta_{0,\mathrm{LF}} = \left(\boldsymbol{1}^T \boldsymbol{R}_{\mathrm{LF}}^{-1} \boldsymbol{1}\right)^{-1} \boldsymbol{1}^T \boldsymbol{R}_{\mathrm{LF}}^{-1} \boldsymbol{y}_{S,\mathrm{LF}}, \\ &\text{and} \quad \boldsymbol{r}_{\mathrm{LF}} = \left[R\left(\boldsymbol{x}, \boldsymbol{x}^{(1)}\right), \ldots, R\left(\boldsymbol{x}, \boldsymbol{x}^{(m)}\right)\right] \in \mathbb{R}^{m_{\mathrm{LF}}} \end{aligned} \tag{3}$$

where $\boldsymbol{r}_{\mathrm{LF}}$ is the correlation vector between the sample data and the new point, $\boldsymbol{R}_{\mathrm{LF}} \in \mathbb{R}^{m_{\mathrm{LF}} \times m_{\mathrm{LF}}}$ represents the correlation matrix between the sample data points and $\boldsymbol{1} \in \mathbb{R}^{m_{\mathrm{LF}}}$ a column vector filled with ones.

With the low-fidelity predictor $\hat{y}_{\mathrm{LF}}(\boldsymbol{x})$, the hierarchical kriging model can be constructed, which is based on a random process representing the high-fidelity function:

$$Y(\boldsymbol{x}) = \beta_0 \hat{y}_{\mathrm{LF}}(\boldsymbol{x}) + Z(\boldsymbol{x}). \tag{4}$$

β_0 is an unknown scaling factor applied to the low-fidelity predictor to represent the trend term of the model and $Z(\boldsymbol{x})$

is a stationary random process. With the high-fidelity sample dataset $(\boldsymbol{S}, y_S)$ consisting of m samples with input variable data $\boldsymbol{S} \in \mathbb{R}^{m\times d}$ and the corresponding output $y_S \in \mathbb{R}^m$ and the kernel function $R(\boldsymbol{x}^{(i)}, \boldsymbol{x}^{(j)})$ as defined above, the HK predictor for the high-fidelity function is given by

$$\begin{aligned}\hat{y}(\boldsymbol{x}) &= \beta_0 \hat{y}_{\mathrm{LF}}(\boldsymbol{x}) + \boldsymbol{r}^T(\boldsymbol{x})\boldsymbol{R}^{-1}(\boldsymbol{y}_S - \beta_0 \boldsymbol{F}) \\ &\text{with} \quad \beta_0 = \left(\boldsymbol{F}^T\boldsymbol{R}^{-1}\boldsymbol{F}\right)^{-1}\boldsymbol{F}^T\boldsymbol{R}^{-1}\boldsymbol{y}_S.\end{aligned} \tag{5}$$

Here, β_0 indicates the correlation between high- and low-fidelity models and $\boldsymbol{F} = [\hat{y}_{\mathrm{LF}}(\boldsymbol{x}^{(1)})...\hat{y}_{\mathrm{LF}}(\boldsymbol{x}^{(n)})]^T, \forall \boldsymbol{x}^{(i)} \in \boldsymbol{S}$ represents the low-fidelity prediction at high-fidelity sample point. $\boldsymbol{r} \in \mathbb{R}^m$ and $\boldsymbol{R} \in \mathbb{R}^{m\times d}$ are defined as introduced for the low-fidelity predictor. In the HK predictor, only $\hat{y}(\boldsymbol{x})$ and $\boldsymbol{r}(\boldsymbol{x})$ depend on the location of the new point. All other factors can be calculated when fitting the model.

Another important quantity that is needed in the later steps of the optimization process is the mean-squared error (MSE) of the HK prediction. It is written here with respect to σ^2, the process variance of $Z(\boldsymbol{x})$

$$\begin{aligned}\mathrm{MSE}(\hat{y}(\boldsymbol{x})) = \sigma^2\Bigg(1.0 - \boldsymbol{r}^T\boldsymbol{R}^{-1}\boldsymbol{r} \\ + \left[\boldsymbol{r}^T\boldsymbol{R}^{-1}\boldsymbol{F} - \hat{y}_{\mathrm{LF}}\right]^2\left(\boldsymbol{F}^T\boldsymbol{R}^{-1}\boldsymbol{F}\right)^{-1}\Bigg).\end{aligned} \tag{6}$$

Based on the initial HK model, several iterations are performed to adaptively improve it until a specific termination criterion is reached. The termination criteria will be covered below. The location of the new adaptive samples is determined by optimizing an infill criterion. When considering multi-fidelity optimization, there are generally two options regarding infill criteria: First, a 'classic' single-fidelity infill criterion can be chosen. Among them, *expected improvement* which was used by Jones et al. (1998) to introduce EGO, remains the most popular. However, several different criteria have been suggested over the years [see, for example, Jones (2001) or Forrester and Keane (2009) for overviews]. The prime disadvantage of this option is that only high-fidelity samples can be added adaptively. Therefore, a multi-fidelity infill criterion is utilized here, called *variable-fidelity expected improvement* (Zhang et al. 2018). It is essentially a multi-fidelity extension of standard EI and in its formulation is very similar to another criterion called augmented EI (Huang et al. 2006). Here, it is favored over the latter because it is free of empirical parameters. More discussion on the comparison between these two criteria can be found in the original publication suggesting VF-EI. VF-EI is defined at location $\boldsymbol{x}$ and fidelity level L as follows:

$$\mathrm{EI}_{vf}(\boldsymbol{x}, L) = \begin{cases} s(\boldsymbol{x}, L)[u\Phi(u) + \phi(u)], & \text{if } s(\boldsymbol{x}, L) > 0 \\ 0, & \text{if } s(\boldsymbol{x}, L) = 0 \end{cases}, \tag{7}$$

where $u = \frac{y_{\min} - \hat{y}(\boldsymbol{x})}{s(\boldsymbol{x}, L)}$ and $y_{\min}$ is the currently best feasible high-fidelity function value. $\Phi(\bullet)$ represents the cumulative distribution of the standard normal distribution and $\phi(\bullet)$ its probability density function. The term $s(\boldsymbol{x}, L)$ denotes the uncertainty of the HK model. The previously introduced scaling factor between fidelity levels β_0 is used here to model the uncertainty in high-fidelity prediction caused by the low-fidelity predictor:

$$s^2(\boldsymbol{x}, L) = \begin{cases} \beta_0^2 \cdot \mathrm{MSE}(\hat{y}_{\mathrm{LF}}(\boldsymbol{x})), & L = 0 \text{ low-fid} \\ \mathrm{MSE}(\hat{y}(\boldsymbol{x})), & L = 1 \text{ high-fid} \end{cases}. \tag{8}$$

$\mathrm{MSE}(\hat{y}(\boldsymbol{x}))$ and $\mathrm{MSE}(\hat{y}_{\mathrm{LF}}(\boldsymbol{x}))$ are the MSEs of the high- and low-fidelity kriging predictors, respectively.

The two summands in Eq. (7) can be identified with exploration and exploitation. The first term $\left(y_{\min} - \hat{y}(\boldsymbol{x})\right)\Phi(u)$ is dominated by the improvement of the solution $\hat{y}(\boldsymbol{x})$ and, thus, represents exploitation, while the second term $s(\boldsymbol{x}, L)\phi(u)$ represents exploration because it is dominated by the uncertainty of the solution $s(\boldsymbol{x}, L)$.

Due to the highly multimodal nature of the EI functions, differential evolution (Storn and Price 1997) is selected for optimization of the infill criterion in the present work.

Two different criteria are used to determine the end of optimization. First, a minimum allowable value is specified for the optimized infill criterion. Second, a maximum total number of (high-fidelity) objective function evaluations is defined. The values of the criteria are problem dependent, and are listed below with the definitions of the problems. The first criterion can be seen as convergence of the algorithm to an (at least near-) optimal point with little expectation of improvement from adding further samples. The other criterion is used to represent budget restrictions on optimization run time that are commonly encountered in application use cases.

The optimization algorithm, along with a part for DoE, is implemented in an in-house Python code from previous work by the authors (Komeilizadeh et al. 2022; Kaps et al. 2022). HK model generation and kernel implementation are based on the scikit-learn library (Pedregosa et al. 2011).

3 Numerical example

Based on the objective functions which are introduced in Sect. 4, two different optimization schemes are compared for an exemplary numerical problem introduced in the following. Here, a cross-die deep-drawing simulation comparable to the one studied by Hoque and Duddeck (2021) is used as a

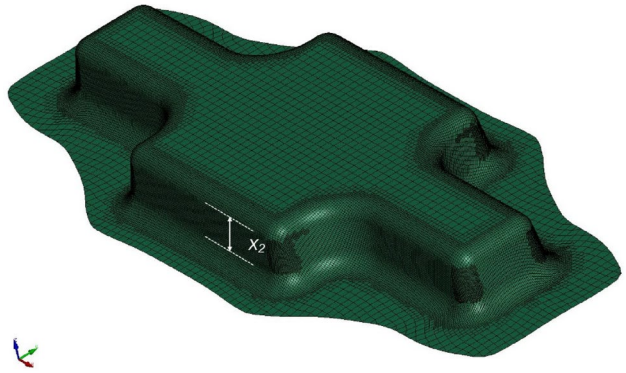

Fig. 2 Exemplary geometry of the cross-die component studied here. The definition of slant depth is indicated in white, i.e., design variable x_2, used here

basis for the optimization problem. An exemplary configuration of the final component is shown in Fig. 2. All tooling is modeled as rigid bodies while the sheet blank is made of steel. Coulomb friction is assumed between the blank and the tools. More detailed information on modeling parameters and numerical values can be found in Table 2 in the Appendix. An incremental explicit simulation in LS-Dyna is utilized for the high-fidelity model. An exemplary high-fidelity simulation model at the initial time step is shown in Appendix Fig. 13. The simulation of deep drawing itself consists of multiple process steps. Initially, the punch moves into contact with the sheet metal blank. The blank itself is pressed to the die by a blankholder. Then, as the punch moves further, the deep drawing, i.e., the nonlinear forming of the blank into its desired shape, is driven by the different contacts between the tools and the blank. Finally, when the punch is removed, an elastic springback of the component occurs. This last step is not considered in the present work because it accounts for dimensional accuracy while the focus here lies on formability. For more detailed overviews of the various details of sheet-metal-forming simulation, readers are referred to the available textbooks on the topic, e.g., Banabic (2010). As the low-fidelity model, the inverse implicit one-step capability of LS-Dyna based on a more coarsely meshed component is utilized. The idea of the inverse one-step approach is to use deformation theory to calculate stresses, strains, and thicknesses in the formed component given the final geometry. A more detailed derivation including the governing equations of the approach can be found, for example, in the original publication (Lee and Huh 1997). The maximum element size is set to 5 mm for the latter, compared to 3 mm for the high-fidelity model. The smallest element size after adaptive mesh refinement in the high-fidelity model is 0.5 mm. Simulation times for high- and low-fidelity simulation models are 10–20 min and 1–2 min, respectively, when running on eight cores.[1] Exact values vary also depending the choice of design variables.

Table 1 Overview of the design variables specified for the optimization problem considered here

Symbol	Name	Bounds	Unit
x_1	Sheet thickness	[0.8, 1.8]	mm
x_2	Slant depth	[12, 35]	mm
x_3	Die radius	[6, 9]	mm
x_4	Lankford coeff	[0.8, 2.5]	–
x_5	Friction coeff	[0.08, 0.12]	–
x_6	Blankholder force	[130, 190]	kN

For the optimization problem studied here, a total of six design variables are selected. All variables and their specified limits are summarized in Table 1. From the literature, the design variables in sheet-metal-forming optimization problems can be divided into three categories: geometry parameters [see, for example, Guo et al. (2000) or Kishor and Kumar (2002)], process parameters [for example, blank holding force, Obermeyer and Majlessi (1998)], and material parameters. In the present work, the design variables are exemplary chosen from all three categories. As geometry parameters, the thickness of the initial sheet metal, the slant depth of the cruciform, which is equivalent to the drawing depth of the process, and the die radius are chosen. The Lankford coefficient, which represents the normal anisotropy of the material, is varied as a material parameter. The Coulomb friction coefficient and the constant blankholder force (BHF) are the two remaining design variables in the class of process parameters.

Previous work has shown that it can be beneficial to vary the BHF in the forming process [e.g., Jakumeit et al. (2005)]. Here, it is kept constant for the sake of simplicity. For the same reason, all design variables in this exemplary problem are considered continuous, even though, for example, the sheet metal thickness or the Lankford coefficient might be more realistically treated as a discrete variable.

The design variable values in the present example are chosen to be very challenging in the sense that they will likely not yield a manufacturable component in the optimization. The main reason is that objective functions f_1 and f_2 are not capable of distinguishing manufacturable components from each other. Both functions take a constant value of zero for manufacturable components. Therefore, manufacturable components in the design space would limit the comparability between objective functions.

[1] The used LS-Dyna version is R12, runs are performed on an AMD Ryzen 9 7950X CPU with 64 GB RAM, running Ubuntu version 22.04.

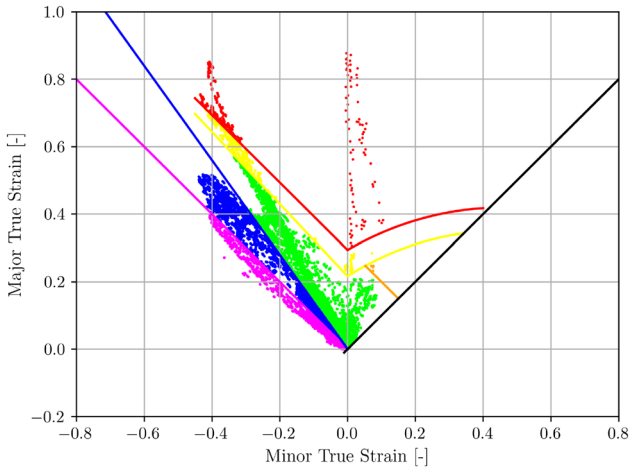

Fig. 3 Exemplary forming limit diagram for a cross-die component. The red line is the FLC and the pink line represents the WLC. Each dot represents an element of the simulation model. Blue and yellow colors indicate crack and wrinkling risk areas, respectively. Orange color shows severe thinning area. The black line marks the limit of strain definitions, i.e., $\epsilon_1 \geq \epsilon_2$. (Color figure online)

4 Objective functions

The three different objective functions used to assess the formability of a component are introduced in the following. All functions are defined here to be minimized during optimization. All three functions have been previously used, sometimes with slight variations, in the literature. Therefore, while the presentation here is kept brief, interested readers are referred to the various original publications for further discussion.

The first two objectives make use of the so-called forming limit diagram (FLD). It includes the forming limit curve (FLC) representing the onset of localized necking in the sheet metal component, as well as a limit curve for the onset of wrinkling. Since their first mention in the 1960s (Goodwin 1968; Keeler 1968), many different variants of FLDs have been studied to remedy some of the initial shortcomings such as strain-path effects on the FLC. One such example is the extension of FLCs to nonlinear strain paths and multi-step forming process by Volk and Suh (2013). Readers are referred to previous works reviewing the topic in more detail [e.g., Paul (2013) or Obermeyer and Majlessi (1998)]. An exemplary FLD used in the present work is shown in Fig. 3. Here, the major and minor true strains for each element of the deep-drawn sheet metal component are plotted against each other. The red line is the FLC and the pink line represents the wrinkling limit curve (WLC). Each dot represents an element in the simulation model.

The first objective function is based on counting the elements in the different categories of the FLD. Subsequently, the objective function f_1 is defined as the share of 'bad' elements:

$$\begin{aligned} f_1 &= \frac{N_{\text{bad}}}{N}, \text{where} \\ N_{\text{bad}} &= N_{\text{C}} + N_{\text{CR}} + N_{\text{W}} + N_{\text{WR}} + N_{\text{TH}} \end{aligned}, \tag{9}$$

where N is the total number of elements. N_{C}, N_{CR}, N_{W}, N_{WR}, and N_{TH} represent the number of elements in the crack, crack risk, wrinkling, wrinkling tendency, and severe thinning categories of the FLD, respectively (compare Fig. 3). This approach is somewhat similar to two of the four criteria suggested by Jakumeit et al. (2005).

The second objective function assessed in the present work is based on the average distance of bad elements to the respective limiting curves. A very similar approach has been originally suggested by Naceur et al. (2004) and applied in a multi-fidelity setup by Sun et al. (2010). In the present work, the different distances are weighed by the area of the respective element [compare Schenk and Hillmann (2004)]. The FLC and WLC are defined here as black-box functions. Given the values of the major and minor true strains of the element e, these functions return the points on the curves $\hat{\boldsymbol{\epsilon}}^{\text{FLC}}$ and $\hat{\boldsymbol{\epsilon}}^{\text{WLC}}$ required for the calculation of the distance. For elements within the domain of the limiting curve, a vertical distance is calculated. The Euclidean distance is utilized for the remaining elements. Therefore, the distance function is defined as follows:

$$d\left(\boldsymbol{\epsilon}^e, \hat{\boldsymbol{\epsilon}}^{\text{LC}}\right) = \begin{cases} |\epsilon_1^e - \hat{\epsilon}_1^{\text{LC}}|, & \epsilon_2^e \in \mathbb{D}_{\text{LC}} \\ \|\boldsymbol{\epsilon}^e - \hat{\boldsymbol{\epsilon}}^{\text{LC}}\|_2, & \text{else} \end{cases}. \tag{10}$$

$\hat{\boldsymbol{\epsilon}}^{\text{LC}}$ represents the major and minor strains of the point on the respective limiting curve (LC), while $\mathbb{D}_{\text{LC}}$ represents the domain of the curve. Therefore, the second objective function is given by

$$\begin{aligned} f_2 &= f_{2,\text{C}} + w f_{2,\text{W}}, \text{where} \\ f_{2,\text{C}} &= \begin{cases} \frac{\sum_{e=1}^{N_{\text{C}}} d(\boldsymbol{\epsilon}^e, \hat{\boldsymbol{\epsilon}}^{\text{FLC}}) A^e}{\sum_{e=1}^{N_{\text{C}}} A^e}, & \epsilon_1^e > \epsilon_1^{\text{FLC}} \\ 0, & \text{else} \end{cases} \\ f_{2,\text{W}} &= \begin{cases} \frac{\sum_{e=1}^{N_{\text{W}}} d(\boldsymbol{\epsilon}^e, \hat{\boldsymbol{\epsilon}}^{\text{WLC}}) A^e}{\sum_{e=1}^{N_{\text{W}}} A^e}, & \epsilon_1^e < \epsilon_1^{\text{WLC}} \\ 0, & \text{else} \end{cases} \end{aligned}. \tag{11}$$

Here, w is a weighting factor balancing the contributions of crack and wrinkling elements. It is set to $w = 0.1$ following the suggestion made in Sun et al. (2010). Initial studies were performed for the present application problem with different values of w. It was found that the value of w does not have a significant impact on the optimization results here; however,

the chosen value provides a nice balance between the two contributions. The element area is given by A^e.

The third objective function f_3 is the thickness variation in the drawn component. This indicator has been widely used for many years [e.g., Guo et al. (2000); Naceur et al. (2001); Sattari et al. (2007)]. The definition used here is very similar to that given by Guo et al. (2000) for the special case $p = 2$:

$$f_3 = \left(\frac{1}{N} \sum_{e=1}^{N} (h_t^e - h_0)^2 \right)^{\frac{1}{2}}. \tag{12}$$

N represents the number of elements, h_0 is the initial constant thickness of the sheet metal, and the elemental sheet thickness at the final simulation time step is given by h_t^e. This function is intuitive because a decrease in thickness during the simulation can lead to necking, while an increase in thickness may be correlated with wrinkling. These are the two main failure modes in sheet metal forming. In contrast to the first two objective functions, this function also allows for the comparison of components considered as manufacturable. Objective functions f_1 and f_2 are always zero when a component is considered formable, whereas function f_3 is not.

Defining the lower and upper bounds of the j-th design variable as $\underline{x}_j$ and $\bar{x}_j$, respectively, (compare Table 1) and considering the three objective functions $f_i(\boldsymbol{x})$ introduced above, the three optimization problems considered here can be formulated as follows:

$$\min_{\boldsymbol{x}} \quad f_i(\boldsymbol{x}), \tag{13a}$$

$$\text{where} \quad \underline{x}_j \le x_j \le \bar{x}_j, \quad j = 1,2,3,4,5,6 \quad . \tag{13b}$$

Here, i will take the values 1, 2, or 3, depending on the objective function considered. The formulation $f_i(\boldsymbol{x})$ includes the whole simulation workflow, where depending on the fidelity level and design variable values either a high-fidelity or a low-fidelity simulation model is generated, evaluated, and the resulting strain field used to calculate the respective objective function value.

Termination criteria for this problem are set to 10^{-5} for the infill criterion threshold and 100 for the maximum number of iterative evaluations of the objective function.

5 Results

In the following, the optimization results of the optimization scheme proposed by Zhang et al. (2018) for the three different objective functions on the given deep-drawing problem are presented separately, discussed, and finally compared. As a reference, a single-fidelity optimization technique based on kriging, EI, and the high-fidelity simulation model is utilized. The latter is referred to as *HF* in the following, while the multi-fidelity scheme is called *MF*.

In general, both techniques are evaluated for the quality, consistency, and computational requirements of the results. Two points are the focus of the present work. First, we assess how each objective function performs in the optimizations and how the optimization results between different objective functions differ. Second, we establish whether the presented multi-fidelity optimization approach shows potential for sheet-metal-forming problems.

All high- and low-fidelity simulations are performed on the same computer using FE software LS-Dyna distributed across eight cores. Each optimization run is repeated ten times to ensure the reliability of the assessment. Unless explicitly stated otherwise, all objective function values listed below are based on the high-fidelity model. For completeness, the average number of simulation model calls for both fidelity level and all objective functions is listed in the Appendix Table 3.

5.1 Objective function f_1

As a first step in assessing the results for objective function f_1, convergence and termination criteria are checked. Only seven out of the total of 20 optimization runs here terminate due to reaching the threshold infill criterion, whereas all others run into the maximum number of allowed iterations. Three and four of these seven runs occur with the *HF* and *MF* techniques, respectively. A convergence plot showing the best current objective function value over the high-fidelity evaluations is shown in Fig. 4. Each gray curve represents repetitions of *MF*, and each black curve represents *HF*. The diagram shows generally good convergence behavior, indicating that the different termination criteria encountered may not be problematic per se. However, it should be noted that there are quite a lot of differences between repetitions of the same optimization technique. Possible reasons for these differences are discussed in the following, after presenting the actual optimization results.

The results of the optimization of objective function f_1, which is based on counting the share of bad elements in the FLD are shown in a parallel coordinates plot in Fig. 5. The two techniques *HF* and *MF* are compared. Each curve represents the optimized result of a single optimization run. The color scale indicates the value of the objective function. Different design variables are listed on the x-axis and their normalized ranges on the y-axis. The values of the objective function here are mostly in the range between 0.38 and 0.40 with a total of six exceptions above or below that (see, for example, the dark blue curve for *HF* or the yellow curve for

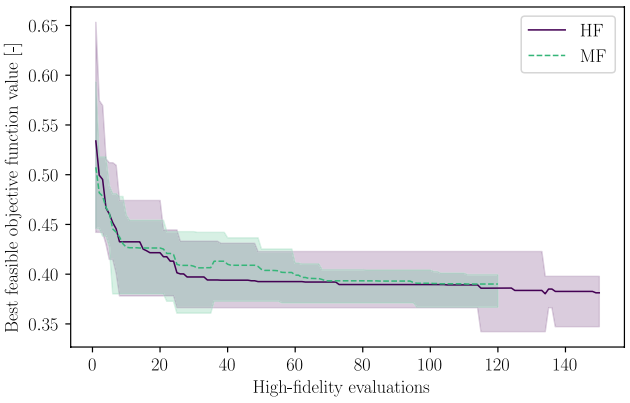

Fig. 4 Objective function f_1: Convergence plot for ten repetitions of the two optimization methods. Mean of the single-fidelity runs is shown as solid black line, multi-fidelity runs as dashed green line. The colored areas represent upper and lower bounds. The first 50 and 20 evaluations are part of the initial design of experiments for *HF* and MF, respectively. (Color figure online)

MF). The average best for the objective function is slightly lower for *HF* compared to *MF*. As this difference is smaller than the variation between repetitions of the same technique, it is not considered significant here. Interestingly, the values of the design variables do not reflect the consistency of the objective function results. In fact, x_3 is the only variable for which a consistent optimal value of around 6.45 mm is found. Intuitively, a higher value for the die radius x_3 should be beneficial to prevent cracks during the drawing process. Here, it is lower, because there is a high number of elements in the wrinkling range where a lower radius can be better. All other design variables vary significantly between different repetitions for both optimization techniques.

The fact that both the convergence plot and the results show significant variations between repetitions across both optimization approaches indicates that the objective function itself might be the problem. Recall that the approach for this objective was to determine the share of 'bad' elements in the FLD. This rather naive approach is tempting because it is very easy to implement and understand. However, it has a number of downsides that could contribute to the inconsistent results reported here. First, counting the categorized elements neglects the degree to which an element violates, for example, the forming limit. In reality, it could make a big difference if an element lies barely above the FLC or is far beyond. Second, the intermediate categorization of elements reduces the influence that design variables have on the objective function. To illustrate this point, imagine an element slightly above the FLC (i.e., in the group of cracked elements) in the basis configuration. Now imagine that this element is experiencing an increased major strain due to, for example, an increase in the blankholder force. Ideally, this worsening state should be reflected in some way in the value of the objective function. However, for f_1 the objective value would not change because the element was already in the group of cracked elements before. This reduced influence of design variables makes any attempt at optimization significantly harder. We believe that this insufficient definition of f_1 is responsible for the inconsistent results reported here. It also leads to 'optimized' designs which are quite different from those found with the other two objective functions, which will be presented below.

For completeness, it should be mentioned that the *MF* approach yields on average a time reduction of around 50% for optimization compared to *HF*. The exact numbers can be found in Table 4 in the Appendix.

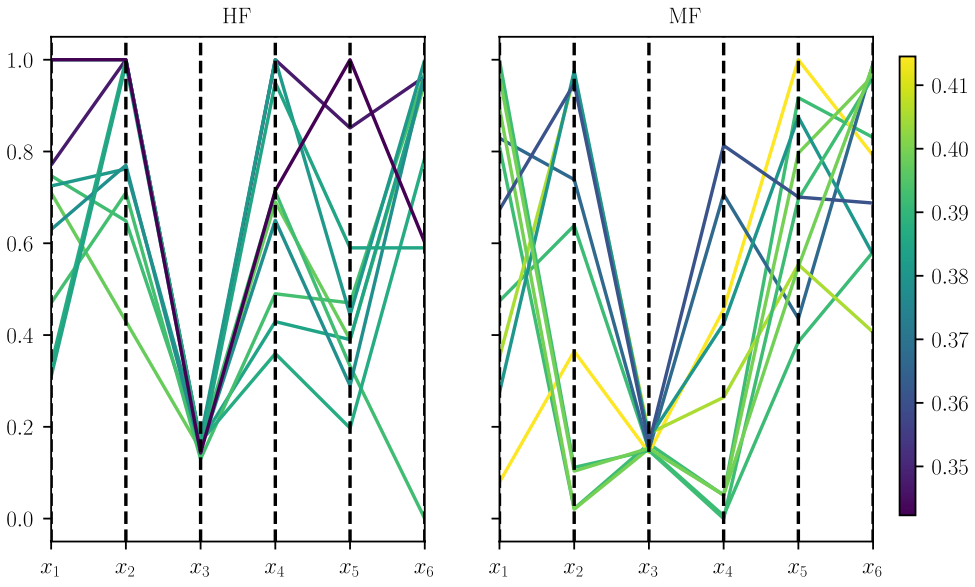

Fig. 5 Objective function f_1: Parallel coordinates plot comparing ten repetitions of the two optimization methods. Design variable values on the y-axis are normalized, actual boundaries can be found in Table 1. The color scale indicates objective function values of the respective results (lower is better). (Color figure online)

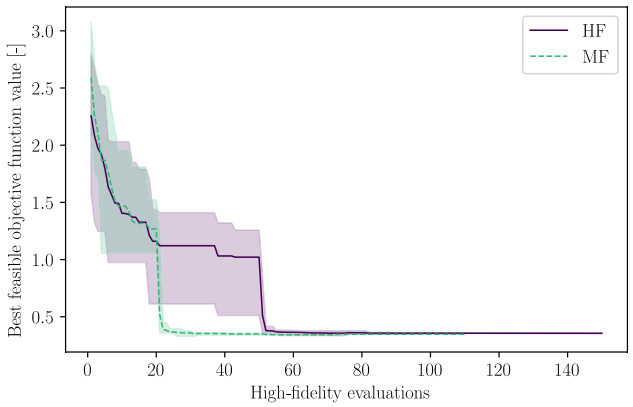

Fig. 6 Objective function f_2: Convergence plot for ten repetitions of the two optimization methods. Mean of the single-fidelity runs is shown as solid black line, multi-fidelity runs as dashed green line. The colored areas represent upper and lower bounds. The first 50 and 20 evaluations are part of the initial design of experiments for *HF* and MF, respectively. (Color figure online)

For the objective function f_1, it can be concluded that the optimization technique *MF* is capable of significantly speeding up the optimization process for the present example problem without reducing the quality of the results. However, the objective function itself is not ideally defined for optimization because the influence of the design variables on the objective function is limited. This leads to very inconsistent optimization results, regardless of the technique used.

5.2 Objective function f_2

The discussion of objective function f_2 which is defined as the weighted average distance of cracked and wrinkle elements to FLC and WLC in the FLD respectively is also started with checking termination conditions and convergence. Here, all *MF* runs and seven of the ten *HF* runs terminate due to the threshold infill criterion indicating good convergence. The remaining three optimizations are terminated after reaching the maximum number of iterations. A convergence plot for this objective function in the same style as above is shown in Fig. 6. Here, repetitions of the same algorithm converge to similar values fairly consistently. In addition, the algorithm reaches values close to the final optimum in very few adaptive high-fidelity evaluations. Just to recall, the adaptive phase starts after 50 and 20 high-fidelity evaluations for *HF* and *MF*, respectively.

A comparison of the optimization results between *HF* and *MF* is shown in Fig. 7. The optimal values of the objective function here are consistently between 0.34 and 0.38, with only one overall worse value in *MF*. Optimal objective function values can also be linked to certain design variable values. x_1 and x_2 are at or close to their lower bounds of 0.8 mm and 12 mm, respectively. x_3 is either at its upper limit 9 mm or around 7.5 mm, x_4 is consistently at its upper limit 2.5, while x_5 and x_6 vary across their entire range between optimizations. The variation in the latter variables indicates that their influence on the objective function is limited. For the Coulomb friction coefficient x_5 this is less surprising as its range was also defined pretty narrowly. For the blankholder force x_6, it can be observed that most of the results are in the lower half of its range, so the best explanation is that its influence diminishes below a certain threshold. Overall, the quality of the results between the two optimization methods is very similar, although there is slightly more variation with *MF*.

To illustrate the progress made during optimization, two designs evaluated during a *MF* optimization run are chosen representatively. The first is the initial evaluation of the

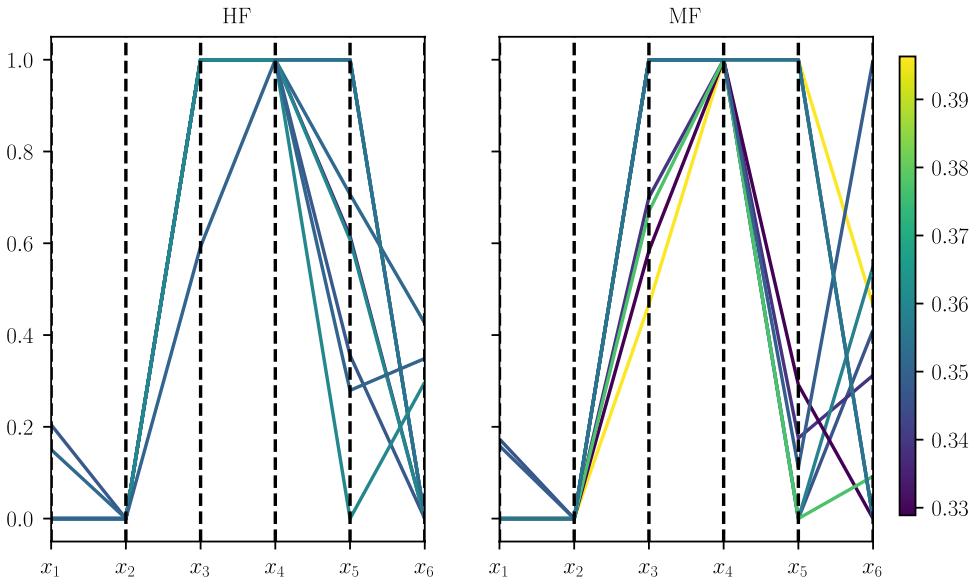

Fig. 7 Objective function f_2: Parallel coordinates plot comparing ten repetitions of the two optimization methods. Design variable values on the *y*-axis are normalized, actual boundaries can be found in Table 1. The color scale indicates objective function values of the respective results (lower is better). (Color figure online)

optimization that produces an objective function value of 2.49 and the second is the optimized evaluation of the same optimization with the objective function value 0.35. FLDs for these two simulations are depicted in Fig. 8. Significant improvements can be seen, particularly with cracked elements, but also in the wrinkling regime. It should be noted here that the optimized result is nevertheless not considered manufacturable, which is expected from the definition of design variable limits (compare Sect. 3).

For computational requirements, *MF* runs on average need around 46% less time to terminate than *HF*. Detailed numbers are listed in Appendix Table 4. These results match fairly well with previously reported time savings of multi-fidelity optimization schemes in structural optimization problems. Compare, for example, Acar et al. (2020) or Kaps et al. (2022) where the authors used multi-fidelity schemes in automotive crashworthiness examples.

In conclusion, *MF* can produce results of comparable quality to *HF*, although they show slightly more variation, while significantly reducing the optimization time using the objective function f_2 in the present example problem. The results with this objective are also significantly more consistent than with f_1, indicating that this is a more suitable objective function for this type of problem.

5.3 Objective function f_3

The results of the thickness reduction objective function f_3 are shown in Fig. 9. Here, good values of the objective function below 0.05 appear to depend on variables x_1, x_2, x_5, and x_6 being close to their respective lower bounds, while x_4 is at its upper bound of 2.5 and x_3 is in the middle between values of 7.5 and 8 mm. We believe that these results are as expected when considering the average thickness reduction of the component over the deep-drawing process. The values of the design variable are also remarkably similar to those observed for f_2. The only exception is the friction coefficient x_5, which is significantly more consistent in its optimal values close to its lower boundary for the present objective function. Interestingly, for this objective function, the *MF* approach yields better and more consistent results than *HF*.

Before looking at the run times and more details of the comparison, convergence information is reported to ensure reliability of the results. For this objective function, all runs of the *HF* method and seven of the ten *MF* runs terminate due to the infill criterion threshold. The other three runs reach the maximum number of iterations. This indicates good convergence of the algorithms. The full convergence plot for all runs, which can be found in Fig. 10, confirms this observation.

The FLD for the best result obtained by the *MF* technique among all repetitions is shown in Fig. 11. As the differences between the repetitions are marginal here, it is also representative of other optimized results from the *MF* method. The component depicted here is not considered manufacturable (see Sect. 3). However, this FLD confirms

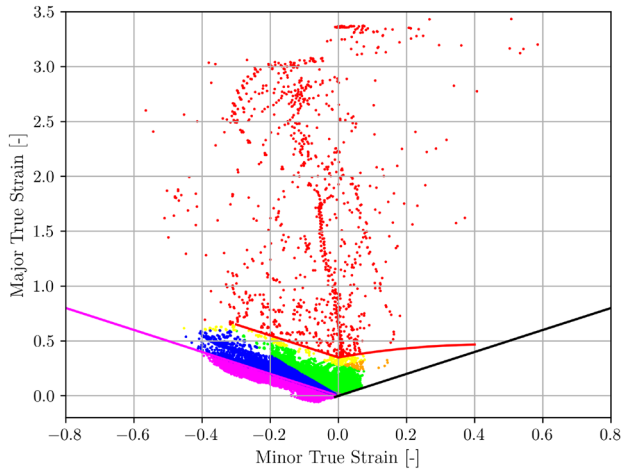

(a) Initial Design.

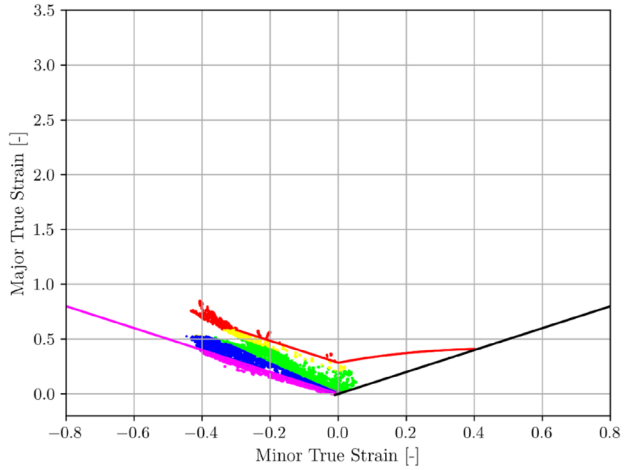

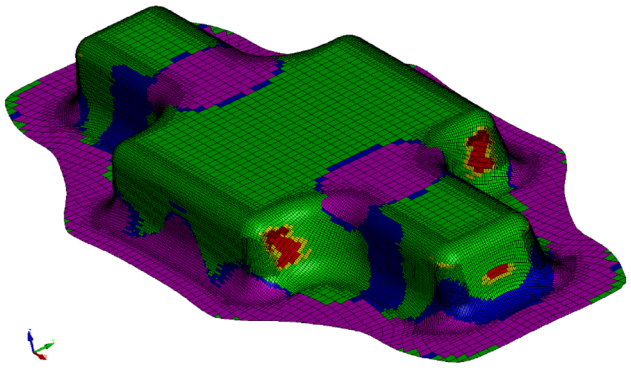

(b) Optimized result.

Fig. 8 Objective function f_2: Comparison of two forming limit diagrams (FLD) of an early simulation and the optimized result of the same optimization run. For the latter, results are also shown mapped onto the final geometry. More details on FLDs can be found in Sect. 4

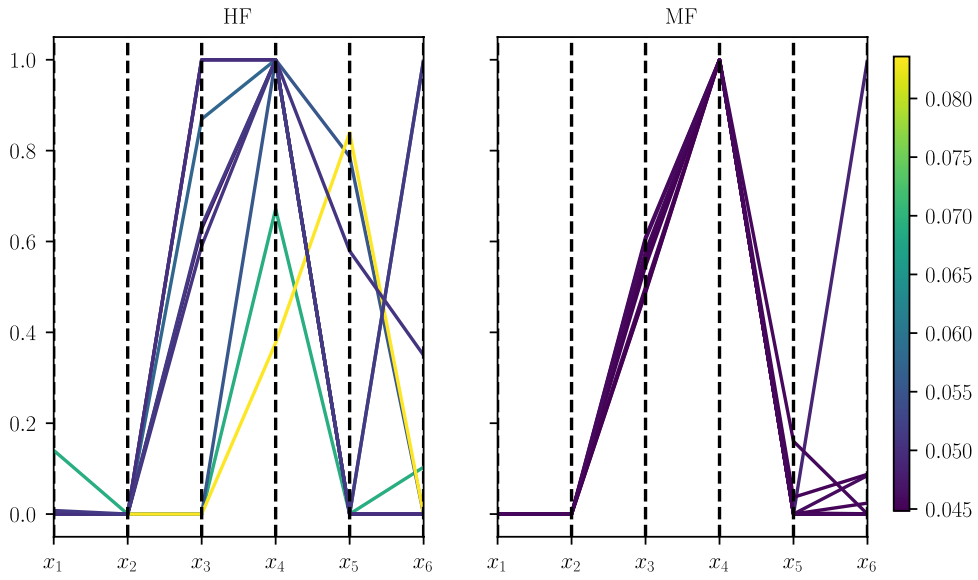

Fig. 9 Objective function f_3: Parallel coordinates plot comparing ten repetitions of the two optimization methods. Design variable values on the y-axis are normalized, actual boundaries can be found in Table 1. The color scale indicates objective function values of the respective results (lower is better). (Color figure online)

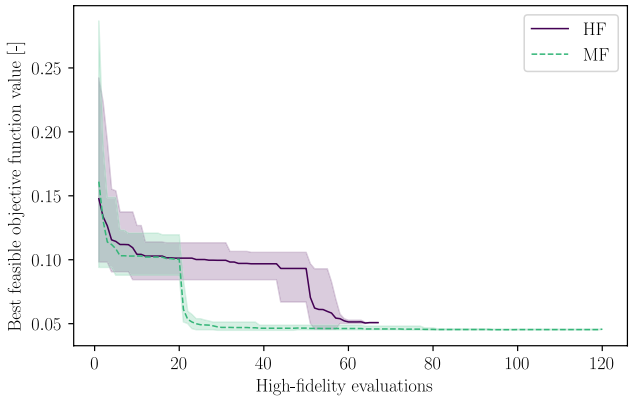

Fig. 10 Objective function f_3: Convergence plot for ten repetitions of the two optimization methods. Mean of the single-fidelity runs is shown as solid black line, multi-fidelity runs as dashed green line. The colored areas represent upper and lower bounds. The first 50 and 20 evaluations are part of the initial design of experiments for *HF* and MF, respectively. (Color figure online)

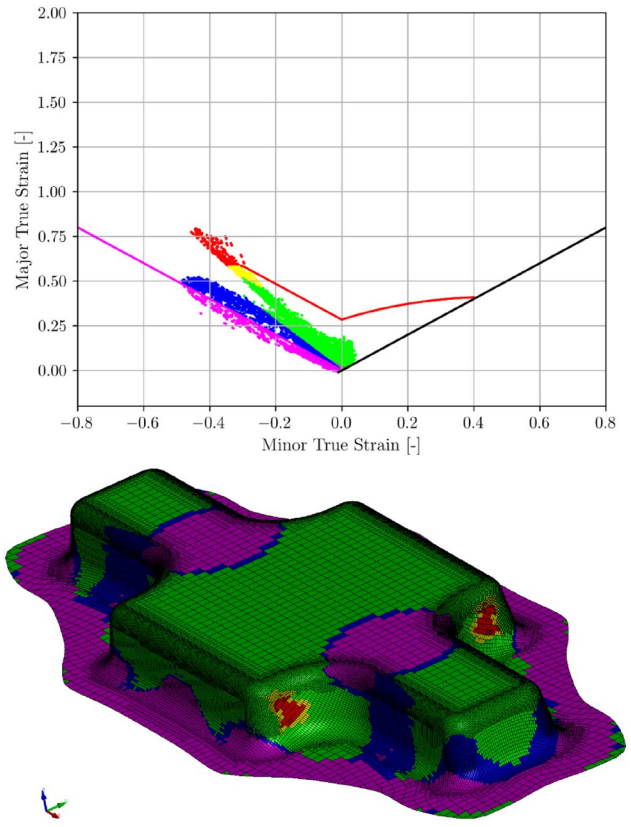

Fig. 11 Objective function f_3: Forming limit diagram of the overall best result obtained with *MF* technique. Results are also shown on the component geometry

the remarkable similarity between the results of f_2 and f_3 (compare Fig. 12c).

For this objective function, optimizations performed with the *MF* technique need on average about 31% longer than *HF* (detailed values are listed in Appendix Table 4). Together with the better and more consistent results found with *MF*, these findings are unexpected. Usually, the aim of a multi-fidelity optimization scheme is to reduce computational effort while not significantly impairing result quality. In this case, the opposite happens, making further investigation of these findings necessary. Several observations can be made as to why in this case *MF* performs better. First, looking at the convergence plots (see Fig. 10), *HF* terminates after fewer high-fidelity evaluations than *MF* for all optimization runs. Usually, the opposite would be expected (compare, for example, Fig. 6). Additionally, all *HF* runs terminate due to the infill criterion threshold, indicating that the algorithm converged and no significant improvements

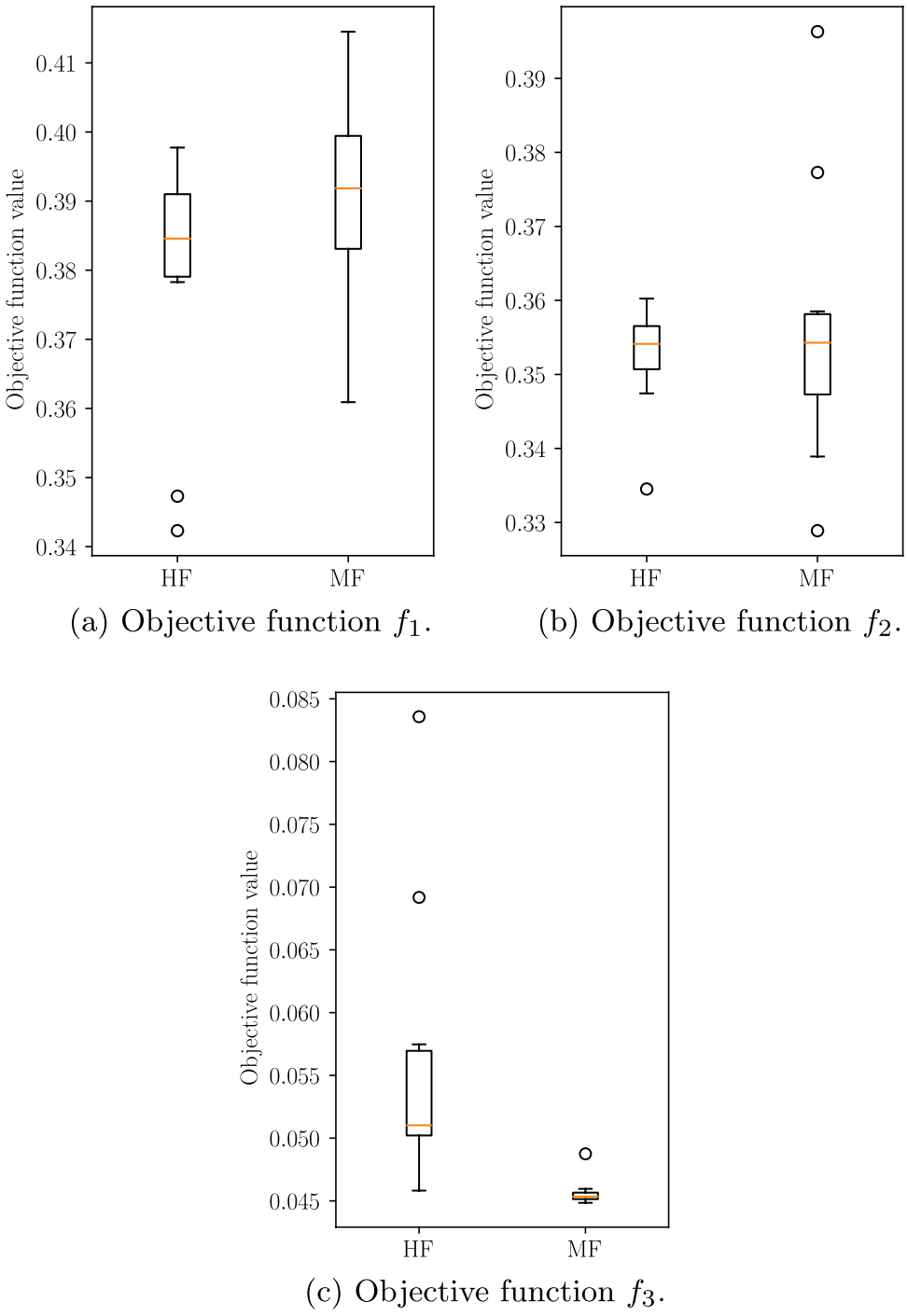

(a) Objective function f_1.

(b) Objective function f_2.

(c) Objective function f_3.

Fig. 12 Box plots comparing results of the different optimization methods. Each method was repeated ten times per objective function

are expected. These two observations show that the kriging model in *HF* may not be sufficiently good and that the optimizer may be stuck at a local optimum. For *MF*, this appears to be less of a problem. Apparently, the additional function evaluations performed with the low-fidelity model, which is then added as a trend term into the HK surrogate model, help the optimizer avoid local optima by better resolving them in the surrogate model.

Overall, the results for this objective function are surprising, as *MF* outperforms *HF* but also requires more computation time. The best current explanation is a higher quality of the surrogate model in *MF* avoiding local minima. We believe that more detailed investigations going beyond the scope of the present work are necessary here. It should also be confirmed whether these results can be repeated for different components and/or design variables.

5.4 Discussion

After presenting the optimization results for all objective functions, some points of discussion will be given below.

Boxplots comparing optimization results for all three objective functions are shown in Fig. 12. The objective function f_1 is found not to be well suited to optimize the example problem chosen here. Both f_2 and f_3 show good performance in the optimization problem. The results between the two are remarkably similar. However, the conclusions drawn are somewhat more differentiated. The objective function f_2 nicely illustrates the potential of a multi-fidelity optimization technique. With very little influence on the result quality, it speeds up the optimization by a factor of two in the present example. The statistical Wilcoxon rank sum test shows that the null hypothesis of equal results for the two methods holds at a 5% significance level ($U = 51$, $p = 0.97$). For the objective function f_3, the same statistical test confirms that the null hypothesis of equal results between the two methods can be rejected at a 5% significance level ($U = 2$, $p < 0.001$). Thus, the multi-fidelity approach even outperforms the classic single-fidelity method for this objective, while also requiring more time to produce results.

The objective functions f_1 and f_2 are not capable of distinguishing manufacturable components from each other. This issue is avoided in the present work through the definition of the optimization problem. Also, it may not be so relevant in practical applications where the main priority is obtaining a manufacturable component. However, in other contexts, such as fitting machine learning models, it could be a challenge. Another possible problem that was observed here is the mesh dependency, especially of objective functions f_1 and f_2. The values of these functions change if the exact same component is meshed differently. In the present work, this is not a concern because all high-fidelity models are meshed the same way. The low-fidelity models used for the *MF* approach are only utilized as a trend term in the HK surrogate model and, thus, are not directly included in comparisons. However, this should be considered in other applications.

6 Conclusions

In the present work, an exemplary cross-die deep-drawing optimization problem is investigated with respect to different objective functions and the use of a multi-fidelity efficient global optimization technique. For the former, three different objective functions are defined, all of which have been previously applied in the literature at least in slightly modified form and primarily for single-fidelity techniques. For the latter, a multi-fidelity efficient global optimization scheme based on hierarchical kriging and variable-fidelity expected improvement is proposed here, which has been successfully used in various fields of applications such as fluid mechanics or automotive crashworthiness.

Two of the three objective functions are based on forming limit diagrams that are commonly used in sheet metal forming to determine the manufacturability of components. The first is based on naively counting elements of different classifications and minimizing the share of bad elements. The second function is defined as minimizing the average violation of the forming and wrinkling limit curves for critical elements. The third objective function to be minimized is the average thickness reduction in the component during the deep-drawing process.

The first objective function is found to be hard to consistently optimize with both the multi-fidelity and a reference single-fidelity efficient global optimization method. The limited influence of design variables on the objective function is identified as one of the main reasons. The second objective function shows consistent result quality across the two optimization techniques and highlights the capability of the multi-fidelity scheme to speed up computation times by a factor up to two. The time gains observed here match well with results previously reported for multi-fidelity optimizations in other fields of application. The third objective function shows surprising results in that the multi-fidelity technique delivers better and more consistent results compared to the single-fidelity reference approach while also increasing the computation times by a factor of approximately 1.3. The currently most likely explanation is the better predictive quality of the surrogate model due to the overall higher number of objective function evaluations in multi-fidelity compared to the single-fidelity technique. However, we believe that these last results warrant a more detailed investigation, which could be interesting for future work.

In addition to that, we believe that it is interesting to further expand the use of multi-fidelity optimization schemes in the field of sheet metal forming. On the basis of the results of the present work, we found a number of additional ideas that we believe to be interesting for future work.

- A number of improvements to the multi-fidelity approach used here have been suggested, which should also be applied to a sheet-metal-forming problem to assess their potential in this field of application.
- Similarly, a number of different multi-fidelity optimization techniques have been suggested which should be compared against other in a sheet-metal-forming problem.
- The results presented here should be confirmed on larger and more complex deep-drawing components.
- Objective functions based on forming limit diagrams cannot distinguish manufacturable components. This might lead to challenges for the optimizer in more realistic problems. An effort should be made to adapt these functions as they are quite intuitive and easily understandable for a human.

Appendix

See Tables 2, 3, 4, and Fig. 13.

Table 2 Cross-die deep-drawing problem: modeling and material properties used to model the steel component

Parameter	Symbol	Value
Component width		290 mm
Component depth		120 mm
Young's modulus	E	205 GPa
Poisson's ratio	ν	0.3
Mass density	ρ	7850 kg m^{-3}
Yield strength	σ_y	160 MPa
Lankford coefficient	R	*Design variable*
Material model (LS-Dyna)	*MAT_037	
1D plasticity	Hockett–Sherby	
	σ_0	160 MPa
	A	600 MPa
	C	0.91
	n	0.518
Element formulation	Belytschko–Lin–Tsay (*HF*)	
	Fully integrated (*LF*)	
Contact formulation	*CONTACT_FORMING_ONE_WAY	
(LS-Dyna; *HF*)	*CONTACT_DRAWBEAD	
Coulomb friction	μ	*Design variable*

*refers to input file keywords of the FE software LS-Dyna

HF incremental (high-fidelity) simulation, *LF* inverse (low-fidelity) simulation

Table 3 Overview of the average number of simulation model calls for different objective functions and optimization methods

Obj	Method	High-fidelity calls	Low-fidelity calls
f_1	*HF*	144.8 (SD 10.7)	–
f_1	*MF*	85.8 (SD 41.9)	100.0 (SD 0.0)
f_2	*HF*	101.5 (SD 33.6)	–
f_2	*MF*	47.7 (SD 24.7)	103.9 (SD 3.2)
f_3	*HF*	58.8 (SD 4.0)	–
f_3	*MF*	88.1 (SD 26.2)	100.7 (SD 0.6)

Each optimization run is repeated ten times. The results are reported as mean and standard deviation (SD). The abbreviations *MF* and *HF* refer to the multi-fidelity and baseline single-fidelity optimization techniques, respectively

Table 4 Overview of the optimization run times for different objective functions and optimization methods

Objective	Method	Run time (s)
f_1	*HF*	150,900 (SD 13,700)
f_1	*MF*	75,900 (SD 25,900)
f_2	*HF*	83,000 (SD 27,200)
f_2	*MF*	44,600 (SD 19,400)
f_3	*HF*	53,600 (SD 3000)
f_3	*MF*	70,400 (SD 16,500)

Each optimization run is repeated ten times. The results are reported as mean and standard deviation (SD) of the run times in seconds, rounded to the nearest 100. The abbreviations *MF* and *HF* refer to the multi-fidelity and baseline single-fidelity optimization techniques, respectively

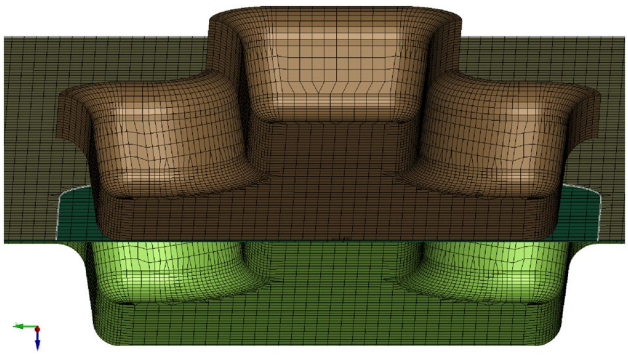

Fig. 13 Exemplary zoom into a high-fidelity simulation model at the initial time step, cut open in the middle. Shown in brown is the punch which moves down to form the component and in light green the die. The blank which is formed into the desired shape is shown in dark green and held in place by a blank holder depicted here in olive. (Color figure online)

Acknowledgements This project is supported by the Federal Ministry for Economic Affairs and Climate Action (BMWK) on the basis of a decision by the German Bundestag (Reference Number KK5339801BD1).

Author contributions AK: Conceptualization, Methodology, Software, Formal analysis, and investigation, Writing—original draft, Writing—review and editing; TL: Software, Writing—review and editing; IL: Software, Writing—review and editing; MW: Writing—review and editing, Supervision; FD: Writing—review and editing, Supervision.

Funding Open Access funding enabled and organized by Projekt DEAL.

Declarations

Conflict of interest On behalf of all authors, the corresponding author declares that there is no conflict of interest.

Replication of results The detailed information on the proposed methods, simulation models, and the software used in this article can be found in the corresponding sections. This includes the algorithms and hyperparameters used. The self-implemented parts of the in-house Python code and exemplary simulation models for high- and low-fidelity models can be obtained from the corresponding author on reasonable request.

References

Ablat MA, Qattawi A (2016) Numerical simulation of sheet metal forming: a review. Int J Adv Manuf Technol 89(1–4):1235–1250. https://doi.org/10.1007/s00170-016-9103-5

Acar E, Yilmaz B, Güler MA, Altin M (2020) Multi-fidelity crashworthiness optimization of a bus bumper system under frontal impact. J Braz Soc Mech Sci Eng 42(9):1–17. https://doi.org/10.1007/s40430-020-02572-3

Andrade-Campos A, Coppieters S, Strano M (2022) Optimization and inverse analysis in metal forming: scientific state-of-the-art and recent trends. Int J Mater Form. https://doi.org/10.1007/s12289-022-01690-8

Banabic D (2010) Sheet metal forming processes. Springer, Berlin. https://doi.org/10.1007/978-3-540-88113-1

Forrester AI, Keane AJ (2009) Recent advances in surrogate-based optimization. Prog Aerosp Sci 45(1–3):50–79. https://doi.org/10.1016/j.paerosci.2008.11.001

Forrester AI, Sóbester A, Keane AJ (2007) Multi-fidelity optimization via surrogate modelling. Proc R Soc A 463(2088):3251–3269. https://doi.org/10.1098/rspa.2007.1900

Garud SS, Karimi IA, Kraft M (2017) Design of computer experiments: a review. Comput Chem Eng 106:71–95. https://doi.org/10.1016/j.compchemeng.2017.05.010

Goodwin GM (1968) Application of strain analysis to sheet metal forming problems in the press shop. In: SAE technical paper series. SAE International. https://doi.org/10.4271/680093

GPy (2012) GPy: a Gaussian process framework in python. http://github.com/SheffieldML/GPy

Guo Y, Batoz J, Naceur H, Bouabdallah S, Mercier F, Barlet O (2000) Recent developments on the analysis and optimum design of sheet metal forming parts using a simplified inverse approach. Comput Struct 78(1–3):133–148. https://doi.org/10.1016/s0045-7949(00)00095-x

Han ZH, Görtz S (2012) Hierarchical kriging model for variable-fidelity surrogate modeling. AIAA J 50(9):1885–1896. https://doi.org/10.2514/1.J051354

Hoque SE, Duddeck F (2021) Experimental and numerical characterization of plasticity and fracture behavior of aluminum 6061-T4 sheet for deep drawing simulation. In: XVI international conference on computational plasticity. Fundamentals and applications. https://doi.org/10.23967/complas.2021.013

Huang D, Allen TT, Notz WI, Miller RA (2006) Sequential kriging optimization using multiple-fidelity evaluations. Struct Multidisc Optim 32(5):369–382. https://doi.org/10.1007/s00158-005-0587-0

Jakumeit J, Herdy M, Nitsche M (2005) Parameter optimization of the sheet metal forming process using an iterative parallel kriging algorithm. Struct Multidisc Optim 29(6):498–507. https://doi.org/10.1007/s00158-004-0455-3

Jansson T, Andersson A, Nilsson L (2005) Optimization of draw-in for an automotive sheet metal part. J Mater Process Technol 159(3):426–434. https://doi.org/10.1016/j.jmatprotec.2004.06.011

Jin R, Chen W, Sudjianto A (2003) An efficient algorithm for constructing optimal design of computer experiments. In: International design engineering technical conferences and computers and information in engineering conference, Chicago, pp 545–554

Jones DR (2001) A taxonomy of global optimization methods based on response surfaces. J Glob Optim 21(4):345–383. https://doi.org/10.1023/A:1012771025575

Jones DR, Schonlau M, Welch WJ (1998) Efficient global optimization of expensive black-box functions. J Glob Optim 13(4):455–492. https://doi.org/10.1023/A:1008306431147

Kaps A, Czech C, Duddeck F (2022) A hierarchical kriging approach for multi-fidelity optimization of automotive crashworthiness problems. Struct Multidisc Optim. https://doi.org/10.1007/s00158-022-03211-2

Keeler SP (1968) Circular grid system—a valuable aid for evaluating sheet metal formability. In: SAE technical paper series. SAE International. https://doi.org/10.4271/680092

Kishor N, Kumar DR (2002) Optimization of initial blank shape to minimize earing in deep drawing using finite element method. J Mater Process Technol 130–131:20–30. https://doi.org/10.1016/s0924-0136(02)00790-2

Komeilizadeh K, Kaps A, Duddeck F (2022) Isovolumetric adaptations to space-filling design of experiments. Optim Eng. https://doi.org/10.1007/s11081-022-09731-6

Krige DG (1951) A statistical approach to some basic mine valuation problems on the Witwatersrand. J South Afr Inst Min Metall 52(6):119–139. https://doi.org/10.10520/AJA0038223X_4792

Lee C, Huh H (1997) Blank design and strain prediction of automobile stamping parts by an inverse finite element approach. J Mater Process Technol 63(1–3):645–650. https://doi.org/10.1016/s0924-0136(96)02700-8

Lee C, Huh H (1998) Three dimensional multi-step inverse analysis for the optimum blank design in sheet metal forming processes. J Mater Process Technol 80–81:76–82. https://doi.org/10.1016/s0924-0136(98)00178-2

Makinouchi A (1996) Sheet metal forming simulation in industry. J Mater Process Technol 60(1–4):19–26. https://doi.org/10.1016/0924-0136(96)02303-5

Matheron G (1963) Principles of geostatistics. Econ Geol 58(8):1246–1266. https://doi.org/10.2113/gsecongeo.58.8.1246

McKay MD, Beckman RJ, Conover WJ (1979) Comparison of three methods for selecting values of input variables in the analysis of output from a computer code. Technometrics 21(2):239–245. https://doi.org/10.1080/00401706.1979.10489755

Morris MD, Mitchell TJ (1995) Exploratory designs for computational experiments. J Stat Plan Inference 43(3):381–402. https://doi.org/10.1016/0378-3758(94)00035-T

Naceur H, Guo Y, Batoz J, Knopf-Lenoir C (2001) Optimization of drawbead restraining forces and drawbead design in sheet metal forming process. Int J Mech Sci 43(10):2407–2434. https://doi.org/10.1016/s0020-7403(01)00014-5

Naceur H, Delaméziere A, Batoz J, Guo Y, Knopf-Lenoir C (2004) Some improvements on the optimum process design in deep drawing using the inverse approach. J Mater Process Technol 146(2):250–262. https://doi.org/10.1016/j.matprotec.2003.11.015

Obermeyer E, Majlessi S (1998) A review of recent advances in the application of blank-holder force towards improving the forming limits of sheet metal parts. J Mater Process Technol 75(1–3):222–234. https://doi.org/10.1016/s0924-0136(97)00368-3

Ohata T, Nakamura Y, Katayama T, Nakamachi E, Omori N (1998) Improvement of optimum process design system by numerical simulation. J Mater Process Technol 80–81:635–641. https://doi.org/10.1016/s0924-0136(98)00170-8

Park C, Haftka RT, Kim NH (2016) Remarks on multi-fidelity surrogates. Struct Multidisc Optim 55(3):1029–1050. https://doi.org/10.1007/s00158-016-1550-y

Paul SK (2013) Theoretical analysis of strain- and stress-based forming limit diagrams. J Strain Anal Eng Des 48(3):177–188. https://doi.org/10.1177/0309324712468524

Pedregosa F, Varoquaux G, Gramfort A, Michel V, Thirion B, Grisel O, Blondel M, Prettenhofer P, Weiss R, Dubourg V, Vanderplas J, Passos A, Cournapeau D, Brucher M, Perrot M, Duchesnay E (2011) Scikit-learn: machine learning in Python. J Mach Learn Res 12:2825–2830

Rajabi MM, Ataie-Ashtiani B, Janssen H (2015) Efficiency enhancement of optimized Latin hypercube sampling strategies: application to Monte Carlo uncertainty analysis and meta-modeling. Adv Water Resour 76:127–139. https://doi.org/10.1016/j.advwatres.2014.12.008

Rasmussen CE, Williams CKI (2005) Gaussian processes for machine learning. MIT Press Ltd, Cambridge. https://doi.org/10.7551/mitpress/3206.001.0001

Ruan X, Jiang P, Zhou Q, Hu J, Shu L (2020) Variable-fidelity probability of improvement method for efficient global optimization of expensive black-box problems. Struct Multidisc Optim 62(6):3021–3052. https://doi.org/10.1007/s00158-020-02646-9

Sacks J, Welch WJ, Mitchell TJ, Wynn HP (1989) Design and analysis of computer experiments. Stat Sci 4(4):409–423. https://doi.org/10.1214/ss/1177012413

Sattari H, Sedaghati R, Ganesan R (2007) Analysis and design optimization of deep drawing process. J Mater Process Technol 184(1–3):84–92. https://doi.org/10.1016/j.jmatprotec.2006.11.008

Schenk O, Hillmann M (2004) Optimal design of metal forming die surfaces with evolution strategies. Comput Struct 82(20–21):1695–1705. https://doi.org/10.1016/j.compstruc.2004.03.055

Storn R, Price K (1997) Differential evolution—a simple and efficient heuristic for global optimization over continuous spaces. J Glob Optim 11(4):341–359. https://doi.org/10.1023/a:1008202821328

Sun G, Li G, Zhou S, Xu W, Yang X, Li Q (2010) Multi-fidelity optimization for sheet metal forming process. Struct Multidisc Optim 44(1):111–124. https://doi.org/10.1007/s00158-010-0596-5

Sun G, Li G, Li Q (2012) Variable fidelity design based surrogate and artificial bee colony algorithm for sheet metal forming process. Finite Elem Anal Des 59:76–90. https://doi.org/10.1016/j.finel.2012.04.012

Toal DJJ, Bressloff NW, Keane AJ (2008) Kriging hyperparameter tuning strategies. AIAA J 46(5):1240–1252. https://doi.org/10.2514/1.34822

Viana FAC (2015) A tutorial on Latin hypercube design of experiments. Qual Reliab Eng Int 32(5):1975–1985. https://doi.org/10.1002/qre.1924

Volk W, Suh J (2013) Prediction of formability for non-linear deformation history using generalized forming limit concept (GFLC). AIP. https://doi.org/10.1063/1.4850035

Wifi AS, Abdelmaguid TF, El-Ghandour AI (2007) A review of the optimization techniques applied to the deep drawing process. In: Proceedings of the 37th international conference on computers and industrial engineering, Alexandria, pp 1111–1121

Ye KQ, Li W, Sudjianto A (2000) Algorithmic construction of optimal symmetric Latin hypercube designs. J Stat Plan Inference 90(1):145–159. https://doi.org/10.1016/S0378-3758(00)00105-1

Zhang Y, Han ZH, Zhang KS (2018) Variable-fidelity expected improvement method for efficient global optimization of expensive functions. Struct Multidisc Optim 58(4):1431–1451. https://doi.org/10.1007/s00158-018-1971-x

A.3 Publication III

Kaps A., Lehrer T., Lepenies I., Wagner M., Quek S.T., Duddeck F.: A novel two-stage multi-fidelity optimization for manufacturability of deep-drawn metal sheets. 2024. (submitted for publication at Structural and Multidisciplinary Optimization)

A novel two-stage multi-fidelity optimization for manufacturability of deep-drawn metal sheets

Arne Kaps[1*], Tobias Lehrer[1], Ingolf Lepenies[2], Marcus Wagner[3], Ser Tong Quek[4] and Fabian Duddeck[1]

[1]TUM School of Engineering and Design, Technical University of Munich, Arcisstr. 21, 80333 Munich, Germany.
[2]SCALE GmbH, Pohlandstr. 19 01309 Dresden, Germany.
[3]Department of Mechanical Engineering, Ostbayerische Technische Hochschule Regensburg, Galgenbergstr. 30, 93053 Regensburg, Germany.
[4]Department of Civil and Environmental Engineering, National University of Singapore, 1 Engineering Drive 2, Singapore 117576, Singapore.

*Corresponding author(s). E-mail(s): arne.kaps@tum.de;

Abstract

In the present work, a two-stage multi-fidelity optimization scheme is proposed and investigated on a cross-die deep drawing application problem. In the novel scheme, a global enrichment with respect to the limit state of the objective function is performed between the initial design of experiments and the adaptive optimization stage. To that end, we propose a multi-fidelity extension of the popular U learning function, which is commonly used in reliability or uncertainty quantification problems. The two-step workflow is compared to a multi-fidelity approach based on hierarchical kriging as a surrogate model and variable-fidelity expected improvement as infill criterion as well as a single-fidelity reference. We find that the novel approach can reduce optimization run times compared to the single-stage approach with minor impact on result quality. Additionally, a combination of the proposed multi-fidelity approach with a modified Latin hypercube sampling is shown to speed up optimization run time compared to the single-fidelity reference by a factor of almost three in our application example.

Keywords: Multi-fidelity optimization, Efficient global optimization, Optimization under uncertainty, Sheet-metal forming, Deep drawing

1 Introduction

Sheet metal forming and specifically deep drawing is one of the most wide spread manufacturing processes for structural components. Its idea is to plastically deform a thin metal sheet into its desired shape. Developing functional deep-drawn parts can be a highly challenging process, because various (conflicting) requirements such as cost reduction, manufacturability, sustainability, or aesthetics are influenced by a variety of parameters. These range from the material properties of the metal sheet to the process parameters and to the geometry parameters of the component itself. To support engineers, numerical methods such as finite element (FE) methods have been in industrial use for decades (Makinouchi, 1996). However, the development of new methods has not stopped

and is, in fact, part of ongoing research (Ablat and Qattawi, 2016; Andrade-Campos et al, 2022).

With the advent of simulation models, researchers have also begun to use optimization algorithms in sheet metal forming applications (Ohata et al, 1998; Guo et al, 2000). One popular example of an algorithm designed for these expensive objective functions is Efficient Global Optimization (EGO; Jones et al (1998)) which utilizes a kriging model (Krige, 1951; Matheron, 1963; Sacks et al, 1989) and performs iterative updates on it by internally optimizing an infill criterion (Jones, 2001). However, in recent years, simulation model sizes and resolutions have increased to the point that even with these specialized techniques, computational costs may be prohibitive. As one remedy, multi-fidelity (MF) schemes have been introduced. An accurate high-fidelity (HF) model is complemented by a less accurate, yet more efficient, low-fidelity (LF) model. This basic idea has already been applied to sheet metal forming problems (Sun et al, 2010, 2012). In the present work, a multi-fidelity surrogate model called hierarchical kriging (HK; Han and Görtz (2012)) and an infill criterion called variable-fidelity expected improvement (VF-EI; Zhang et al (2018)) are applied in an MF version of EGO. We have shown in a previous work that this type of algorithm can perform very well in improving the manufacturability of a deep-drawn component (Kaps et al, 2023). Interested readers are referred to previous work on multi-fidelity surrogate models and optimization for more information on different available approaches (Forrester et al, 2007; Park et al, 2016; Zhou et al, 2023).

The aim in reliability analysis is commonly to determine the limit state of a function and to estimate the probability of failure for a given structural problem. In the context of expensive functions, surrogate-based reliability analysis has also been well established in the literature. An adaptively improving kriging model was suggested by (Bichon et al, 2008) that is conceptually inspired by the EGO optimization technique except for the novel infill criterion called *expected feasibility function* (EFF). The approach was then extended among other things with a new infill criterion called U learning function (Echard et al, 2011) which is inspired by the lower confidence bound criterion in optimization (Cox and John, 1992). A review of existing methodology as well as the development of a unified framework for reliability analysis and design optimization are given by Moustapha and Sudret (2019). More recently, these methods and, particularly, the U learning function were also applied in a multi-fidelity setting (Chakroborty et al, 2023; Dhulipala et al, 2022).

In the present work, we aim to improve the optimization performance of an HK-based multi-fidelity approach. Inspired by previous work (Pei et al, 2023) we propose a two-stage optimization technique in which a global enrichment with respect to the limit state of the objective function is performed between the initial design of experiments (DoE) and the subsequent adaptive objective function improvement. One of the main contributions of the present work alongside the two-stage multi-fidelity optimization technique is the proposal of a novel multi-fidelity extension to the popular U learning function. This function is used here to facilitate the global enrichment. Its use is inspired by the fact that drawability measures have a limit state just like the one encountered in reliability analysis, the drawability limit. Additionally, we investigate the influence of a modified DoE scheme on optimization performance. All approaches are investigated on a cross-die deep drawing application problem.

This paper is structured as follows. In Section 2, the cross-die deep drawing optimization problem is presented, including simulation models, parameters, and the objective function. The basics of the multi-fidelity optimization scheme including HK and the relevant infill criteria are summarized in Section 3. Subsequently, the proposed optimization scheme is introduced in Section 4. Optimization results are shown and discussed in Section 5, followed by our conclusions and an outlook into possible future work (Section 6).

2 Application example

The exemplary optimization problem used here to compare different optimization algorithms is introduced below. The optimization problem is based on a cross-die deep-drawing simulation similar to the one studied by Hoque and Duddeck (2021) and previously utilized by the authors in Kaps et al (2023) and Lehrer et al (2023). Initially, the simulation model is presented in Subsection 2.1, subsequently, the design and noise variables, as

well as the objective function, are introduced in Subsections 2.2 and 2.3, respectively.

2.1 Simulation models

An exemplary configuration of the component after drawing is shown in Figure 1. The modeling parameters along with numerical values can be found in Table A2 in the Appendix. As a high-fidelity model, an incremental explicit simulation in LS-Dyna is used. Here, all the tooling is modeled as rigid, and the sheet blank is made of steel. Coulomb friction is assumed between the blank and the tools. A high-fidelity simulation model with all tooling at the initial time step is depicted in the Appendix Figure A1 for illustrative purposes. The simulation of a deep drawing process consists of many process steps which are only outlined here. Readers are referred to the available textbooks on the topic for more detailed presentations of the various details (e.g., Banabic (2010)). Initially, the blank is pressed to the die by the blankholder while the punch moves into contact with the blank. As the punch then moves further, the deep drawing itself occurs, which describes the non-linear forming of the blank into its final shape. Finally, an elastic springback of the component occurs when the punch is removed. This step is not considered here due to the focus of the present work on drawability rather than on dimensional accuracy. The inverse implicit one-step capability of LS-Dyna is utilized as a low-fidelity model. The idea of an inverse one-step approach is to apply deformation theory to derive stresses, strains, and thicknesses in the formed component given the final geometry of the component. For more detailed elaborations on the inverse approach including the governing equations, readers are referred to the research articles on the topic, such as the original publication (Guo et al, 1990).

The maximum element size is set to 5 mm for the low-fidelity model, compared to 3 mm for the high-fidelity model. The smallest element size after adaptive mesh refinement in the high-fidelity model is 0.5 mm. Simulation times are approximately ten minutes and one minute, for high- and low-fidelity simulation models, respectively, when running on eight cores[1]. The exact run times also vary depending on the choice of design variables.

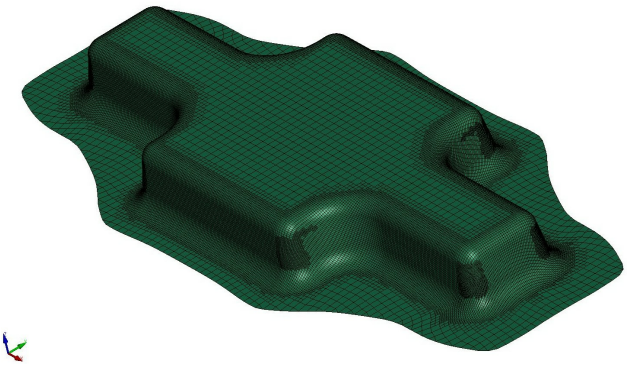

Fig. 1: Exemplary geometry of the cross-die component studied here (adapted from Kaps et al (2023)).

2.2 Parameters

Four design variables and two uncertain noise variables are selected for the problem studied here. All design variables and their specified limits are summarized in Table 1. Noise variables and their assumed distributions are listed in Table 2.

Table 1: Overview of the design variables specified for the optimization problem considered here.

Symbol	Name	Bounds	Unit
x_1	sheet thickness	$[0.8, 1.8]$	mm
x_2	die radius	$[6, 9]$	mm
x_3	Lankford coeff.	$[0.8, 2.5]$	-
x_4	blankholder force	$[130, 190]$	kN

In the present work, the design variables are chosen as examples from the three categories of variables found in sheet metal forming applications: geometry parameters (see, for example, Guo et al (2000) or Kishor and Kumar (2002)), process parameters (for example, blank holding force, Obermeyer and Majlessi (1998)), and material parameters. The thickness of the initial sheet metal and the die radius are chosen as geometry parameters. As a process parameter, the

[1]The used LS-Dyna version is R12, runs are performed on an Intel Core i9-10900 CPU with 64GB RAM, running Ubuntu version 20.04.

Table 2: Overview of the noise variables specified for the present optimization problem. The notation $\mathcal{N}(\mu, \sigma^2)$ refers to a normal distribution with mean μ and standard deviation σ.

Symbol	Name	Distribution	Unit
x_5	yield strength	$\mathcal{N}(160, 6.67^2)$	MPa
x_6	static frict. coeff.	$\mathcal{N}(0.1, 0.0067^2)$	-

blankholder force is chosen. The Lankford coefficient, which represents the normal anisotropy of the material, is varied as a material parameter.

Yield strength and friction coefficient are defined as noise variables to represent commonly encountered uncertainties in material and process parameters, respectively. Noise variables are assumed to not be directly controllable here and defined to follow a normal distribution around an expected value. Previous work on optimization under uncertainty in deep drawing applications such as by Nguyen and Reiter (2015) or Merten et al (2021) was used as orientation in the definition of noise variable distributions.

Some of the design variables such as sheet metal thickness or material parameters would be treated as discrete in a more realistic application. Here, they are considered continuous for the sake of simplicity.

The sizes of the initial DoEs used with the different optimization techniques in this example are listed in the Appendix Table A1 .

2.3 Objective function

The objective function utilized here is based on the forming limit diagram (FLD). It was initially suggested in a similar form by Naceur et al (2004) and applied in a multi-fidelity setup by Sun et al (2010). The authors used it previously in Kaps et al (2023) and extended it in Lehrer et al (2023) to be able to distinguish drawable parts from each other. The latter extended form is used in the present work and is briefly introduced in the following.

Initially defined in the 1960s (Goodwin, 1968; Keeler, 1968) an FLD defines two material-dependent curves for the limits of the sheet metal component. The forming limit curve (FLC) represents the onset of localized necking in the component, while the wrinkling limit curve (WLC) represents the onset of wrinkling. Over the years, many improvements and variations of FLDs have been suggested, and readers are referred to previous publications that review the topic in more detail (such as Obermeyer and Majlessi (1998) or Paul (2013)).

An exemplary FLD in the definition used in the present work is shown in Figure 2. The red and pink lines represent FLC and WLC, respectively. The major and minor true strains in each element of the final deep-drawn sheet metal component are plotted against each other.

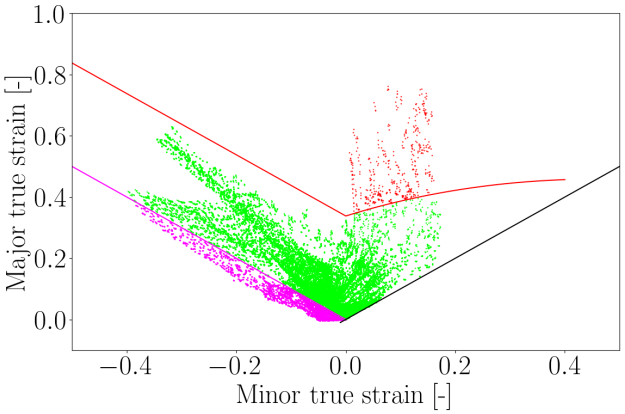

Fig. 2: Exemplary forming limit diagram for a cross-die component. The red line is the FLC and the pink line represents the WLC. Each dot represents an element of the simulation model. The black line marks the limit of strain definitions, i.e. $\epsilon_1 \geq \epsilon_2$.

The calculation process of the objective function introduced in the following is also summarized as Algorithm 1 in the Appendix for clarity. The calculation of the objective function starts by calculating the average distance of 'bad' elements from their respective limit curve (LC). Here, the FLC and WLC are assumed to be black-box functions. Given the major and minor true strain values $\boldsymbol{\epsilon}^e$ of an element e, they return the closest points on the respective curves $\hat{\boldsymbol{\epsilon}}^{FLC}$ and $\hat{\boldsymbol{\epsilon}}^{WLC}$. These are subsequently used for distance calculation as

$$d\left(\boldsymbol{\epsilon}^e, \hat{\boldsymbol{\epsilon}}^{LC}\right) = \|\boldsymbol{\epsilon}^e - \hat{\boldsymbol{\epsilon}}^{LC}\|_2. \tag{1}$$

The non-drawable factor of the objective function f_{nd} is then defined as the weighted average of these distances

$$f_{nd} = f_c + w_w f_w, \text{where}$$
$$f_c = \begin{cases} \frac{\sum_{e=1}^{N_c} d\left(\boldsymbol{\epsilon}^e, \hat{\boldsymbol{\epsilon}}^{FLC}\right) A^e}{\sum_{e=1}^{N_c} A^e} & , \epsilon_1^e > \epsilon_1^{FLC} \\ 0 & , \text{else} \end{cases}, \tag{2}$$
$$f_w = \begin{cases} \frac{\sum_{e=1}^{N_w} d\left(\boldsymbol{\epsilon}^e, \hat{\boldsymbol{\epsilon}}^{WLC}\right) A^e}{\sum_{e=1}^{N_w} A^e} & , \epsilon_1^e < \epsilon_1^{WLC} \\ 0 & , \text{else} \end{cases}.$$

Here, A^e is the element area utilized as weight. N_c and N_w represent the number of cracked and wrinkling elements, respectively. w_w is a weighting factor that balances the contributions of crack and wrinkling elements. It is set to $w_w = 0.1$ following previous experiences of the authors with very similar cross-die deep drawing examples (Kaps et al, 2023; Lehrer et al, 2023).

The function f_{nd} is not able to distinguish drawable components from each other because it only considers cracked and wrinkle elements. Therefore, it is extended with a drawable factor f_d that represents the average distance of good elements to the two LCs and is defined as follows:

$$f_d = -w_g \sum_{e=1}^{N_g} A^e \frac{d\left(\boldsymbol{\epsilon}^e, \hat{\boldsymbol{\epsilon}}^{FLC}\right) + w_w d\left(\boldsymbol{\epsilon}^e, \hat{\boldsymbol{\epsilon}}^{WLC}\right)}{1 + w_w}. \tag{3}$$

The weighting factor w_g that is introduced to balance the magnitudes of f_d and f_{nd} is set to $w_g = 0.2$ following the suggestion of Lehrer et al (2023).

The complete objective function f is then defined as

$$f = \begin{cases} f_{nd} & , \text{if } f_{nd} > f_{thr} \\ f_d & , \text{else} \end{cases}, \tag{4}$$

where $f_{thr} = 0.005$ is a threshold value to account for components with only minor wrinkling in non-critical regions that could be considered drawable.

Given the objective function f, as well as the design and noise variables introduced in the previous subsection, the optimization problem discussed here is defined as

$$\min_{\boldsymbol{x}} \quad f(\boldsymbol{x}), \tag{5a}$$
$$\text{where} \quad \underline{x}_i \leq x_i \leq \bar{x}_i, \quad i = 1, 2, 3, 4, \tag{5b}$$
$$\text{subject to} \quad x_j \sim \mathcal{N}(\mu_j, \sigma_j^2), \quad j = 5, 6. \tag{5c}$$

The formulation $f(\boldsymbol{x})$ includes the entire simulation workflow, where, depending on the fidelity level and design variable values, a high-fidelity or low-fidelity simulation model is generated, evaluated, and the resulting strain field is used to calculate the objective function value. Here, $\underline{x}_i$ and $\bar{x}_i$ represent the lower and upper limits of the four design variables introduced in Table 1. μ_j and σ_j are the mean and standard deviation of the Gaussian distributions of the two noise variables, as shown in Table 2.

The noise variables in this work are included in the surrogate model by extending the design space with a $\pm 3\sigma$ interval around their mean value (see also Section 4 below). The surrogate model is then used in the optimization phase of the algorithm to provide an estimation of the optimized results being non-drawable under the influence of the noise variables. To that end, 10^4 Monte Carlo samples drawn from the distributions of the noise variables are evaluated on the respective surrogate model.

3 Multi-fidelity optimization

The multi-fidelity EGO approach which is based on HK and VF-EI and used as a baseline is introduced below. The extended approach proposed here is presented in Section 4. The optimization scheme consists of two major parts. Initially, a surrogate model is fitted from a set of design samples, which is generated using design of experiments. Kriging is commonly used in single-fidelity applications. Here, HK is employed due to its ability to provide superior error approximations compared to other multi-fidelity kriging methods (Han and Görtz, 2012). Subsequently, this surrogate model is iteratively updated using an infill criterion to determine the location of new samples. In the present work, VF-EI is utilized, because it has been shown to work well in the metal forming application (Kaps et al, 2023).

DoE is the first step in this optimization scheme. As there is no unique best way to distribute samples, it is still an active field of research (Garud et al, 2017). Here, an optimal Latin hypercube (OLH) method is used because

it generally performs well in these types of lower-dimensional applications. In OLH, an initial Latin hypercube design (LHD) is adaptively improved following a so-called space-filling criterion (Morris and Mitchell, 1995; Ye et al, 2000; Jin et al, 2005). Here, the method suggested by Morris and Mitchell (1995) is applied. An LHD itself is constructed as follows to draw N samples from a d-dimensional design space. Each dimension of the design space is divided into N bins of equal probability. N cells of the total N^d created cells are then randomly selected so that each bin in each dimension only contains a single selected cell (McKay et al, 1979).

In the present work, we compare an OLH approach with a modified version of the DoE scheme called optimal isovolumetric Latin hypercube (OIVLH; Komeilizadeh et al (2022)). The idea of this variant is to transform Latin hybercube samples depending on the number of design space dimensions and pushing samples closer to design space boundaries while maintaining LHS properties. Specifically, assuming a uniform probability distribution, the bin boundaries p_i and sizes a_j are defined as

$$p_i = \begin{cases} 0.5\left(1 - \left(\frac{N_v+1-i}{N_v}\right)^{1/d}\right), & i \in [1, N_v] \\ 0.5\left(1 + \left(\frac{i-(N_v+1)}{N_v}\right)^{1/d}\right), & i \in (N_v, N+1] \end{cases} \tag{6}$$

$$a_j = p_{j+1} - p_j,\ j \in [1, N] \tag{7}$$

instead of the usual $p_i = \frac{i}{N}$ and $a_j = \frac{1}{N}$. Here, $N_v = \frac{N}{2}$ is defined for convenience of notation. The only previously published application of OIVLH is the successful integration into the multi-fidelity optimization of an automotive crashworthiness problem (Kaps et al, 2022).

After generating the DoE, the initial HK model is fitted to the objective functions based on the sampling data. HK is a multi-fidelity extension to the kriging model (Krige, 1951; Matheron, 1963; Sacks et al, 1989) which has been extensively discussed in the literature (e.g., Rasmussen and Williams (2005)). A more detailed derivation of the HK predictor can be found in the original publication (Han and Görtz, 2012). In HK, the trend term of the multi-fidelity predictor is the low-fidelity predictor. To determine the latter, we assume an LF sample data set $(\boldsymbol{S}_{LF}, \boldsymbol{y}_{S,LF})$ consisting of m_{LF} samples with input variable data $\boldsymbol{S}_{LF} \in \mathbb{R}^{m_{LF} \times d}$ and the corresponding output $\boldsymbol{y}_{S,LF} \in \mathbb{R}^{m_{LF}}$. Additionally, a so-called kernel modeling the correlation between sample points has to be defined. Here, a squared-exponential kernel, also called a Gaussian radial-basis function (RBF) kernel, is utilized due to its smoothness and infinite differentiability:

$$R(\boldsymbol{x}^{(i)}, \boldsymbol{x}^{(j)}) = \prod_{k=1}^{d} \exp\left(-\theta_k |x_k^{(i)} - x_k^{(j)}|^2\right), \tag{8}$$

where θ_k denotes the kernel length scale that represents the hyperparameter(s) of the kriging / HK model. The kernel utilized here is called anisotropic because there is a separate parameter for each dimension of the design space. Over the years, a wide variety of different kernel functions has been suggested (Rasmussen and Williams, 2005) and implemented in popular software libraries (for example, Pedregosa et al (2011); GPy (since 2012)). With the sample data set from above, the respective model is fitted by running an optimization for the kernel hyperparameters θ_k. Differential evolution (DE; Storn and Price (1997)) is used here due to its effectiveness and ease of use. More advanced methods of optimizing hyperparameters have been suggested (Toal et al, 2008). Given the sampling data and the kernel function, the low-fidelity predictor for a new design point $\boldsymbol{x}$ is defined as

$$\begin{aligned} &\hat{y}_{LF}(\boldsymbol{x}) = \beta_{0,LF} + \boldsymbol{r}_{LF}^T(\boldsymbol{x}) \boldsymbol{R}_{LF}^{-1} (\boldsymbol{y}_{S,LF} - \beta_{0,LF}\mathbf{1}), \\ &\text{with} \quad \beta_{0,LF} = (\mathbf{1}^T \boldsymbol{R}_{LF}^{-1} \mathbf{1})^{-1} \mathbf{1}^T \boldsymbol{R}_{LF}^{-1} \boldsymbol{y}_{S,LF}, \\ &\text{and} \quad \boldsymbol{r}_{LF} = [R(\boldsymbol{x}, \boldsymbol{x}^{(1)}), ..., R(\boldsymbol{x}, \boldsymbol{x}^{(m)})] \in \mathbb{R}^{m_{LF}}, \end{aligned} \tag{9}$$

where $\boldsymbol{r}_{LF}$ is the correlation vector between the sample data and the new point, $\boldsymbol{R}_{LF} \in \mathbb{R}^{m_{LF} \times m_{LF}}$ represents the correlation matrix between the sample data points and $\mathbf{1} \in \mathbb{R}^{m_{LF}}$ a column vector filled with ones.

Combining the low-fidelity predictor $\hat{y}_{LF}(\boldsymbol{x})$ as a trend term with the high-fidelity sample data set

$(\boldsymbol{S}, y_S)$ consisting of m samples with input variable data $\boldsymbol{S} \in \mathbb{R}^{m \times d}$ and the corresponding output $y_S \in \mathbb{R}^m$, the HK predictor is given by

$$\hat{y}(\boldsymbol{x}) = \beta_0 \hat{y}_{LF}(\boldsymbol{x}) + \boldsymbol{r}^T(\boldsymbol{x})\boldsymbol{R}^{-1}(\boldsymbol{y}_S - \beta_0 \boldsymbol{F}) \quad \text{with} \quad \beta_0 = (\boldsymbol{F}^T\boldsymbol{R}^{-1}\boldsymbol{F})^{-1}\boldsymbol{F}^T\boldsymbol{R}^{-1}\boldsymbol{y}_S. \tag{10}$$

Here, β_0 indicates the correlation between high- and low-fidelity models. $\boldsymbol{r} \in \mathbb{R}^m$ and $\boldsymbol{R} \in \mathbb{R}^{m \times d}$ are defined as introduced for the low-fidelity predictor using the same kernel function $R(\boldsymbol{x}^{(i)}, \boldsymbol{x}^{(j)})$. The low-fidelity prediction at high-fidelity sample points is represented by $\boldsymbol{F} = [\hat{y}_{LF}(\boldsymbol{x}^{(1)})...\hat{y}_{LF}(\boldsymbol{x}^{(n)})]^T, \forall \boldsymbol{x}^{(i)} \in \boldsymbol{S}$. All factors in the above equation except for $\hat{y}(\boldsymbol{x})$ and $\boldsymbol{r}(\boldsymbol{x})$ can be calculated at model fitting time as they do not depend on the location of the new point.

The mean squared error (MSE) of the HK prediction that is required for the adaptive stage of the optimization can be written with respect to the process variance σ^2 of the underlying random process as

$$MSE(\hat{y}(\boldsymbol{x})) = \sigma^2(1.0 - \boldsymbol{r}^T\boldsymbol{R}^{-1}\boldsymbol{r} + \left[\boldsymbol{r}^T\boldsymbol{R}^{-1}\boldsymbol{F} - \hat{y}_{LF}\right]^2 \left(\boldsymbol{F}^T\boldsymbol{R}^{-1}\boldsymbol{F}\right)^{-1}). \tag{11}$$

After fitting the initial HK model, several iterations are performed to adaptively improve it until the specified termination criterion is reached. The latter is discussed in Section 4. Each new adaptive sample is determined by internally optimizing an infill criterion. More general overviews on adaptive improvement methods for surrogate models can be found in one of the available overview works (e.g., Liu et al (2017); Fuhg et al (2020)). In the present work, two classes of infill criteria are introduced based on their aim. First, there are the more classic infill criteria used in optimization. Among them, *expected improvement* (EI; Jones et al (1998)) remains the most popular, but several other criteria have been suggested (see, for example, Jones (2001) or Forrester and Keane (2009) for an overview). In the present work, a multi-fidelity extension to EI called *variable-fidelity expected improvement* (Zhang et al, 2018) is utilized, as it allows adaptive sampling of low- and high-fidelity instead of just high-fidelity samples. Here, it is favored over other multi-fidelity infill criteria because it has been successfully applied in challenging structural applications by Kaps et al (2022, 2023).

VF-EI is defined at location $\boldsymbol{x}$ and fidelity level L as

$$EI_{vf}(\boldsymbol{x}, L) = \begin{cases} s(\boldsymbol{x}, L)\left[u\Phi(u) + \phi(u)\right], & \text{if } s(\boldsymbol{x}, L) > 0 \\ 0, & \text{if } s(\boldsymbol{x}, L) = 0, \end{cases} \tag{12}$$

where $u = \frac{y_{min} - \hat{y}(\boldsymbol{x})}{s(\boldsymbol{x}, L)}$ and y_{min} is the best feasible high-fidelity function value currently available. $\Phi(\bullet)$ and $\phi(\bullet)$ represent the cumulative distribution and probability density functions of the standard normal distribution, respectively. The term $s(\boldsymbol{x}, L)$ denotes the uncertainty of the HK model. As suggested in the original publication, the scaling factor β_0 that was previously introduced can be used to model the uncertainty in the high-fidelity prediction caused by the low-fidelity predictor

$$s^2(\boldsymbol{x}, L) = \begin{cases} \beta_0^2 \cdot MSE(\hat{y}_{LF}(\boldsymbol{x})), & L = 0 \text{ low-fid.} \\ MSE(\hat{y}(\boldsymbol{x})), & L = 1 \text{ high-fid.} \end{cases}. \tag{13}$$

$MSE(\hat{y}(\boldsymbol{x}))$ and $MSE(\hat{y}_{LF}(\boldsymbol{x}))$ are the MSEs of the high- and low-fidelity kriging predictors, respectively.

The second class of criteria discussed here is typically used in reliability analysis rather than optimization. Here, the aim is to improve the prediction of the limit state of a function by adaptively sampling close to it. This type of infill criterion in combination with a kriging model is also known as active learning kriging. One of the more popular functions of the category is the so-called U learning function (Echard et al, 2011). The motivation for using this particular infill criterion for the adaptive improvement of the surrogate model is twofold. First, it is observed from the problem definition in Subsection 2.3 that the objective function of the present application problem has an obvious limit state, the drawability limit. Therefore, while the problem considered here is not directly related to reliability analysis, this class of criteria is still applicable and

the idea is that adaptive sampling around the limit state will help guide the following optimization and increase convergence speeds. Second, the noise variables included in the optimization problem allow for the calculation of a probability of non-drawability to components predicted to be drawable in the mean state. Here, the improvement of the surrogate model around the limit state enables the surrogate-based estimation of this probability as described in Subsection 2.3. Therefore, the U learning function is used here as a basis instead of one of the many other available infill criteria. It is defined for a single-fidelity predictor $\hat{y}_{SF}(\boldsymbol{x})$ and the corresponding MSE as

$$U(\boldsymbol{x}) = \frac{|\hat{y}_{SF}(\boldsymbol{x})|}{\sqrt{MSE(\hat{y}_{SF}(\boldsymbol{x}))}}. \tag{14}$$

In the present work, we propose a new multi-fidelity extension of the U learning function inspired by the VF-EI infill criterion which uses the correlation factor β_0 to estimate the uncertainty in the high-fidelity prediction due to the low-fidelity prediction. Our multi-fidelity U learning function is defined depending on the design space location $\boldsymbol{x}$ and the fidelity level L as

$$U_{MF}(\boldsymbol{x}, L) = \frac{|\hat{y}(\boldsymbol{x})|}{s(\boldsymbol{x}, L)}. \tag{15}$$

Here, $s(\boldsymbol{x}, L)$ is defined as in Equation (13) and $\hat{y}(\boldsymbol{x})$ is the HK predictor from Equation (10). Due to the typically highly multimodal nature of the infill criteria, DE (Storn and Price, 1997) is selected for optimization of all infill criteria in the present work.

4 Proposed Approach

In the present work, a two-stage multi-fidelity optimization approach inspired by previous work in the literature (Pei et al, 2023) is proposed. Its target is twofold. First, it aims to increase the convergence speed of the algorithm in optimization problems by better resolving the relevant regions of the objective function. Second, it enables straightforward inclusion of input parameter uncertainties into the optimization process.

A schematic overview of the proposed multi-fidelity scheme is depicted in Figure 3. Initially, the design space is extended with sensible intervals for the noise variables (here: $\pm 3\sigma$ around their mean value). A DoE using OLH or OIVLH

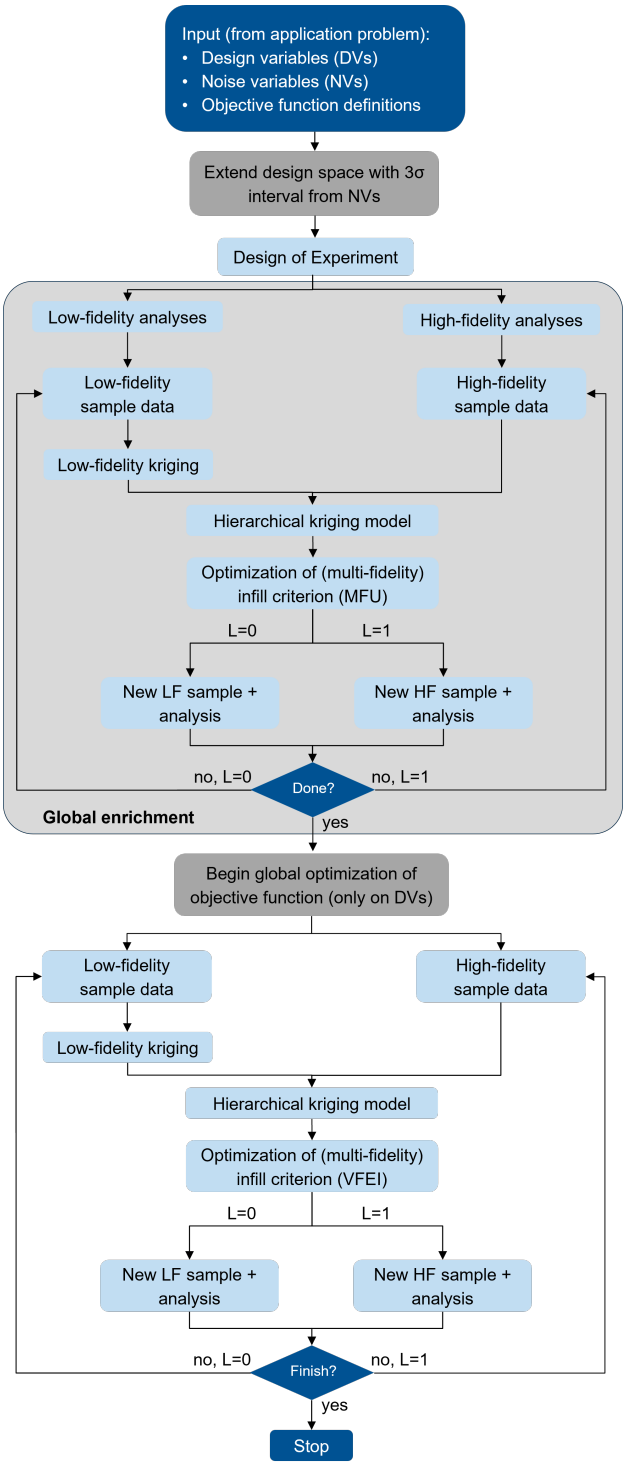

Fig. 3: Schematic overview of the proposed optimization scheme. The difference to the original multi-fidelity scheme (Zhang et al, 2018) is the possible inclusion of noise variables and the global enrichment phase. The different design of experiment methods are not shown. Termination criteria for the phases are discussed in Section 4.

sampling is created to fit an HK surrogate model on the extended design space including design and noise variables. Then, the global enrichment phase is started whereby an infill criterion (Eq. (15)) is optimized on the extended design space to add new samples to the surrogate model and subsequently refit it. In this phase, the aim is to improve the resolution of the limit state in the objective function (or a possible failure constraint). After a termination criterion is reached for the enrichment phase, the algorithm moves to the global optimization of the objective function. Details on termination criteria for both enrichment and optimization phases are discussed in the upcoming paragraph below. For the optimization, the surrogate model is restricted to design variables only. The previously included noise variables may be used, for example, to enforce failure constraints or simply to estimate the probability of failure of a given design point. The treatment of noise variables in the present work is explained in Subsection 2.3 where the exemplary application problem is introduced. The adaptive optimization itself consists of iteratively running DE on the infill criterion (here: VF-EI), calculating the determined design sample, and finally refitting the surrogate model(s). The algorithm finishes once a termination criterion is reached.

Three different termination criteria are utilized in the optimization process. They are independently defined for the global enrichment phase, where applicable, and the adaptive optimization phase. First, a threshold value is specified for the optimized infill criterion. Second, the number of adaptive objective function evaluations is limited. Third, the number of adaptive high-fidelity objective function evaluations is also limited for multi-fidelity techniques. The former criterion indicates convergence of the algorithm. The latter two criteria represent a budget restriction on optimization run time. For the adaptive optimization phase in all the investigated methods, the threshold value of (VF)EI is set to 10^{-5} and the number of total adaptive samples to 100, while the third criterion is not enforced here. The criteria applied for the global enrichment phase are listed in Table 3.

In the present work, a total of six different optimization techniques are compared. An overview of them is given in Table 4. In the following, they are referred to by the respective abbreviations given in the first column of the table.

Table 3: Overview of the termination criteria applied for the global enrichment phase of the optimization process. Methods are named according to Table 4.

Method name	IC_{th}	Max. it.	Max. HF it.
HF	-	-	-
HF + U	2	10	-
MF	-	-	-
MF(IV)	-	-	-
MF + MFU	2	60	10
MF(IV) + MFU	2	60	10

Table 4: Overview of different optimization schemes applied in the following deep drawing example. All techniques are referred to by the abbreviation given in the first column.

method name	surr. model	DoE method	enrich. crit.	infill crit.
HF	kriging	OLH	-	EI
HF + U	kriging	OLH	U	EI
MF	HK	OLH	-	VF-EI
MF(IV)	HK	OIVLH	-	VF-EI
MF + MFU	HK	OLH	MFU	VF-EI
MF(IV) + MFU	HK	OIVLH	MFU	VF-EI

The optimization algorithm, along with a part for DoE, is implemented in an in-house Python code from previous work by the authors (Komeilizadeh et al, 2022; Kaps et al, 2022, 2023). The generation of HK models and the implementation of kernels are based on the *scikit-learn* library (Pedregosa et al, 2011).

5 Results

A total of six optimization schemes are compared in the optimization problem introduced in Section 2. They are referred to below by the abbreviations introduced in Table 4. All techniques are evaluated here for result quality, computational costs, and result consistency. Specifically, we establish which of the methods can benefit from the inclusion of an enrichment phase into the optimization. To ensure reliability of the assessment, all simulations are performed on the same PC running LS-Dyna on eight cores. Additionally, each optimization run is repeated ten times. Unless explicitly stated otherwise, all objective function values given in the following refer to the high-fidelity model.

As a first step, the convergence of the algorithms and the respective termination criteria are checked to ensure comparability of the results. Convergence plots for all techniques are shown in Figure 4. Bold lines indicate the respective mean values, while the shaded areas represent the upper and lower bounds. All graphs include the complete optimization workflow including the initial DoE and, if applicable, enrichment phase. The diagrams indicate that all methods show very consistent convergence behavior and tend to very similar final results of the optimization.

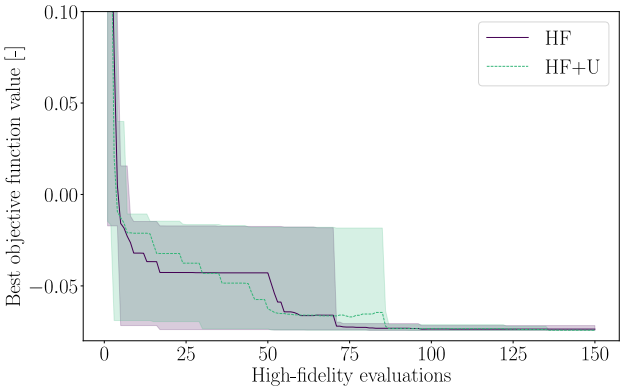

(a) Single-fidelity methods.

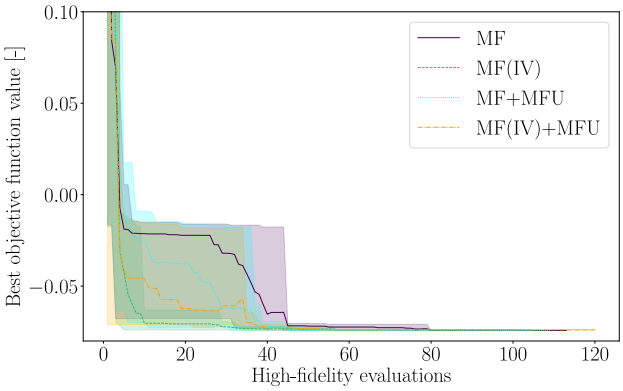

(b) Multi-fidelity methods.

Fig. 4: Convergence plots for ten repetitions of the six optimization methods. The mean of the respective runs is shown as a bold line. Areas of the same color represent upper and lower bounds. Plots include the initial design of experiments (see Table A1 in the Appendix) and, where applicable, the enrichment phase.

The enrichment phase is included in three of the six techniques, namely *HF+U*, *MF+MFU* and *MF(IV)+MFU*. It is terminated in all *HF+U* runs due to the iteration limit. In the multi-fidelity cases, seven runs reach the high-fidelity iteration limit and 13 runs the limit for adaptive HF samples. For *HF+U*, this is likely due to the definition of the threshold value, which is a common value used in reliability applications without optimization. Here, a more relaxed threshold value such as in (Pei et al, 2023) may have been beneficial. For the *MF+MFU* and *MF(IV)+MFU* techniques, the additional LF samples are likely to lead to a reduction in HK prediction uncertainty. This increases the MFU values to the point of termination of the enrichment phase. The impact on optimization results is discussed in more detail in the following.

The termination of the optimization phase shows a remarkable difference between *HF* and *MF* as well. For the former, only eight of the total 20 single-fidelity runs terminate due to the EI threshold value. All remaining runs reach the maximum number of iterations. On the other hand, only one run from *MF(IV)+MFU* of the total 40 multi-fidelity runs terminates due to reaching the iteration limit while all other reach the VF-EI threshold. The findings here together with the convergence plots above indicate, that a modification of the number of allowed adaptive samples, i.e., the second and/or third termination criterion, would not significantly change overall results. The explanation for the observed difference is probably the same as that for the enrichment phase. The additional LF samples reduce the prediction uncertainties of the HK model, thus reducing the VF-EI values. Implications are discussed below after a more detailed coverage of the optimization results.

A number of boxplots comparing the results of the optimization for the different techniques are shown in Figure 5. Given the scaling of the y-axis, all objective function results are very close to each other between values of -0.064 and -0.074. However, a pure visual comparison indicates that *HF* produces the best and most consistent results. *MF*, *MF(IV)* and *HF+U* are slightly less consistent but show the same median value, while *MF+MFU* and *MF(IV)+MFU* additionally have a slightly worse median value in the results. To check whether any of the observed differences with *HF* are statistically significant, each of the other five sets of results is individually tested against *HF* using a

Wilcoxon rank sum test. The null hypothesis of equal results is found to hold at a 5 % significance level for all tests. For completeness, the test statistics and p-values of all tests performed are listed in Table 5.

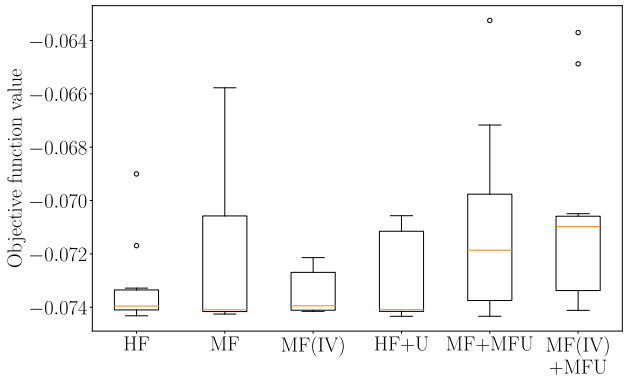

Fig. 5: Boxplots comparing optimization results for different techniques. Each method was repeated ten times. The red lines indicate median values and the boxes show the range between first and third quartile (interquartile range). The whiskers extend to the furthest point within 1.5 times the interquartile range and the dots represent outliers.

Table 5: Wilcoxon rank sum test statistics performed to check differences in the quality of objective function results at a 5 % significance level. Each method is tested against *HF* results.

Method name	U	p
HF + U	45	0.73
MF	50	1.00
MF(IV)	49	0.96
MF + MFU	66	0.24
MF(IV) + MFU	73.5	0.08

Given the optimized objective function values, a look is taken at the respective design variable values corresponding to the results. Therefore, six parallel coordinate plots comparing the different techniques are depicted in Figure 6. Each curve represents the optimized results of an optimization run. The color map indicates the values of the objective function. Different design variables are listed on the x-axis and their normalized ranges on the y-axis.

It is observed that optimized results appear to correspond to x_1, x_2 and x_3 at or somewhat close to their respective upper bounds 1.8 mm, 9 mm and 2.5. Most of the runs find the optimal value for x_4 very close to its lower bound 130 kN. However, in this case there are also a significant number of runs with different results throughout the design range of x_4. The larger variation in x_4 likely means that the variable is somewhat limited in its influence on the objective function, at least compared to the other variables. Apart from that, the results are as expected when considering cracks and wrinkles as the main modes of failure in deep drawing. Furthermore, they match very well with the results found in Kaps et al (2023) for a very similar application problem. The same observations regarding the quality and consistency of the results that are made above for the boxplot in Figure 5 apply here also. *HF*, *MF*, *MF(IV)* and *HF+U* show consistent and very similar results, while for *MF+MFU* and *MF(IV)+MFU*, there is slightly more variation and a total of three outliers among the two techniques for which the algorithm terminates with worse results.

To illustrate the progress made during an optimization run, a representative initial design and the respective optimal design from one run of *HF+U* are depicted in Figure 7. The respective FLDs are mapped onto the final geometry of the manufactured component to show the location of the remaining bad elements. The initial design produces an objective function value of 0.756, the optimized result −0.0744. The latter is the best objective function value found across all techniques and repetitions. Notably, the optimized result still contains a few bad elements. This stems from the definition of the objective function (Eq. (4)) where small violations, e.g. due to minor wrinkling, are still considered manufacturable. However, all cracked elements are removed here.

In a final step, the computational requirements of the different methods are compared by the average total optimization run time shown in Figure 8. Average run times in seconds are depicted as bars together with their standard deviations. The inclusion of the enrichment phase using the (MF)U learning function is found to result in about 15 % and 33 % faster run times for *HF+U* and *MF+MFU* compared to their respective counterparts *HF* and *MF*. The difference is

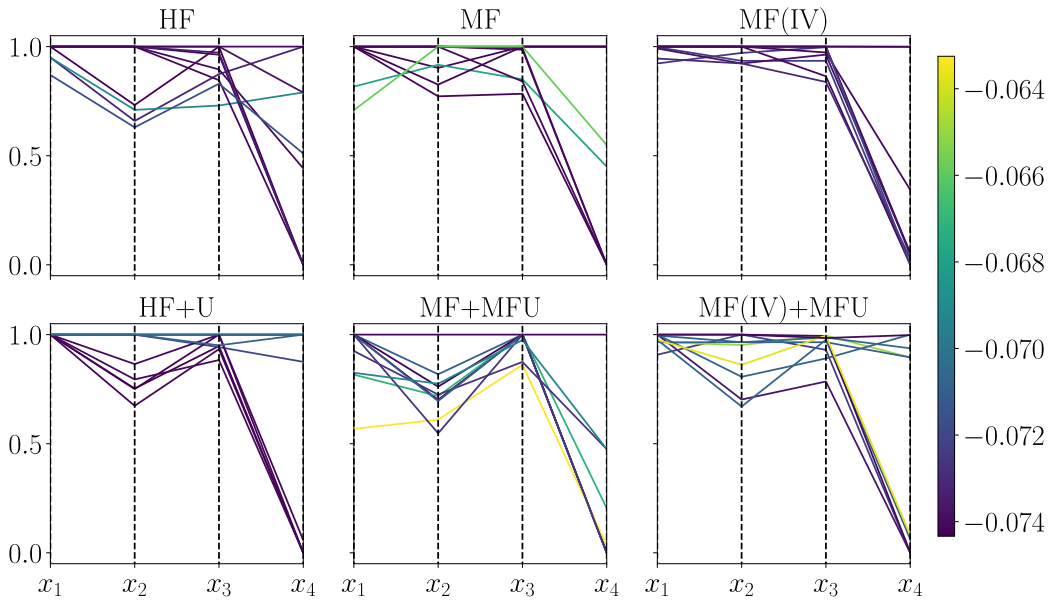

Fig. 6: Parallel coordinates plot comparing ten repetitions of the six optimization methods. Design variable values on the y-axis are normalized, actual boundaries can be found in Table 1. The color scale indicates objective function values of the respective results (lower is better).

the smallest for *MF(IV)+MFU* where the average run time is approximately 12 % less than for *MF(IV)*. However, both of these methods produce very good results, as they save approximately 58 % and 64 % optimization run time for *MF(IV)* and *MF(IV)+MFU*, respectively compared to the baseline *HF* technique. The best explanation for the run time differences throughout lies in the different termination criteria for the algorithms, which was shown above. Additionally, the introduction of an enrichment phase results in a lower average number of overall calculated samples prior to termination of the algorithm (compare also Table A3 in the Appendix).

In the introduction of the application problem, two noise variables are defined in addition to the four design variables. In this work, the noise variables are only used to give an estimation of the probability of non-drawability of the optimized drawable components using Monte Carlo sampling. Here, the probability is negligible in all runs, indicating that the components are considered drawable also under the influence of the noise variables. We believe it could be interesting to extend the treatment of noise variables in future work, for example, by defining a failure constraint that is enforced by the surrogate model predictions in the optimization phase.

It is shown that the inclusion of a global enrichment phase into the optimization workflow by itself already benefits the algorithm performance by reducing average run times with little compromise on the result quality. In the example presented here, the *MF+MFU* technique utilizing the newly proposed MFU enrichment criterion saves a third of run time compared to the multi-fidelity reference. The example problem investigated has a clear limit state in the objective function. We believe that the proposed approach is applicable to arbitrary objective functions as long as some information on the range of objective function values is available. However, this remains to be investigated further in future work.

6 Conclusions

In the present work, a novel two-stage multi-fidelity optimization scheme is proposed and investigated on a cross-die deep drawing problem. The workflow of an efficient global optimization scheme is extended by a global enrichment stage in between the initial surrogate model fitting and the actual adaptive optimization stage. To that end, a novel multi-fidelity extension of the popular U learning function is proposed that aims at improving the surrogate model quality at a limit state of

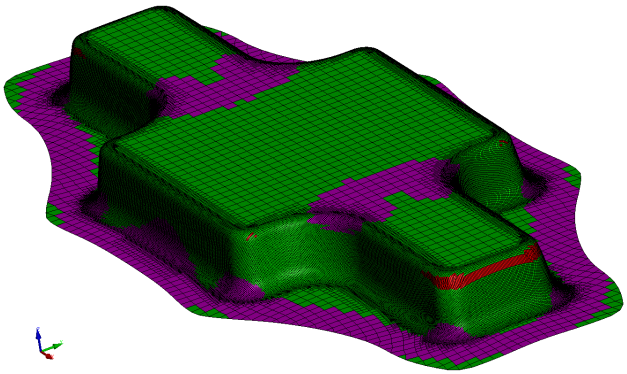

(a) Representative initial design.

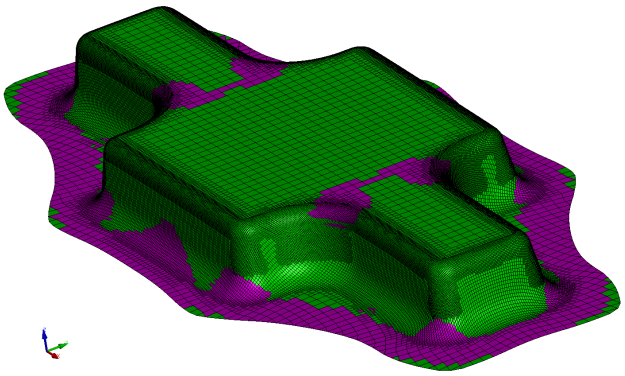

(b) Optimal design.

Fig. 7: FLDs of an early simulation and the optimized result mapped onto the respective final component geometry. Green, red and pink colors represent good, cracked and wrinkling elements, respectively (see Figure 2).

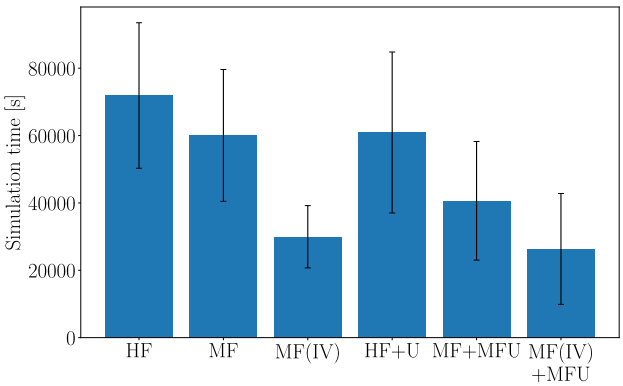

Fig. 8: Average run times of the compared optimization techniques in seconds. Error bars indicate the standard deviation out of the ten repetitions.

the function. The two-stage workflow is compared to a multi-fidelity approach based on hierarchical kriging as a surrogate model and variable-fidelity expected improvement as an infill criterion. A single-fidelity EGO method is used for reference. To illustrate the benefits of the two-stage approach, a single-fidelity two-stage approach is also extended with an enrichment phase using the U learning function as infill criterion. In addition, a modified sampling approach, which was recently proposed and successfully applied by our group, is investigated in this multi-fidelity context.

The application problem here aims at improving the manufacturability of a cross-die component. The high-fidelity simulation model is an explicit incremental formation simulation, whereas the low-fidelity model is an inverse one-step simulation. A drawability measure based on the forming limit diagram is used to determine manufacturability. For illustrative purposes, two noise variables are included in the problem.

It is found that all of the optimization approaches investigated yield very similar results, although there is a slightly higher variation in result quality compared to the single-fidelity reference approach. The inclusion of the enrichment stage into the optimization scheme saves between 12 % and 33 % in optimization run time compared to the respective single-stage optimization techniques. Particularly, the multi-fidelity approach using isovolumetric sampling performed well in our example. A speed-up factor in run time of more than two was observed for the classic single-stage approach and the novel two-stage approach, with the latter yielding a speed-up of approximately 2.7. All observed run time benefits are best explained by faster algorithm convergence due to lower uncertainty in surrogate model predictions.

On the basis of the promising results of the presented work, we have identified a number of ideas that we believe to be interesting for future work.

- Include a failure constraint into the optimization problem or enforce the sampling of manufacturable components in the adaptive phase.
- Apply the suggested optimization technique to a larger, possibly more realistic deep drawing component.
- Compare some of the various different multi-fidelity optimization techniques that have been

suggested in recent years against each other in a sheet metal forming problem.

Acknowledgments. This project is supported by the Federal Ministry for Economic Affairs and Climate Action (BMWK) on the basis of a decision by the German Bundestag.

Declarations

Competing interests. On behalf of all authors, the corresponding author declares that there is no conflict of interest.

Replication of results. The detailed information on the proposed methods, simulation models, and software used in this article can be found in the corresponding sections. This includes the algorithms and hyperparameters used. The self-implemented parts of the in-house Python code and exemplary simulation models for high- and low-fidelity models can be obtained from the corresponding author on reasonable request.

Authors' contributions. AK: Conceptualization, Methodology, Software, Formal analysis and investigation, Writing - original draft, Writing - review and editing; TL: Software, Writing - review and editing; IL: Software, Writing - review and editing; MW: Writing - review and editing, Supervision; STQ: Writing - review and editing, Supervision; FD: Writing - review and editing, Supervision.

Appendix A

Table A1: Overview of the initial design of experiments (OLH / OIVLH) used for the optimization techniques. Methods are named according to Table 4.

Method name	HF samples	LF samples
HF	50	-
HF + U	40	-
MF	30	100
MF(IV)	30	100
MF + MFU	20	100
MF(IV) + MFU	20	100

Table A2: Cross-die simulation model: Geometrical and material properties used to model the steel component. *HF*: Incremental (high-fidelity) simulation; *LF*: Inverse (low-fidelity) simulation.

Parameter	Symbol	Value
component width		290mm
component depth		120mm
component height (excl. radii)		12mm
die radius		*design variable*
Young's modulus	E	205GPa
Poisson's ratio	ν	0.3
mass density	ρ	$7850\,\frac{\mathrm{kg}}{\mathrm{m}^3}$
yield strength	σ_y	*noise variable*
Lankford coefficient	R	*design variable*
material model	*MAT_037	
1D plasticity	Hockett-Sherby	
	σ_0	*noise variable*
	σ_s	600MPa
	C	0.91
	n	0.518
element formulation	Belytschko-Lin-Tsay (*HF*)	
	fully integrated (*LF*)	
contact formulation	*CONTACT_FORMING_ONE_WAY	
(LS-Dyna; *HF*)	*CONTACT_DRAWBEAD	
Coulomb friction	μ	*noise variable*

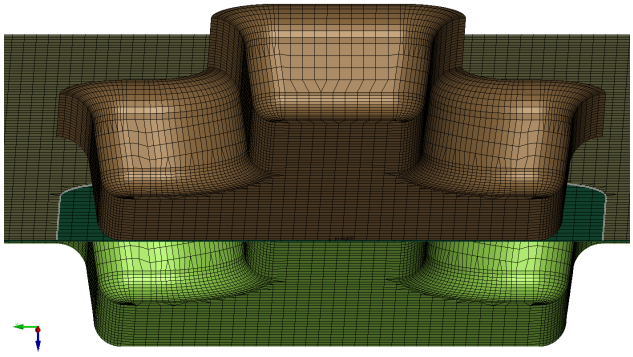

Fig. A1: Exemplary zoom into a high-fidelity simulation model at the initial time step, cut open in the middle. Shown in brown is the punch which moves down to form the component and in light green the die. The blank which is formed into the desired shape is shown in dark green and held in place by a blank holder depicted here in olive. (Kaps et al, 2023)

Algorithm 1 Calculation of the objective function

Require:

$d\left(\boldsymbol{\epsilon}^e, \hat{\boldsymbol{\epsilon}}^{LC}\right)$: Distance function (see Eq. (1))

N_g, N_c, N_w: Number of good, cracked and wrinkled elements, respectively

$f_{thr} \leftarrow 0.005$

$w_g \leftarrow 0.2$

$w_w \leftarrow 0.1$

$f_{nd} \leftarrow Eq.(2)$

if $f_{nd} <= f_{thr}$ **then**

  $f \leftarrow f_{nd}$

else

  $f \leftarrow Eq.(3)$

end if

Table A3: Overview of the average number of simulation model calls for different objective functions and optimization methods. Each optimization run is repeated ten times. The results are reported as mean and standard deviation (SD). Abbreviations follow the nomenclature introduced in Table 4.

Method	High-fidelity calls	Low-fidelity calls
HF	129.2 (SD 32.7)	-
HF + U	119.2 (SD 35.0)	-
MF	69.5 (SD 25.6)	100.0 (SD 0.0)
MF(IV)	52.9 (SD 20.3)	100.0 (SD 0.0)
MF + MFU	47.0 (SD 22.7)	109.3 (SD 7.5)
MF(IV) + MFU	48.5 (SD 36.1)	105.5 (SD 5.2)

References

Ablat MA, Qattawi A (2016) Numerical simulation of sheet metal forming: a review. The International Journal of Advanced Manufacturing Technology 89(1-4):1235–1250. https://doi.org/10.1007/s00170-016-9103-5

Andrade-Campos A, Coppieters S, Strano M (2022) Optimization and inverse analysis in metal forming: scientific state-of-the-art and recent trends. International Journal of Material Forming 15(3). https://doi.org/10.1007/s12289-022-01690-8

Banabic D (2010) Sheet Metal Forming Processes. Springer Berlin Heidelberg, https://doi.org/10.1007/978-3-540-88113-1

Bichon BJ, Eldred MS, Swiler LP, Mahadevan S, McFarland JM (2008) Efficient global reliability analysis for nonlinear implicit performance functions. AIAA Journal 46(10):2459–2468. https://doi.org/10.2514/1.34321

Chakroborty P, Dhulipala SLN, Che Y, Jiang W, Spencer BW, Hales JD, Shields MD (2023) General multifidelity surrogate models: Framework and active-learning strategies for efficient rare event simulation. Journal of Engineering Mechanics 149(12). https://doi.org/10.1061/jenmdt.emeng-7111

Cox D, John S (1992) A statistical method for global optimization. In: [Proceedings] 1992 IEEE International Conference on Systems, Man, and Cybernetics. IEEE, Chicago, IL, USA, https://doi.org/10.1109/icsmc.1992.271617

Dhulipala SL, Shields MD, Spencer BW, Bolisetti C, Slaughter AE, Labouré VM, Chakroborty P (2022) Active learning with multifidelity modeling for efficient rare event simulation. Journal of Computational Physics 468:111,506. https://doi.org/10.1016/j.jcp.2022.111506

Echard B, Gayton N, Lemaire M (2011) AK-MCS: An active learning reliability method combining kriging and Monte Carlo simulation. Structural Safety 33(2):145–154. https://doi.org/10.1016/j.strusafe.2011.01.002

Forrester AI, Keane AJ (2009) Recent advances in surrogate-based optimization. Progress in Aerospace Sciences 45(1-3):50–79. https://doi.org/10.1016/j.paerosci.2008.11.001

Forrester AI, Sóbester A, Keane AJ (2007) Multi-fidelity optimization via surrogate modelling. Proceedings of the Royal Society A: Mathematical, Physical and Engineering Sciences 463(2088):3251–3269. https://doi.org/10.1098/rspa.2007.1900

Fuhg JN, Fau A, Nackenhorst U (2020) State-of-the-art and comparative review of adaptive sampling methods for kriging. Archives of Computational Methods in Engineering 28(4):2689–2747. https://doi.org/10.1007/s11831-020-09474-6

Garud SS, Karimi IA, Kraft M (2017) Design of computer experiments: A review. Computers & Chemical Engineering 106:71–95. https://doi.org/10.1016/j.compchemeng.2017.05.010

Goodwin GM (1968) Application of strain analysis to sheet metal forming problems in the press shop. In: SAE Technical Paper Series. SAE International, https://doi.org/10.4271/680093

GPy (since 2012) GPy: A Gaussian process framework in python. http://github.com/SheffieldML/GPy, [Date accessed: 20.11.2023]

Guo Y, Batoz J, Naceur H, Bouabdallah S, Mercier F, Barlet O (2000) Recent developments on the analysis and optimum design of sheet metal forming parts using a simplified inverse approach. Computers & Structures 78(1-3):133–148. https://doi.org/10.1016/s0045-7949(00)00095-x

Guo YQ, Batoz JL, Detraux JM, Duroux P (1990) Finite element procedures for strain estimations of sheet metal forming parts. International Journal for Numerical Methods in Engineering 30(8):1385–1401. https://doi.org/10.1002/nme.1620300804

Han ZH, Görtz S (2012) Hierarchical kriging model for variable-fidelity surrogate modeling. AIAA Journal 50(9):1885–1896. https://doi.org/10.2514/1.J051354

Hoque SE, Duddeck F (2021) Experimental and numerical characterization of plasticity and fracture behavior of aluminum 6061-T4 sheet for deep drawing simulation. In: XVI International Conference on Computational Plasticity. Fundamentals and Applications, https://doi.org/10.23967/complas.2021.013

Jin R, Chen W, Sudjianto A (2005) An efficient algorithm for constructing optimal design of computer experiments. Journal of Statistical Planning and Inference 134(1):268–287. https://doi.org/10.1016/j.jspi.2004.02.014

Jones DR (2001) A taxonomy of global optimization methods based on response surfaces. Journal of Global Optimization 21(4):345–383. https://doi.org/10.1023/A:1012771025575

Jones DR, Schonlau M, Welch WJ (1998) Efficient global optimization of expensive black-box functions. Journal of Global Optimization 13(4):455–492. https://doi.org/10.1023/A:1008306431147

Kaps A, Czech C, Duddeck F (2022) A hierarchical kriging approach for multi-fidelity optimization of automotive crashworthiness problems. Structural and Multidisciplinary Optimization 65(4). https://doi.org/10.1007/s00158-022-03211-2

Kaps A, Lehrer T, Lepenies I, Wagner M, Duddeck F (2023) Multi-fidelity optimization of metal sheets concerning manufacturability in deep-drawing processes. Structural and Multidisciplinary Optimization 66(8). https://doi.org/10.1007/s00158-023-03631-8

Keeler SP (1968) Circular grid system — a valuable aid for evaluating sheet metal formability. In: SAE Technical Paper Series. SAE International, https://doi.org/10.4271/680092

Kishor N, Kumar DR (2002) Optimization of initial blank shape to minimize earing in deep drawing using finite element method. Journal of Materials Processing Technology 130-131:20–30. https://doi.org/10.1016/s0924-0136(02)00790-2

Komeilizadeh K, Kaps A, Duddeck F (2022) Isovolumetric adaptations to space-filling design of experiments. Optimization and Engineering 24(2):1267–1288. https://doi.org/10.1007/s11081-022-09731-6

Krige DG (1951) A statistical approach to some basic mine valuation problems on the Witwatersrand. Journal of the Southern African Institute of Mining and Metallurgy 52(6):119–139. https://doi.org/10520/AJA0038223X_4792

Lehrer T, Kaps A, Lepenies I, Duddeck F, Wagner M (2023) 2S-ML: A simulation-based classification and regression approach for drawability assessment in deep drawing. International Journal of Material Forming 16(5). https://doi.org/10.1007/s12289-023-01770-3

Liu H, Ong YS, Cai J (2017) A survey of adaptive sampling for global metamodeling in support of simulation-based complex engineering design. Structural and Multidisciplinary Optimization 57(1):393–416. https://doi.org/10.1007/s00158-017-1739-8

Makinouchi A (1996) Sheet metal forming simulation in industry. Journal of Materials Processing Technology 60(1-4):19–26. https://doi.org/10.1016/0924-0136(96)02303-5

Matheron G (1963) Principles of geostatistics. Economic Geology 58(8):1246–1266. https://doi.org/10.2113/gsecongeo.58.8.1246

McKay MD, Beckman RJ, Conover WJ (1979) Comparison of three methods for selecting values of input variables in the analysis of output from a computer code. Technometrics 21(2):239–245. https://doi.org/10.1080/00401706.1979.10489755

Merten M, Liebold K, Haufe A (2021) Robustness analysis with LS-OPT® and LS-DYNA® for sheet metal forming simulations. IOP Conference Series: Materials Science and Engineering 1157(1):012,088. https://doi.org/10.1088/1757-899x/1157/1/012088

Morris MD, Mitchell TJ (1995) Exploratory designs for computational experiments. Journal

of Statistical Planning and Inference 43(3):381–402. https://doi.org/10.1016/0378-3758(94)00035-T

Moustapha M, Sudret B (2019) Surrogate-assisted reliability-based design optimization: a survey and a unified modular framework. Structural and Multidisciplinary Optimization 60(5):2157–2176. https://doi.org/10.1007/s00158-019-02290-y

Naceur H, Delaméziere A, Batoz J, Guo Y, Knopf-Lenoir C (2004) Some improvements on the optimum process design in deep drawing using the inverse approach. Journal of Materials Processing Technology 146(2):250–262. https://doi.org/10.1016/j.matprotec.2003.11.015

Nguyen AT, Reiter S (2015) A performance comparison of sensitivity analysis methods for building energy models. Building Simulation 8(6):651–664. https://doi.org/10.1007/s12273-015-0245-4

Obermeyer E, Majlessi S (1998) A review of recent advances in the application of blank-holder force towards improving the forming limits of sheet metal parts. Journal of Materials Processing Technology 75(1-3):222–234. https://doi.org/10.1016/s0924-0136(97)00368-3

Ohata T, Nakamura Y, Katayama T, Nakamachi E, Omori N (1998) Improvement of optimum process design system by numerical simulation. Journal of Materials Processing Technology 80-81:635–641. https://doi.org/10.1016/s0924-0136(98)00170-8

Park C, Haftka RT, Kim NH (2016) Remarks on multi-fidelity surrogates. Structural and Multidisciplinary Optimization 55(3):1029–1050. https://doi.org/10.1007/s00158-016-1550-y

Paul SK (2013) Theoretical analysis of strain- and stress-based forming limit diagrams. The Journal of Strain Analysis for Engineering Design 48(3):177–188. https://doi.org/10.1177/0309324712468524

Pedregosa F, Varoquaux G, Gramfort A, Michel V, Thirion B, Grisel O, Blondel M, Prettenhofer P, Weiss R, Dubourg V, Vanderplas J, Passos A, Cournapeau D, Brucher M, Perrot M, Duchesnay E (2011) Scikit-learn: Machine learning in Python. Journal of Machine Learning Research 12:2825–2830

Pei P, Quek ST, Peng Y (2023) Enriched global–local multi-objective optimization scheme for fuzzy logic controller-driven magnetorheological damper-based structural system. Mechanical Systems and Signal Processing 193:110,267. https://doi.org/10.1016/j.ymssp.2023.110267

Rasmussen CE, Williams CKI (2005) Gaussian Processes for Machine Learning. MIT Press Ltd, https://doi.org/10.7551/mitpress/3206.001.0001

Sacks J, Welch WJ, Mitchell TJ, Wynn HP (1989) Design and analysis of computer experiments. Statistical Science 4(4):409–423. https://doi.org/10.1214/ss/1177012413

Storn R, Price K (1997) Differential evolution – a simple and efficient heuristic for global optimization over continuous spaces. Journal of Global Optimization 11(4):341–359. https://doi.org/10.1023/a:1008202821328

Sun G, Li G, Zhou S, Xu W, Yang X, Li Q (2010) Multi-fidelity optimization for sheet metal forming process. Structural and Multidisciplinary Optimization 44(1):111–124. https://doi.org/10.1007/s00158-010-0596-5

Sun G, Li G, Li Q (2012) Variable fidelity design based surrogate and artificial bee colony algorithm for sheet metal forming process. Finite Elements in Analysis and Design 59:76–90. https://doi.org/10.1016/j.finel.2012.04.012

Toal DJJ, Bressloff NW, Keane AJ (2008) Kriging hyperparameter tuning strategies. AIAA Journal 46(5):1240–1252. https://doi.org/10.2514/1.34822

Ye KQ, Li W, Sudjianto A (2000) Algorithmic construction of optimal symmetric Latin hypercube designs. Journal of Statistical Planning and Inference 90(1):145–159. https://doi.org/10.1016/S0378-3758(00)00105-1

Zhang Y, Han ZH, Zhang KS (2018) Variable-fidelity expected improvement method for efficient global optimization of expensive functions. Structural and Multidisciplinary Optimization 58(4):1431–1451. https://doi.org/10.1007/s00158-018-1971-x

Zhou Q, Zhao M, Hu J, Ma M (2023) Multi-fidelity Surrogates. Springer Nature Singapore, https://doi.org/10.1007/978-981-19-7210-2

Appendix B

Summaries of supervised theses

B.1 Master's thesis I (Wang, 2022)

When performing MF surrogate modeling or MF surrogate-based optimization, it seems very useful to consider the MF context already in the initial DoE and determine sample locations accordingly. As these MF-DoE methods are not commonly applied in MF optimization literature, they are evaluated in this Master's thesis utilizing HK surrogate models and the same MF optimization technique based on HK and VFEI that is used in the appended publications (Kaps et al., 2022, 2023, 2024). Based on a literature study on previously proposed MF-DoE techniques, three approaches are identified and studied more closely. An investigation of multiple influence parameters on HK model quality is carried out using two common analytical test functions. These include the question of how to distribute the sampling budget between LF and HF samples. Subsequently, the optimization performance is studied on the same analytical test functions as well as a lateral impact application example (the same one studied in appended publication I (Kaps et al., 2022)). In addition, the IV sampling modification is applied to the MF-DoE approaches to check its influence.

The findings of this work can be summarized in the following points. First, the allocation of the sampling budget to the LF and HF levels can be optimized if prior information is available about the correlation between the models. That is, if the two are highly correlated, more LF samples should be used. Without prior knowledge, a balanced approach has to be taken to avoid deterioration of the quality of the surrogate model. Second, it is found that here, IV sampling does not improve the global surrogate model quality measures and does not improve the optimization performance in the studied examples when using MF-DoE. Finally, it is found that the use of an MF-DoE technique does not significantly improve optimization performance in the study example problems compared to creating separate DoEs for the fidelity levels.

B.2 Master's thesis II (Krivacic, 2023)

In this Master's thesis, different MF optimization techniques are compared. Specifically, the approach based on HK and VFEI is compared with a cokriging-based approach as well as two different infill criteria, namely MES (maximum value entropy search) and upper confidence bound. The different methods are evaluated using two analytical test functions and the same

lateral impact example considered in appended publication I (Kaps et al., 2022) and in the previous Master's thesis (Wang, 2022).

One finding is that in the investigated examples, the difference between cokriging and HK as the underlying MF surrogate model is minimal. The infill criteria have a somewhat larger influence on optimization performance, and it is found that MES performs best in the analytical test cases. For the impact example, the results between all surrogate models and infill criteria are quite similar to previous findings from the analytical functions. However, the optima are found to vary significantly from previously reported results in Kaps et al. (2022) and Wang (2022). Therefore, results cannot be compared between works. Also, the optimization run times cannot be compared on the basis of the results in this Master's thesis.